2002

STRAIN CONTROL OF PIEZOELECTRIC MATERIALS USING AN APPLIED ELECTRON FLUX

Philip Clark Hadinata
University of Kentucky, pchodi0@engr.uky.edu

ABSTRACT OF DISSERTATION

Philip Clark Hadinata

The Graduate School

University of Kentucky

2002

STRAIN CONTROL OF PIEZOELECTRIC MATERIALS USING AN APPLIED ELECTRON FLUX

ABSTRACT OF DISSERTATION

This dissertation is submitted as one of fulfillment of the requirements for the degree of Doctor of Philosophy in the College of Engineering at the University of Kentucky

By

Philip Clark Hadinata

Lexington, Kentucky

Director: Dr. John A. Main, Associate Professor of Mechanical Engineering

University of Kentucky

Lexington, Kentucky

2002

ABSTRACT OF DISSERTATION

STRAIN CONTROL OF PIEZOELECTRIC MATERIALS USING AN APPLIED ELECTRON FLUX

This dissertation examines the response of piezoelectric material strain to electron flux influence. A plate of PZT5h is prepared as the specimen. The positive electrode is removed, and the negative electrode is connected to a power amplifier. Sixteen strain gages are attached as the strain sensor. The specimen is placed in a vacuum chamber, then the positive side is illuminated by electron beam.

The characteristic of the static strain response is predicted by deriving the equation strain/deflection of the plate. Two methods are used, the Electro-Mechanical Equations and numerical analysis using Finite Element Method.

The settings of the electron gun system (energy and emission current), along with the electric potential of the negative electrode (back-pressure), are varied to examine piezoelectric material responses under various conditions. Several material characteristics are examined: current flow to and from the material, time response of material strain, charge and strain distribution, and blooming.

Results from these experiments suggest several conditions control the strain development in piezoelectric material. The current flow and strain on the material is stable if the backpressure voltage is positive. As a comparison, the current flow is small and the strain drifts down if the backpressure voltage is significantly negative.

The material needs only 1 second to follow a positive step in backpressure voltage, but needs almost 1 minute to respond to a negative step backpressure change. This phenomenon is a result of secondary electron emission change and the energy transfer from the primary electrons to the local electrons on the material. The time needed to achieve steady state condition is also a dependent of emission current.

After a period of time the primary electron incidence induces strain throughout the 7.5-cm-by-5-cm plate despite the fact that the beam diameter is only 1 cm^2. One possibility is blooming due to electron movement under intense electric fields in the dielectric material.

KEYWORDS: piezoelectric, electron flux, quasi-static, strain, control

Philip Clark Hadinata

January 25, 2002

STRAIN CONTROL OF PIEZOELECTRIC MATERIALS USING AN APPLIED ELECTRON FLUX

By

Philip Clark Hadinata

Dr. John A. Main
Director of Dissertation

Dr. George Huang
Director of Graduate Studies

January 25, 2002

RULES FOR THE USE OF DISSERTATIONS

Unpublished dissertations submitted for the Doctor's degree and deposited in the University of Kentucky Library are as a rule open for inspections, but are to be used only with due regard to the rights of the authors. Bibliographical references may be noted, but quotations or summaries of parts may be published only with the permission of the author, and with the usual scholarly acknowledgments.

Extensive copying or publication of the dissertation in whole or in part also requires the consent of the Dean or the Graduate School of the University of Kentucky.

DISSERTATION

Philip Clark Hadinata

The Graduate School
University of Kentucky
2002

STRAIN CONTROL OF PIEZOELECTRIC MATERIALS USING AN APPLIED ELECTRON FLUX

DISSERTATION

This dissertation is submitted as one of fulfillment of the requirements for the degree of Doctor of Philosophy in the College of Engineering at the University of Kentucky

By

Philip Clark Hadinata

Lexington, Kentucky

Director: Dr. John A. Main, Associate Professor of Mechanical Engineering

University of Kentucky

Lexington, Kentucky

2002

To Flora

My true delight

ACKNOWLEDGMENT

First and foremost, I owe my greatest gratitude to my dissertation chair, Dr. John A. Main, for his on-going serenity and effort to get the best and finest of me. Dr. Main's critiques, suggestions and evaluations enlightened me throughout each step of this dissertation. Furthermore, Dr. Main provided me with unlimited resources of fund and instrumental assistance as well as information, with which I am able to pull all the stops to finish this dissertation with aspiring finesse.

I also wish to give my meritorious thanks to my advisory committee: Dr. Jamey D. Jacob, Dr. Suzanne W. Smith, Dr. Horn S. Tzou, Dr. Keith E. Rouch, Dr. Seongjai Kim, and Dr. Syed Nasar. Each individual endowed me with guidance and different thoughts, enriched me with constructive mind.

No one I ever knew of is as supportive and persevered in pushing me forward as Flora Djojo. Her entity in my arsenal of assistance is far from scientific and technical terms, but simply is her being. To her I bestow this work.

My Advance Structure Laboratory fellows: George Nelson, Jeff Martin, Todd Griffith and Mike Roche, I owe them a great deal of gratitude for technical support and guide, and for sharing their knowledge through my first difficult months in University of Kentucky. My new fellow Haiping Song, I thank him for his generosity in helping me with Matlab. My other fellows, Vijay Kulkarni, Ben Macke, and Eric Herndon, I appraise them for programming support. And my Indonesian fellow Ferdy Martinus, I thank him for his kindness in providing me with books and other theoretical resources.

I graciously thank Pilgrim Bible Assembly, especially Rachel and Annie Sloan for their astounding dishes on my defense. I wish to thank National Science Foundation, especially the program chair Dr. Allison Flatau, for the fund and opportunity they spent throughout this research. I hope this work is answering enough to their support.

Finally, I am truly indebted to my beloved family: my Mom, Dad, and brother Leonard, for their love and faith. Their undying esteem in my true self will be heralded forever in this dissertation, not as my meager attempt to repay their faith, but as my continuing deed to be their pride.

TABLE OF CONTENTS

LIST OF TABLES

LIST OF FIGURES

LIST OF FILES

Disst.pdf …… 1.8Mbyte

CHAPTER ONE
INTRODUCTION

Piezoelectric Phenomenon

Piezoelectric materials are used extensively as actuators in many aerospace structures. The word “piezoelectric” comes from greek term “piezo” meaning “pressure”[1]. This material can convert mechanical energy that distorts the material into electrical energy, and vice versa. One simple argument about this mutual aspect is the lack of a center of symmetry in the crystal structure. If a structure with center of symmetry is exposed to mechanical stress, the dimension changes but no net electric dipole moment is created. If a structure without center of symmetry is exposed to the same stress, the center of positive and negative charge no longer coincide, and a dipole moment is produced.

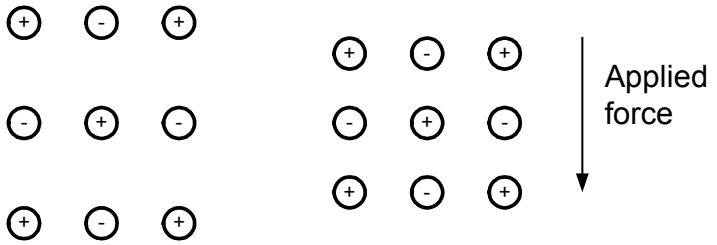

Figure 1.1. Material with center of symmetry

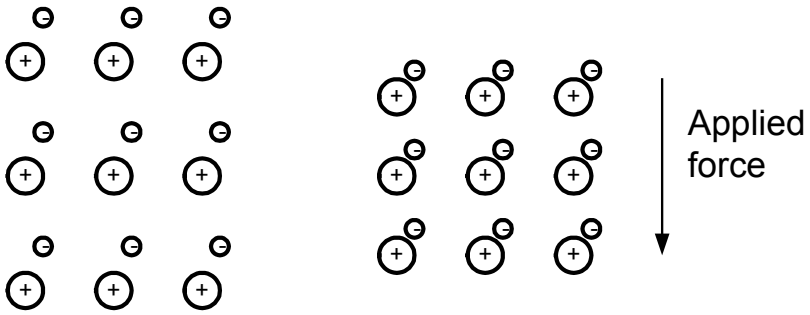

Figure 1.2. Material without center of symmetry

Other properties common to these materials are a high dielectric resistance, i.e., it is an excellent insulator, and some polymeric piezoelectric materials posses a long molecular chain structure having an unbalanced electric charge at the ends of the chains. The positive charge at one end of the chain will attract a free electron while the negative charge at the other end will repel free electrons.

Because the material is an excellent insulator, electrons are free to move only at the boundaries of the material. The unbalanced charge from the bipolar molecules will create a net deficiency of free electrons at one surface of the structure and a surplus of free electrons at the other surface. Generally the surfaces are coated with a conductive material or the material is mounted between conductors to form what is essentially a capacitor having a bipolar center.

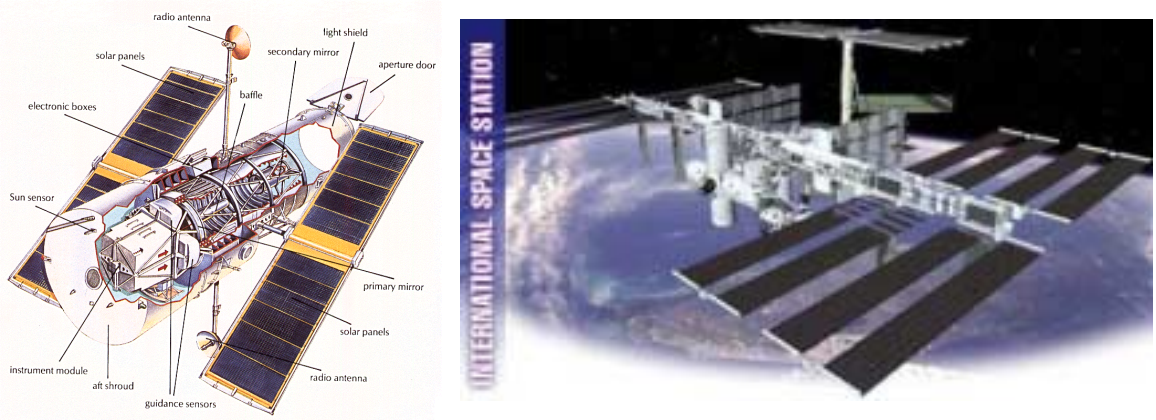

Figure 1.3. Space structures: Hubble Telescope and International Space Station

The goal of this research is to explore an alternative method for applying electrical control signals to piezoelectric materials. The classical “capacitor” approach relies upon two plates maintained a different electric potential levels. The electric field created between the plates strains the material by changing the dipole moment. In this research control charges are applied to piezoelectric materials by applying an electron flux to the bare surface of the piezoelectric material.

The main advantage of using electron flux to stimulate strain in piezoelectric materials is the potential for high spatial resolution and flexible actuation area. High spatial resolution means that the actuation area can be made as small as possible by

focusing the electron beam. Flexible actuation area means that the actuation area can be of any shape (round, rectangular, etc.) through beam scanning.

Secondary Electron Emission Mechanism

When an electron hits the surface of a piece of piezoelectric material there are a number of interactions that can take place. Ganachaud and Mokrani [3], Attard and Ganachaud [5] described the interactions as electron-electron collision, electron-phonon (light particle) collision (though it is more likely that a phonon is generated as a product of this interaction), electron-solid elastic collision, polarization and polaronic effects. A polaron is a conducting electron in an ionic crystal together with the induced polarization of the surrounding lattice. All of these interactions allow energy transfer, with the incoming electron as an energy donor and the electrons on the material as the recipient. The latter then are excited to the next energy band, and can eventually become a free electron known as “secondary electron”.

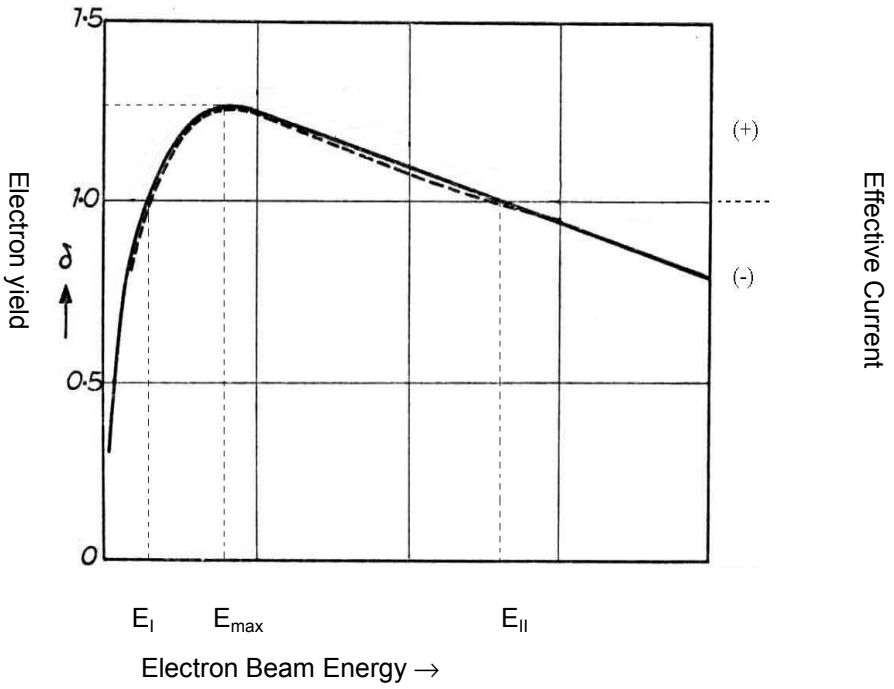

Figure 1.4. Plot of secondary electron yield against incoming energy

The following explanation of the secondary electron yield can be found in Hajo Bruining's book [2]. The chart of secondary electron yield versus energy at primary electrons can be seen in Figure 1.4. When an incoming electron with energy < E_I (as shown in Figure 1.4.) hits the dielectric surface, it will stick on the plate (since the secondary yield <1), making the plate more negative. So the next incoming electron will come with reduced speed, and also with reduced energy. So the electron beam energy moves to the left, and at some point it will die out. If the electrons have energy between E_I and E_{II}, the secondary electron yield >1, so they will kick out more and more electrons out of the plate, making the plate more positive if there is a collector present to attract the freed secondary electrons. So the next incoming electrons will hit the plate with higher speed, thus higher energy. So the electron energy moves to the right, passing through E_{II} point. As soon as it exceed E_{II}, the same phenomenon takes place when the energy < E_I. So as long as the electron energy is greater than E_I, it will reach E_{II}. E_{II} is the stable point.

Ganachaud and Mokrani [3] presented a thorough, detailed analysis of electron-material interactions. Also, some influences of internal electric field and surface potential barrier are discussed. These effects were also taken into account in Monte Carlo simulations, which are discussed in detail by Ganachaud, Attard and Renoud [4].

Ganachaud and Mokrani [3], Ganachaud, Attard and Renoud [4] built a model of space charge build-up in an insulating target under electron bombardment. Electron-insulator interaction was evaluated by considering electron-electron, electron-phonon, and elastic collisions. The charging of the plate was modeled using Monte Carlo simulation. Figure 1.5 shows the results of one simulation. Note the expansion of charge across the surface (0-axis) and into the material as a function of primary electron number.

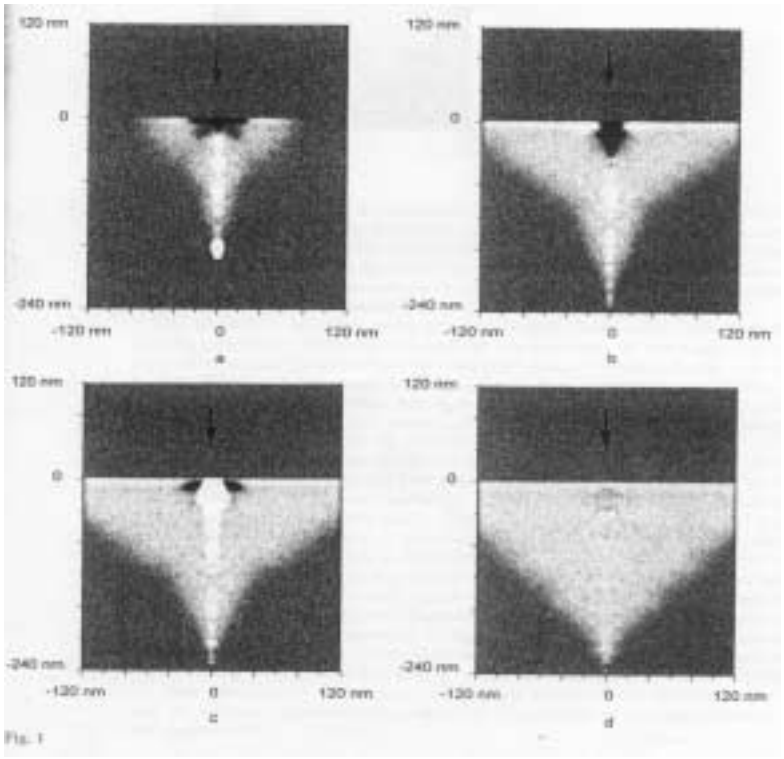

Figure 1.5. Charge blooming from Monte Carlo Simulation by Attard and Ganachaud [5]
a. 1000, b. 5000, c. 10000, d. 15000 electrons

The results, taking into account some parameters such as primary electron energy, electron traps, surface potential, and external electrostatic fields, were discussed extensively by Attard and Ganachaud [5], and Renoud et al [6]. Attard and Ganachaud [5] found out that as the target charge builds up, the potential at the surface and the secondary yield vary. The amplitude of the electrostatic field depends on the density of traps. For the energies considered, the target charged positively and the secondary electrons emitted at low energies could be attracted back to the surface. Renoud et al. [6] specifically examined in this effect and pointed out that the total secondary electron yield tends to unity and the surface potential stabilized at a low positive value, correlated with the explanation of Figure 1.4 presented by Hajo Bruining[2].

Charge build-up and distribution in the material is the main topic for Bibi, Lazurik and Rogov [7]-[9]. A probability method called the Trajectory Translation method, based on the new Monte Carlo method was developed to calculate charge and electric field

distribution on the materials. Bibi, Lazurik and Rogov [7] computed data examining charge profiles in thin materials. The charge distribution depended on energy of the primary electrons, atomic number and thickness of the materials investigated.

Bibi, Lazurik and Rogov [8] used the Trajectory Translation method to simulate the charge deposition density of several materials with different thicknesses subjected to electron flux. An analytic expression for the charge deposition profiles based on what they got from the simulation results was developed. Using the same data, once again Bibi, Lazurik and Rogov [9] used the Trajectory Translation method to simulate the electric field distribution in the same materials.

Nazarov [10] was interested in electron energy loss when electrons collide with the material. A semi-infinite solid model was used and the surface energy loss function was built. The analysis was based on the theory of inelastic electron scattering by surfaces of materials and took into account both the spatial dispersion of the dielectric response and the structure of the near-surface region. The energy loss function was expressed in terms of the dielectric function of the material.

Gross et al. [11] explained the charge storage and transport in materials under electron flux and corona charge influence. The relationship between the current density of the beam and the electric field in the material was derived from Maxwell's current equation.

Schou [12] presented a thorough explanation on his paper about transport theory of electrons under electron flux influence. The energy and angular distribution and the yield of secondary electron for a random target utilizing Boltzmann transport equations were calculated. The liberated electrons of low energy were pointed out to be moving isotropically inside the target in the limit of high primary energy, as compared to the instantaneous energy of the liberated electrons. The connection between the spatial distribution of kinetic energy of the liberated electrons and the secondary electron current from solid was also derived. Boltzmann transport equations can be examined in further details in a paper by Rösler et al. [13], along with explanations of other electron-solid interactions.

Electron Transport Through a Dielectric Solid

When the primary electron hits plate, there are a number of interactions between the electron and the local particles (electron, phonon, atom) as is described by Ganachaud and Mokrani [3] and Ganachaud, Attard and Renoud [4]. This interaction induces energy transfer from the primary electrons to the local electrons.

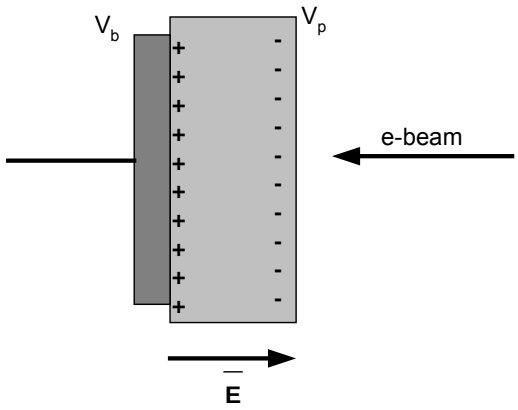

Figure 1.6. Electric field in piezoelectric material under electron flux influence

The primary electrons also shroud the positive surface of the plate with negative ions (electrons). This polarizes the material so that the negative charges (i.e. electrons) are stacked up on the positive surface, and the positive charges (i.e. holes) are gathered at the negative surface (electrode). An electric field is induced from the positive charges to the negatives, as is depicted on Figure 1.6. The constitutive relationship between the mechanical and electrical aspects of piezoelectric material is given by:

$$T = cS - e\bar{E} \quad (1.1)$$

$$D = \in \bar{E} + eS \quad (1.2)$$

The homogeneous electric field strength between positive and negative surface is given by [14]:

$$\bar{E} = \in 4\pi q = \in \bar{E}_v \quad (1.3)$$

where q = surface charge density

$\bar{E}_v$ = electric field in vacuum

$$\in = \in_r \in_o \tag{1.4}$$

$\in_r$ = relative dielectric constant

$\in_o$ = permitivity of vacuum = 8.85 x 10^{-12} F/m

As discussed in detail in the previous subchapter, an electron can only move through the lattice in the material if its energy exceeds the potential energy barrier. This potential energy can be considered to be constant throughout the material.[15] In the absence of an external electric field, the probability that the electron flux will cause an ion (electron) to jump across a barrier is:

$$p^* = Ae^{\frac{-E_b}{E_t}} \tag{1.5}$$

where E_b = energy barrier

E_t = the total energy received from the interaction with primary electron

A = frequency factor, obtained from the probability of a jump caused by an average energy $h_P\omega_o$ with respect to all probable energy

h_P = Planck constant (6.63 x 10^{-34} J.s)

The electron flux causes a different polarity on both surfaces, thus induces an electric field. The total probability that an electron will travel in a direction to the field is given by:

$$p_t^* = p^* \left(\frac{\bar{E} q_e a}{E_t} \right) \tag{1.6}$$

where $\bar{E}$ = the electric field

q_e = electron charge (1.6 x 10^{-19} C)

a = distance between lattice

The electric polarity for one jump is ea. The current density is:

$$j = np_t^* q_e a = np^* \left(\frac{\bar{E} q_e a}{E_t} \right) \tag{1.7}$$

where n = density of electron

The conductivity of the material is determined by utilizing Ohm's Law and Equation (1.7) above:

$$\sigma = \frac{j}{E} = np * \left(\frac{q_e{}^2 a^2}{E_t} \right) \tag{1.8}$$

The ionic mobility is given by:

$$\sigma = nq_e\mu \tag{1.9}$$

which leads to the mobility of the electron in the material as:

$$\chi = p * \left(\frac{q_e a^2}{E_t} \right) \tag{1.10}$$

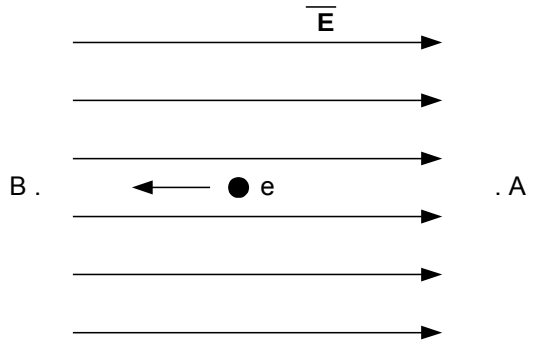

Figure 1.7. Electron movement in the opposite direction of the electric field.

Equation (1.10) suggests that despite the fact that piezoelectric material is a perfect insulator, there is a possibility that the electrons travel through the material. The electric field induces force on an electron with magnitude eE and in the opposite direction with the electric field [35], as is described in Figure 1.6. The elemental work done by the electric field through a displacement dL is eE.dL. To find the total work from A to B, integrate all the work contributions for all the infinitesimal segments. This leads to the following equation

$$W_{AB} = -q_e \int_A^B \bar{E} dL \tag{1.11}$$

The electric potential difference is derived from

$$V_B - V_A = \frac{W_{AB}}{q_e} \tag{1.12}$$

Substituting Equation (1.12) to Equation (1.11) leads to

$$V_B - V_A = -\int_A^B \bar{E} dL \tag{1.13}$$

The trajectory of the electron on the electric field is represented by Boltzmann Transport Equation. [16] The electrons in a material can be considered as a form of "cloud" with density ρ(k,r,t), where k is the wave vector, r is the position vector and t is time. The continuity equation has to be derived to find the actual motion of the electron in this cloud:

$$\frac{\partial \rho}{\partial t} + \nabla_k \bullet (\dot{k}\rho) + \nabla_r \bullet (\dot{r}\rho) = \left(\frac{\partial \rho}{\partial t}\right)_{coll} \tag{1.14}$$

Because of the independence of the variables, Equation (1.14) can be rewritten:

$$\frac{\partial \rho}{\partial t} + \dot{k} \bullet \nabla_k \rho + v \bullet \nabla_r \rho = \left(\frac{\partial \rho}{\partial t}\right)_{coll} \tag{1.15}$$

where $v = \dot{r}$

In the electron cloud argument, the mass density ρ can actually be replaced by the average occupancy f(k,r,t) of an electronic state. Equation (1.15) can be rewritten:

$$\frac{\partial f}{\partial t} + \dot{k} \bullet \nabla_k f + v \bullet \nabla_r f = \left(\frac{\partial f}{\partial t}\right)_{coll} \tag{1.16}$$

This is Boltzmann Transport Equation. This equation is based on classical motion, and is not expected to be valid when the external fields are too large. The right hand expression is an integral over the unknown function f(k,r,t), while the left-hand side contains the derivative of f(k,r,t).

Background on Piezoelectric Materials

Studies concerning piezoelectric materials, especially studies about the material properties, are still conducted in order to have good understanding on its behavior.

Studies have been conducted in control aspects, i.e. preliminary studies to use the material as actuators of smart structures. Batra et al. [17] investigated the optimum location of a given rectangular piezoceramic actuator that will require the minimum voltage to null the deflections of a simply supported rectangular linear elastic plate vibrating near one of its fundamental frequencies. The relationship between the voltage required and the length of its diagonal was investigated and derived.

Ghosh and Batra [18] conducted research on shape control of plates using piezoceramic elements. A fiber-reinforced laminated composite plate with 4 small piezoceramic actuator attached on top surface are used for experimental sample, and the Galerkin formulation was used to calculate the parameters for the computer code. The piezoelectric actuators could be used to nullify the deflection of the plate. Two common quasistatic problems were taken into account: simply-simply supported and cantilever plate.

Main, Nelson and Martin [19-20] demonstrated that strains in piezoelectric materials could be controlled through a combination of applied electron fluxes and potentials. It was also shown the changes in structure remained after the input signals were removed, indicating that there is some potential for energy efficient static strain control in adaptive structures using this method. This explanation is strengthened by a paper by Nelson and Main [21].

Crawley and deLuis [22] constructed a model of static and dynamic behavior of segmented piezoelectric actuator under load influences, either bonded to an elastic structure, or embedded in a laminated composite. These models enable prediction of the response of the structure to a control signal, and permit the determination of optimal locations for actuator placement. The independence of the effectiveness of piezoelectric actuators from the size of the structure was demonstrated and various piezoelectric

materials (based on their effectiveness in transmitting strain to the substructure) were evaluated.

Crawley and Lazarus [23] dealt with induced strain on isotropic and anisotropic plates subject to different loads. The equations relating the strains and the energy are derived, and some solutions are presented using Rayleigh-Ritz method.

Lee and Moon [24] derived and examined experimentally the modal sensor or actuator relationship, and derived the one-dimensional modal equations experimentally. These equations showed that distributed piezoelectric sensors/actuators could be adopted to measure specific modes of one-dimensional plate or beam. A mode 1 and 2 sensor for one-dimensional cantilever plate were constructed and tested to examine the applicability of the modal sensors/actuators. Tzou and Ye [25] examined its behavior under different steady-state temperature fields by means of finite element method.

Gopinathan, Varadan and Varadan [26] developed a 3-dimensional complete field solution for active laminates based on a modal, Fourier series solution approach that was used to compute all the through-thickness electromechanical fields near the dominant resonance frequency of a sandwiched-beam plate. This solution was then used to verify the result from the most accepted finite element model for piezoelectric (classical laminate of first-order shear deformation theory).

Purpose of the Research

A complete understanding of piezoelectric behavior under various electron flux conditions needs to be developed. This understanding can be achieved through several steps:

- Obtaining the static and quasi-static characteristic of piezoelectric material under vacuum environment, exposed to electron flux, from experimental data.
- Developing a theoretical understanding the electron-material interaction and process of mass-charge transfer on the contact area.

Outline

Chapter I is comprised of introductory explanations of piezoelectric material characteristics, electron gun strain control, secondary electron emission, and several related previous developments. Chapter II consists of theoretical explanation of piezoelectric shape control. A brief explanation using Finite Element Method is presented. Chapter III shows the specimen, vacuum chamber and data acquisition system in detail. A preliminary experiment to determine the sensitivity of electron flux induced strain to location within the vacuum chamber is also conducted. Chapter IV is a presentation of the effect of electron flux on the current flowing through a piezoelectric plate. Chapter V is a presentation of piezoelectric strain results due to various excitation and backpressure conditions. Chapter VI is a discussion of the experiments.

CHAPTER TWO

THEORY OF PIEZOELECTRIC RESPONSE UNDER ELECTRON FLUX INFLUENCE

In this chapter the strain and displacement distribution on piezoelectric material under electron flux influence is studied using two methods: Electro-mechanical equations developed by Tzou [27] and Finite Element Method. Both methods will be discussed to gain a clearer understanding of the state of strain in a rectangular piezoelectric plate due to externally applied electric fields.

Piezoelectric Electro-mechanical Equations

This method starts with a thin, isotropic and homogeneous shells of constant thickness with curvilinear surface coordinates α_1, α_2, α_3, as is shown in Figure 2.1.

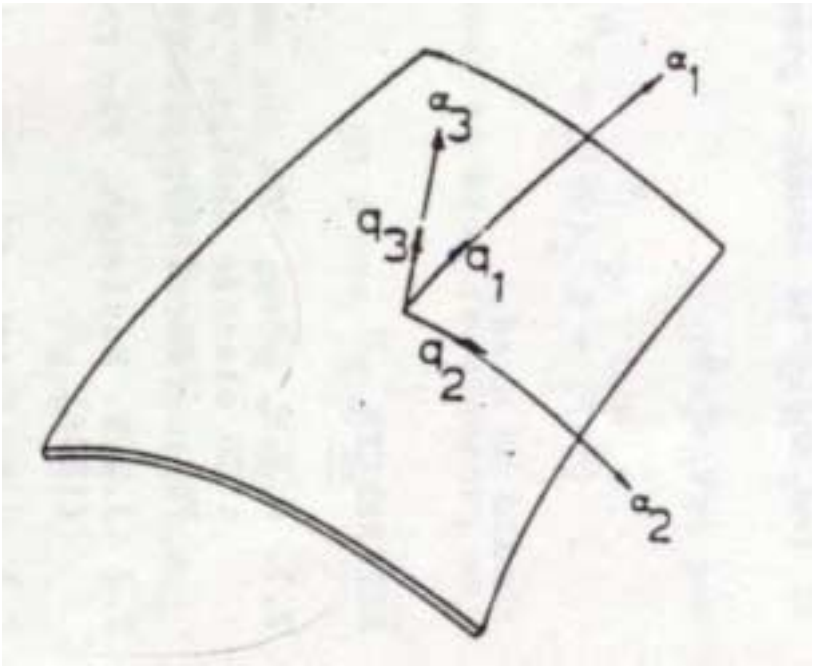

Figure 2.1. Generic piezoelectric shell [27]

The electro-mechanical equations for piezoelectric shell force, as developed by Tzou [27] based on Love's equations:

$$\frac{\partial\left[\left(N_{11}^{m}-N_{11}^{e}\right)A_2\right]}{\partial\alpha_1}+\frac{\partial\left(N_{21}^{m}A_1\right)}{\partial\alpha_2}+N_{12}^{m}\frac{\partial A_1}{\partial\alpha_2}-\left(N_{22}^{m}-N_{22}^{e}\right)\frac{\partial A_2}{\partial\alpha_1}+$$

$$\left(Q_{13}^{m}-Q_{13}^{e}\right)A_1A_2\frac{1}{R_1}+A_1A_2(\sigma_{13}-e_{15}\overline{E}_1)\Big|_{-h/2}^{h/2}=\rho hA_1A_2\ddot{u}_1 \qquad (2.1)$$

$$\frac{\partial\left[\left(N_{22}^{m}-N_{22}^{e}\right)A_1\right]}{\partial\alpha_2}+\frac{\partial\left(N_{12}^{m}A_2\right)}{\partial\alpha_1}+N_{21}^{m}\frac{\partial A_2}{\partial\alpha_1}-\left(N_{11}^{m}-N_{11}^{e}\right)\frac{\partial A_1}{\partial\alpha_2}+$$

$$+\left(Q_{23}^{m}-Q_{23}^{e}\right)A_1A_2\frac{1}{R_2}+A_1A_2(\sigma_{23}-e_{25}\overline{E}_2)\Big|_{-h/2}^{h/2}=\rho hA_1A_2\ddot{u}_2 \qquad (2.2)$$

$$\frac{\partial\left[\left(Q_{23}^{m}-Q_{23}^{e}\right)A_1\right]}{\partial\alpha_2}+\frac{\partial\left[\left(Q_{13}^{m}-Q_{13}^{e}\right)A_2\right]}{\partial\alpha_1}-\left(N_{11}^{m}-N_{11}^{e}\right)\frac{A_1A_2}{R_1}-$$

$$\left(N_{22}^{m}-N_{22}^{e}\right)\frac{A_1A_2}{R_2}+A_1A_2(\sigma_{33}-e_{33}\overline{E}_3)\Big|_{-h/2}^{h/2}=\rho hA_1A_2\ddot{u}_3 \qquad (2.3)$$

where A_1, A_2 = Lamé parameters

α_1, α_2, α_3 = coordinate in 1st, 2nd, and 3rd direction as in Figure 2.1.

R_1, R_2 = radii of curvature

N^{m}_{ij} = mechanical membrane forces = $\int_{\alpha_3}\sigma_{ij}d\alpha_3$

N^{e}_{ij} = electrical membrane forces = $\int_{\alpha_3}e_{3j}\overline{E}_3d\alpha_3$

M^{m}_{ij} = mechanical bending moments = $\int_{\alpha_3}\sigma_{ij}\alpha_3d\alpha_3$

M^{e}_{ij} = electric bending moments = $\int_{\alpha_3} e_{3j}\bar{E}_3\alpha_3 d\alpha_3$

Q^{m}_{ij} = mechanical transverse shear forces = $\int_{\alpha_3} \sigma_{ij} d\alpha_3$

Q^{e}_{ij} = electrical transverse shear forces = $\int_{\alpha_3} e_{3j}\bar{E}_3 d\alpha_3$

e_{ij} = conventional mechanical stress

ρ = mass density of piezoelectric

h = piezoelectric thickness

$\bar{E}_j$ = electric field in i^{th} direction

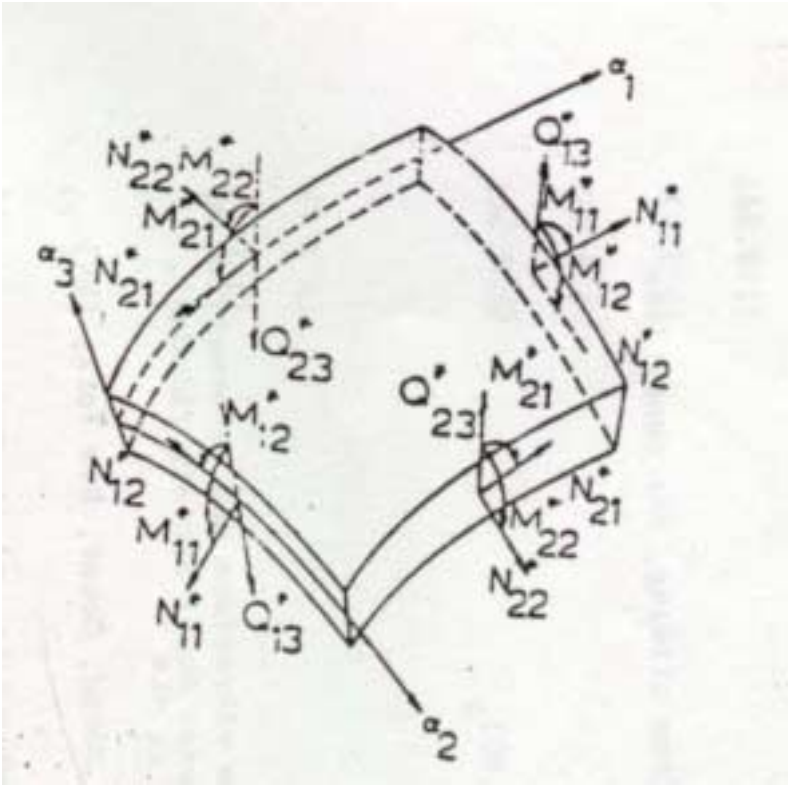

Figure 2.2. Generic piezoelectric shell with all its forces and moments [27]

For a thin piezoelectric shell, $\bar{E}_1 = \bar{E}_2 = 0$, leaving only $\bar{E}_3$. For thin piezoelectric plate, $A_1 = A_2 = 1$, $R_1 = R_2 = \infty$. This greatly reduces Equations (2.1) through (2.3).

$$\frac{\partial\left[\left(N_{xx}^{m}-N_{xx}^{e}\right)\right]}{\partial x}-\frac{\partial N_{yx}^{m}}{\partial y}=\rho h\ddot{u}_{x} \tag{2.4}$$

$$-\frac{\partial\left[\left(N_{yy}^{m}-N_{yy}^{e}\right)\right]}{\partial y}+\frac{\partial N_{xy}^{m}}{\partial x}=\rho h\ddot{u}_{y} \tag{2.5}$$

$$\frac{\partial Q_{x3}^{m}}{\partial x}+\frac{\partial Q_{y3}^{m}}{\partial y}+\left(\sigma_{33}-e_{33}\overline{E}_{3}\right)\Big|_{-h/2}^{h/2}=\rho h\ddot{u}_{3} \tag{2.6}$$

where $$Q_{x3}^{m}=\frac{\partial\left[\left(M_{xx}^{m}-M_{yy}^{e}\right)\right]}{\partial x}+\frac{\partial\left(M_{yx}^{m}\right)}{\partial y} \tag{2.7}$$

$$Q_{y3}^{m}=\frac{\partial\left[\left(M_{yy}^{m}-M_{xx}^{e}\right)\right]}{\partial y}+\frac{\partial\left(M_{xy}^{m}\right)}{\partial x} \tag{2.8}$$

The thin piezoelectric plate assumption also means that the displacements in the α_1 and α_2 directions vary linearly through the shell thickness, while displacement in the α_3 direction is independent of α_3.

The transverse displacement (and strain) is taken into consideration, i.e. Equation (2.6). The last factor on the left-hand side of Equation (2.6) can be neglected, resulting in

$$YI\nabla^{4}u_{3}(x,y,t)+\rho h\frac{\partial^{2}u_{3}(x,y,t)}{\partial t^{2}}=p(x,y,t) \tag{2.9}$$

where $\nabla^{4}(\bullet)=\nabla^{2}\nabla^{2}(\bullet)$ = Laplacian operator (2.10)

$$\nabla^{2}(\bullet)=\frac{1}{A_{1}A_{2}}\left[\frac{\partial(\bullet)}{\partial\alpha_{1}}\left(\frac{A_{2}}{A_{1}}\frac{\partial(\bullet)}{\partial\alpha_{1}}\right)+\frac{\partial(\bullet)}{\partial\alpha_{2}}\left(\frac{A_{1}}{A_{2}}\frac{\partial(\bullet)}{\partial\alpha_{2}}\right)\right] \tag{2.11}$$

A_1, A_2 = Lamé parameters in 1st and 2nd direction

α_1, α_2 = coordinate in 1st and 2nd direction

YI = bending stiffness

$$= \frac{Yh^{3}}{12(1-\mu^{2})}$$

Y = Young modulus

I = inertia

μ = Poisson ratio

p(x,y,t) = force acting on x-y plane

h = thickness of plate

For a plate in a cartesian coordinate system,

A_1, A_2 = 1,

α_1, α_2 = x, y,

$$\nabla^2(\bullet) = \frac{\partial^2(\bullet)}{\partial x^2} + \frac{\partial^2(\bullet)}{\partial y^2} \tag{2.12}$$

Substitution into equation (2.9) results

$$YI\left[\frac{\partial^4 u_3(x,y,t)}{\partial x^4} + 2\frac{\partial^4 u_3(x,y,t)}{\partial^2 x.\partial^2 y} + \frac{\partial^4 u_3(x,y,t)}{\partial y^4}\right] + \rho h \frac{\partial^2 u_3(x,y,t)}{\partial t^2} = p(x,y,t) \tag{2.13}$$

Assume that $u_3(x,y,t)$ and p(x,y,t) are divided into two parts, the time-dependant part and spatially-dependant part, each is independent from the other.

$$u_3(x,y,t) = U_3(x,y)\, U_3(t) \tag{2.14}$$

$$p(x,y,t) = P(x,y)\, P(t) \tag{2.15}$$

Substituting into equation (2.13) results in

$$YI\left[\frac{\partial^4 U_3(x,y)}{\partial x^4} + 2\frac{\partial^4 U_3(x,y)}{\partial^2 x.\partial^2 y} + \frac{\partial^4 U_3(x,y)}{\partial y^4}\right] U_3(t) + \rho h \frac{\partial^2 U_3(t)}{\partial t^2} U_3(x,y) = P(x,y) P(t) \tag{2.16}$$

There are numerous ways to find the solution for Equation (2.16). One method is presented here, as is presented in more detail by Tzou [27]. The time-dependent part of $u_3(x,y,t)$ can be represented as

$$U_3(t) = e^{j\omega t} \tag{2.17.a}$$

$$P(t) = e^{j\omega t} \tag{2.17.b}$$

Thus Equation (2.16) becomes

$$YI\left[\frac{d^4U_3(x,y)}{dx^4}+2\frac{d^4U_3(x,y)}{d^2xd^2y}+\frac{d^4U_3(x,y)}{dy^4}\right]e^{j\omega t}+\rho h\omega^2U_3(x,y)e^{j\omega t}=P(x,y)e^{j\omega t} \quad (2.18)$$

Assume that there is no displacement at y-axis (i.e. the plate is reduced to a beam in x-axis). This will make all the derivations with respect to y direction zero. First, the general solution is found

$$YI\frac{d^4}{dx^4}U_3(x)+\rho h\omega_x^2U_3(x)=0 \quad (2.19)$$

Then

$$\frac{d^4U_3(x)}{dx^4}+\lambda^4U_3(x)=0 \quad (2.20)$$

$$\text{where } \lambda^4=\frac{\rho h\omega^2}{YI} \quad (2.21)$$

The natural frequency is given as

$$\omega_x=\sqrt{\frac{YI}{\rho h}}\lambda^2 \quad (2.22)$$

Taking Laplace transform of Equation (2.12) results in

$$s^4U_3(s)-s^3U_3(0)-s^2U_3'(0)-sU_3''(0)-U_3'''(0)-\lambda^4U_3(s)=0 \quad (2.23)$$

Solving for U_3 generates

$$U_3(s)=\frac{1}{s^4-\lambda^4}[s^3U_3(0)+s^2U_3'(0)+sU_3''(0)+U_3'''(0)] \quad (2.24)$$

Applying the inverse Laplace transform results in

$$U_3(x)=A(\lambda x)U_3(0)+\frac{B(\lambda x)}{\lambda}U_3'(0)+\frac{C(\lambda x)}{\lambda^2}U_3''(0)+\frac{D(\lambda x)}{\lambda^3}D(\lambda x)U_3'''(0) \quad (2.25)$$

$$\text{where } A(\lambda x)=\frac{1}{2}(\cosh\lambda x+\cos\lambda x) \quad (2.26.a)$$

$$B(\lambda x) = \frac{1}{2}(\sinh \lambda x + \sin \lambda x) \quad (2.26.b)$$

$$C(\lambda x) = \frac{1}{2}(\cosh \lambda x - \cos \lambda x) \quad (2.26.c)$$

$$D(\lambda x) = \frac{1}{2}(\sinh \lambda x - \sin \lambda x) \quad (2.26.d)$$

$U_3(x)$ is the natural mode, $U_3'(x)$ corresponds to slope, $U_3''(x)$ corresponds to moment, and $U_3'''(x)$ corresponds to the shear force. Deriving the above equation gives the following equations

$$U_3'(x) = \lambda D(\lambda x)U_3(0) + A(\lambda x)U_3'(0) + \frac{B(\lambda x)}{\lambda}U_3''(0) + \frac{C(\lambda x)}{\lambda^2}U_3'''(0) \quad (2.27.a)$$

$$U_3''(x) = \lambda^2 C(\lambda x)U_3(0) + \lambda . D(\lambda x)U_3'(0) + A(\lambda x)U_3''(0) + \frac{B(\lambda x)}{\lambda^2}U_3'''(0) \quad (2.27.b)$$

$$U_3'''(x) = \lambda^3 B(\lambda x)U_3(0) + \lambda^2 C(\lambda x)U_3'(0) + \lambda D(\lambda x)U_3''(0) + A(\lambda x)U_3'''(0) \quad (2.27.c)$$

A matrix of equations can be set up based on the above equations

$$\begin{bmatrix} A(\lambda x) & \frac{B(\lambda x)}{\lambda} & \frac{C(\lambda x)}{\lambda^2} & \frac{D(\lambda x)}{\lambda^2} \\ \lambda D(\lambda x) & A(\lambda x) & \frac{B(\lambda x)}{\lambda} & \frac{C(\lambda x)}{\lambda^2} \\ \lambda^2 C(\lambda x) & \lambda D(\lambda x) & A(\lambda x) & \frac{B(\lambda x)}{\lambda} \\ \lambda^3 B(\lambda x) & \lambda^2 C(\lambda x) & \lambda D(\lambda x) & A(\lambda x) \end{bmatrix} \begin{bmatrix} U_3(0) \\ U_3'(0) \\ U_3''(0) \\ U_3'''(0) \end{bmatrix} = \begin{bmatrix} U_3(x) \\ U_3'(x) \\ U_3''(x) \\ U_3'''(x) \end{bmatrix} \quad (2.28)$$

To solve this set of equations, the boundary conditions are needed. By assuming that the plate is simply-simply supported, the boundary conditions are

$U_3(0) = 0$, $U_3''(0) = 0$,

$U_3(L) = 0$, $U_3''(L) = 0$,

$U_3'(0) \neq 0$, $U_3'''(0) \neq 0$,

$U_3'(L) \neq 0$, $U_3'''(L) \neq 0$,

where L is the length of the plate.

Substitute these set of equations into Equation (2.28)

$$\begin{bmatrix} A(\lambda L) & \frac{B(\lambda L)}{\lambda} & \frac{C(\lambda L)}{\lambda^2} & \frac{D(\lambda L)}{\lambda^3} \\ \lambda D(\lambda L) & A(\lambda L) & \frac{B(\lambda L)}{\lambda} & \frac{C(\lambda L)}{\lambda^2} \\ \lambda^2 C(\lambda L) & \lambda D(\lambda L) & A(\lambda L) & \frac{B(\lambda L)}{\lambda} \\ \lambda^3 B(\lambda L) & \lambda^2 C(\lambda L) & \lambda D(\lambda L) & A(\lambda L) \end{bmatrix} \begin{bmatrix} 0 \\ U_3' \\ 0 \\ U_3'''(0) \end{bmatrix} = \begin{bmatrix} 0 \\ U_3'(L) \\ 0 \\ U_3'''(L) \end{bmatrix} \tag{2.29}$$

Simplifying the equations

$$\begin{bmatrix} \frac{B(\lambda L)}{\lambda} & \frac{D(\lambda L)}{\lambda^3} \\ \lambda D(\lambda L) & \frac{B(\lambda L)}{\lambda} \end{bmatrix} \begin{bmatrix} U_3'(0) \\ U_3'''(0) \end{bmatrix} = \begin{bmatrix} 0 \\ 0 \end{bmatrix} \tag{2.30}$$

This is a non-trivial equation, so the determinant of the first matrix has to be zero. This will lead to characteristic equation of the matrix

$$B^2(\lambda L)-D^2(\lambda L) = 0 \tag{2.31}$$

Using Equation (2.26.b) and (2.26.d), Equation (2.31) can be simplified to

$$\sinh(\lambda L)\sin(\lambda L) = 0 \tag{2.32}$$

The solution for Equation (2.32) is

$$U_{3m}(x) = \sum_{m=1}^{\infty} \sin\frac{m\pi x}{L_x} \tag{2.33}$$

The same result can be generated for displacement in the y-direction (by considering no displacement in x-axis)

$$U_{3n}(y) = \sum_{n=1}^{\infty} \sin\frac{n\pi y}{L_y} \tag{2.34}$$

The total general solution is gained by multiplying x- and y-axis solutions.

$$U_3(x,y) = \sum_{m=1}^{\infty}\sum_{n=1}^{\infty}\sin\frac{m\pi x}{L_x}\sin\frac{n\pi y}{L_y} \tag{2.35}$$

Now the response to electron flux can be found. The modal response to the external forces (i.e. electron flux) can be represented by

$$u_k(x,y) = \sum_{k=1}^{\infty}\eta_k(t)U_k(x,y) \tag{2.36}$$

where $\eta_k(t)$ = modal participation factor

$$= \frac{F_k^*}{\omega_k^2} \tag{2.37}$$

$$F_k^* = \frac{\sum_{j=1}^{3}\int_0^W\int_0^L q_j U_{jk}\,dxdy}{\rho h N_k} \tag{2.38}$$

$$N_k = \int_0^W\int_0^L\sum_{j=1}^{3}U_{jk}^2\,dxdy \tag{2.39}$$

Again, only the static part of the equation is considered, so q_j is not time dependent. The trace of electron beam on the plate surface can be considered as a constant point load, so

$$q_k = \Pi.\delta(x-x^*)\,\delta(y-y^*) \tag{2.40}$$

Π = charge build-up when the electrons hit the plate, determined from the experiments.

x*,y* = the point/points where p applies

Substituting Equation (2.40) to (2.38) results in

$$F_k^* = \frac{\Pi}{\rho h N_k}U_{3k}(x^*,y^*) \tag{2.41}$$

$$\eta_k(x,y,t) = \frac{F_k^*}{\omega_k^2\sqrt{\left(1-\left(\frac{\omega}{\omega_k}\right)^2\right)^2 + 4\xi_k^2\left(\frac{\omega}{\omega_k}\right)^2}} \tag{2.42}$$

$$= \frac{F_k^*}{\omega_k^2} \text{ since } \omega = 0 \tag{2.43}$$

and the total solution for the static part is obtained

$$u_k = \sum_{k=1}^{\infty} \eta_k(x,y,t) U_k(x,y) \tag{2.44}$$

The largest strain response should be located directly under the electron flux. To visualize this more thoroughly, a simulation of a piezoelectric plate with dimensions 7.5 cm x 5 cm x 0.1975 cm is presented. The beam effect is represented a round area of electric field $\bar{E} = 76 \times 10^3$ V/m with area of 10 mm^2 applied through the plate thickness. The plate is considered to be simply-simply supported. The material is a PZT5h, whose properties are extracted from Morgan Matroc Piezoelectric Manual [28]

$\rho = 7500$ kg/m^3;

$Y = 48$ GPa

$\mu = 0.31$

$d_{31} = -274 \times 10^{12}$ m/v

Substituting the constants for PZT5h to Equations (2.36) to (2.42), the strain response from the plate of piezoelectric material exposed to an electric field can be simulated. It can be seen from the result on Figure 2.3 that the highest displacement is in the area where the electric field is applied, i.e. 1 cm^2 in the middle of the plate. The Matlab code for this simulation can be found in Appendix C1.

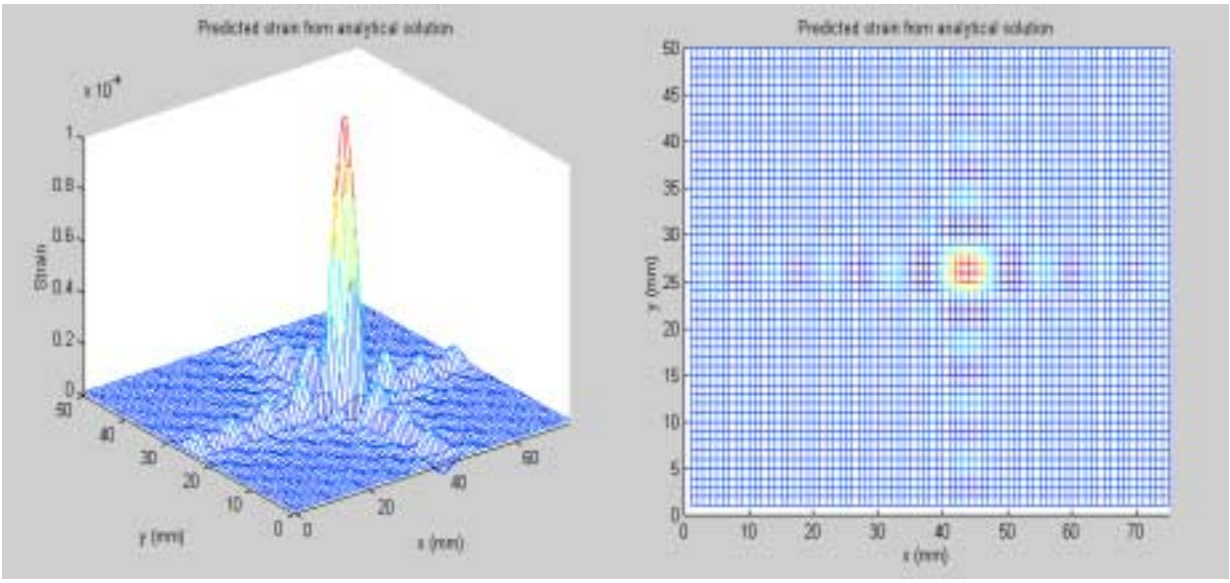

(a) (b)

Figure 2.3. Spatial response from piezoelectric plate exposed to an applied electric field: (a) in 3-D, (b) in 2-D

Finite Element Approach

The relationships between the mechanical and electrical aspects of piezoelectric material are

$$T = [c]S - [e]\bar{E} \tag{2.45}$$

and

$$D = [\in]\bar{E} + [e]S \tag{2.46}$$

where T = stress tensor

S = strain

D = electric flux density

$\bar{E}$ = electric field

[c] = elastic constant matrix

[e] = piezoelectric constant matrix

[$\in$] = dielectric constant matrix

In the Finite Element approach [27,29], piezoelectricity can be divided into mechanical and electrical components. From the mechanical standpoint, strain tensor is determined by the spatial gradient of mechanical displacement, i.e.

$$S_{ij} = \frac{1}{2}\left(u_{i,j} + u_{j,i}\right) \tag{2.45}$$

$$\text{where } u_{i,j} = \frac{\partial u_i}{\partial x_j} \tag{2.46}$$

Traction tensor T_i is defined by the mechanical interaction between 2 portions of the continuum separated by a surface

$$T_i = \frac{F_i}{S} \tag{2.47}$$

The stress tensor is defined by

$$T_{ij} = \frac{T_j}{n_i} \tag{2.48}$$

where n_i is the component of the outwardly directed unit normal to the surface across which the traction vector acts.

From electrical standpoint, the electric field intensity and electric displacement are related by

$$D_i = \in_0 \bar{e}_i + P_i \tag{2.49}$$

where D_i = electric displacement

$\in_0$ = permitivity of free space = 8.854 x 10^{-12} F/m

$\bar{e}_i$ = electric field intensity

P_i = components of polarization vector

Using the law of thermodynamics, the conservation energy between the mechanical and electrical components can be represented as

$$\dot{U} = T_{ij}\dot{S}_{ij} + \overline{E}_i\dot{D}_i \tag{2.50}$$

where U is the total energy density for the piezoelectric continuum. The electric enthalpy density H is defined by

$$H = U - \bar{E}_i D_i \tag{2.51}$$

Substituting Equation (2.52) into (2.53) results in

$$\dot{H} = T_{ij}\dot{S}_{ij} - D_i\dot{\overline{E}}_i \tag{2.52}$$

In linear piezoelectric theory H can be written as

$$H = \frac{1}{2}c^E_{ijkl}S_{ij}S_{kl} - e_{kij}E_kS_{ij} - \frac{1}{2}\in^S_{ij}\overline{E}_i\overline{E}_j \tag{2.53}$$

where c^E_{ijkl} = elastic constant

e_{kij} = piezoelectric constant

$\in^S_{ij}$ = dielectric constant

The piezoelectric constitutive equations can then be represented by

$$T_{ij} = c^E_{ijkl}S_{kl} - e_{kij}E_k \tag{2.54}$$

$$D_i = e_{ikl}S_{kl} + \in^S_{ij} E_k \tag{2.55}$$

where $c_{ijk} = \begin{bmatrix} c_{11} & c_{12} & c_{13} & 0 & 0 & 0 \\ c_{12} & c_{11} & c_{13} & 0 & 0 & 0 \\ c_{13} & c_{13} & c_{33} & 0 & 0 & 0 \\ 0 & 0 & 0 & c_{44} & 0 & 0 \\ 0 & 0 & 0 & 0 & c_{44} & 0 \\ 0 & 0 & 0 & 0 & 0 & c_{66} \end{bmatrix}$

$e_{kij} = \begin{bmatrix} 0 & 0 & 0 & 0 & e_{15} & 0 \\ 0 & 0 & 0 & e_{15} & 0 & 0 \\ e_{31} & e_{31} & e_{33} & 0 & 0 & 0 \end{bmatrix}$

$\in^s_{ij} = \begin{bmatrix} \in_{11} & 0 & 0 \\ 0 & \in_{11} & 0 \\ 0 & 0 & \in_{33} \end{bmatrix}$

Rearranging Equations (2.54) and (2.55) to get strain expression results in the following equations

$$S_{ij} = s^{E}_{ijkl} T_{kl} + d_{kij} E_k \tag{2.56}$$

$$D_i = d_{ikl} T_{kl} + \in^{T}_{ik} E_k \tag{2.57}$$

For specific structures these equations can be solved with Finite Element Method using Ansys56. The coefficients $c^{E}_{ijkl}, e_{kij}, \in_{ij}$ are found in the Morgan Matroc Piezoelectric Manual [28]. Substituting these constants to Equations (2.56) and (2.57), and running an ANSYS® program for the same conditions as the analytical solution presented previously, the results shown in Figure 2.4 are obtained for the 1-direction strain due to the spot excitation. Again, the highest strain can be found in the area directly under the applied electric field, while the rest of the area remains low in strain. The Ansys code file can be found in Appendix B.

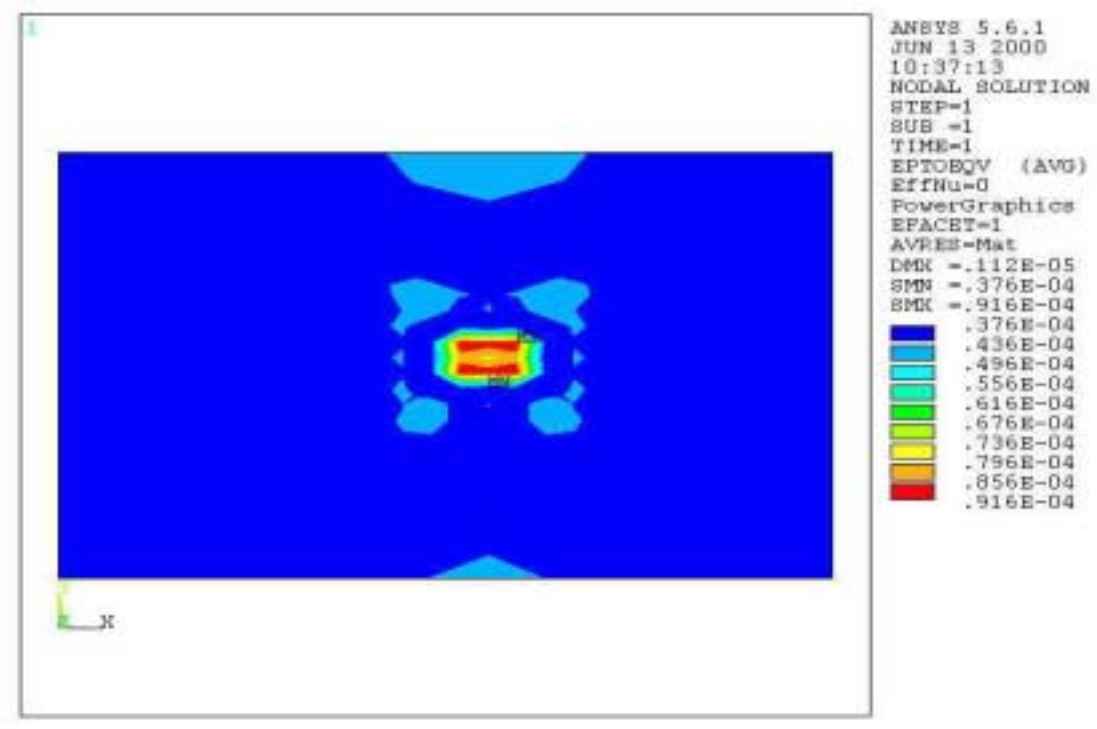

Figure 2.4. ANSYS® solution for static strain of piezoelectric material

CHAPTER THREE
EXPERIMENTAL SETUP AND SENSITIVITY ANALYSIS

The first part of this chapter contains a detailed view of the experiment setup. A complete description of specimen preparation is presented. Brief information of each of the component of the setup is also presented. The second part explains a sensitivity experiment, purposed to see the sensitivity of the material to the distance between the material and the source of excitation (i.e. electron gun).

Experimental Setup

The test specimen is a rectangular PZT-5H plate (length 7.5 cm, width 5 cm, and thickness 1.975 mm) purchased from Morgan Matroc Inc. The plate was procured from the manufacturer with silver electrodes distributed on both sides, as can be seen in Figure 3.1.a. The manufacturer denoted the positive side by a small dot on one of the edge. The positive electrode was removed with a combination of swabbing with nitric acid and light sanding to reveal the dielectric piezoelectric material as a target for the electron beam, Figure 3.1.b.

The negative surface is cleansed with isopropyl alcohol to remove grease and dirt. Sixteen Measurement Group strain gages are attached atop the negative electrode using M-Bond 200 catalyst and adhesive, Figure 3.1.c. These strain gages have 350 Ω resistance with 0.3% tolerance, 2.095 gage factor with 0.5% tolerance, and are arranged in 4x4 matrix, Figure 3.1.d. The gages' numbering is presented in Figure 3.1.e.

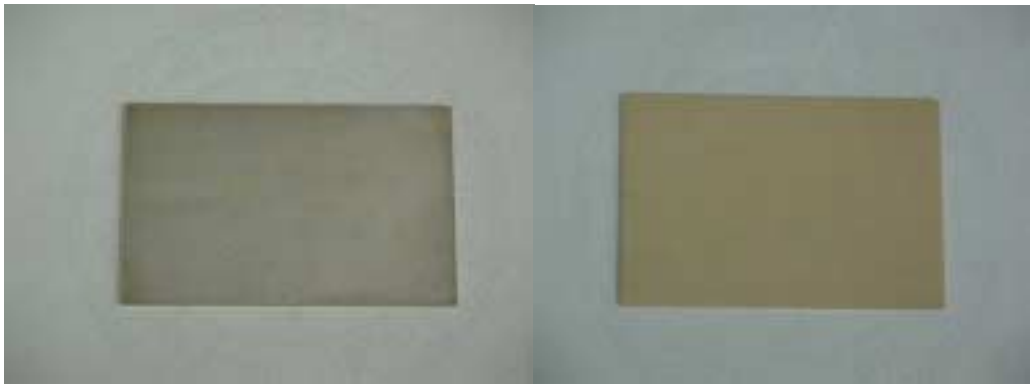

a. b.

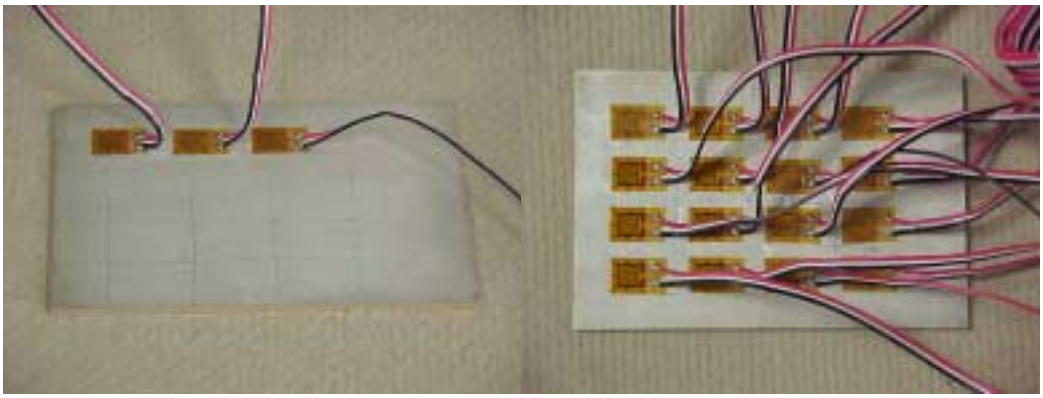

c. d

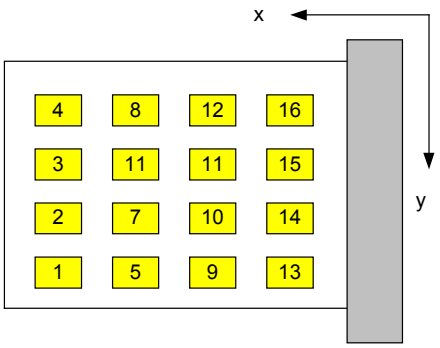

e.

Figure 3.1. Test specimen: a. PZT5h with electrode on both surface
b. PZT5h with electrode on positive surface removed
c. Strain gages are attached to the negative surface
d. PZT5h with all strain gages
e. Strain gage numbering and axis

The positive (stripped) side of piezoelectric plate is oriented toward a Kimball Physics EFG-7 electron gun, which is designed as a flood gun. This means that it is designed to distribute the electron flux over a wide angle. The negative (electroded) side of the piezoelectric plate is connected to a power amplifier to allow the potential of the electrode to be controlled, which subsequently will be called backpressure voltage (V_b). The experimental protocol required the apparatus to be enclosed in a vacuum chamber and exposed to a vacuum condition, $2x10^{-7}$ torr (mm Hg). A sketch of the standard experimental setup is included as Figure 3.2. The schematic of the vacuum chamber can be found in Appendix A.

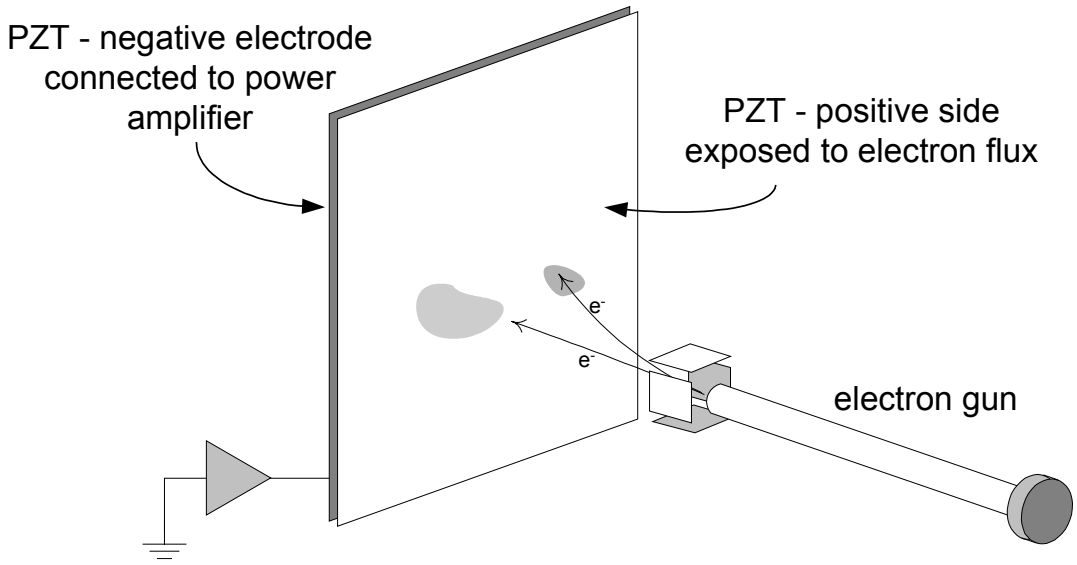

Figure 3.2. Standard experiment setup.

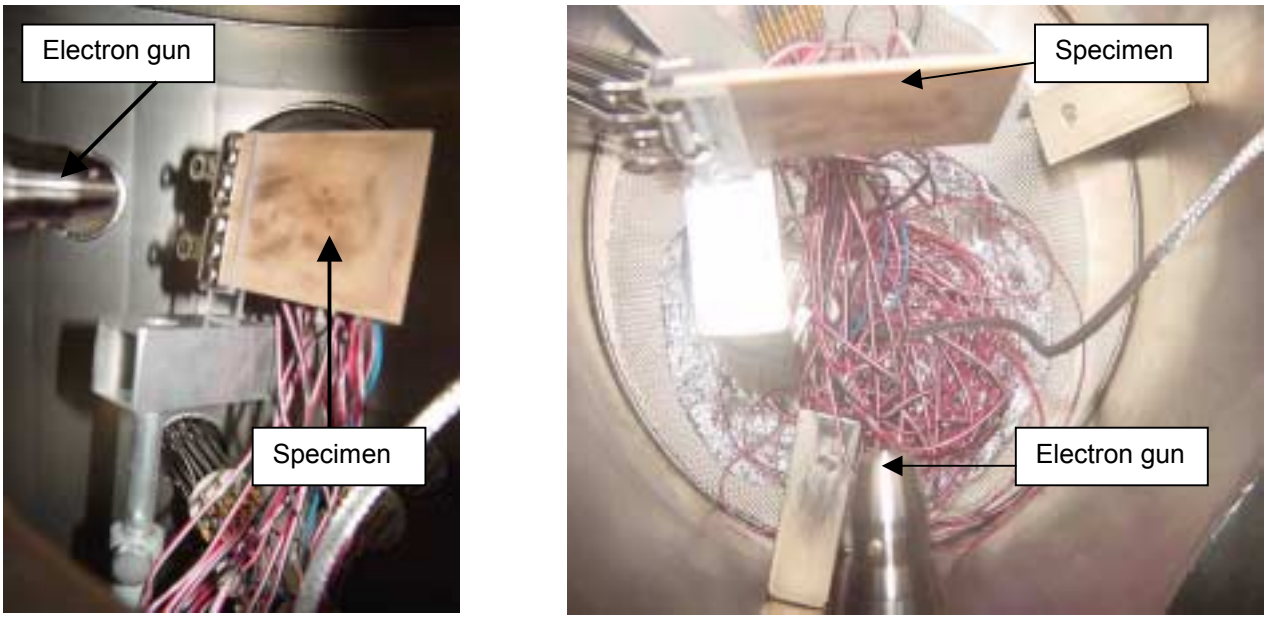

Figure 3.3. Specimen and electron gun position in vacuum chamber

Sensitivity Analysis

This experiment is designed to investigate the effect of specimen location in the vacuum chamber on the strain response to the electron flux. The plate is removed from initial charge and strain by shaking and rubbing both surfaces. Then the plate is placed in a vacuum chamber and exposed to vacuum condition. This condition is considered to be zero strain absolute. The plate is first placed 5 cm from the electron gun. The negative surface electrode is connected to ground while the positive surface is hit by a flood electron beam (all areas received the same intensity of beam) with 400 eV energy, 60 μA emission current. The resulting strain is considered to be the zero strain relative. All subsequent strains are measured from this condition. Then the backpressure voltage is varied sinusoidally at 20 mHz, 200 V peak-to-peak amplitude. The procedure was repeated for various distance from the electron gun: 7.5 cm, 10 cm, and 17.78 cm, as is seen in Figure 3.4.

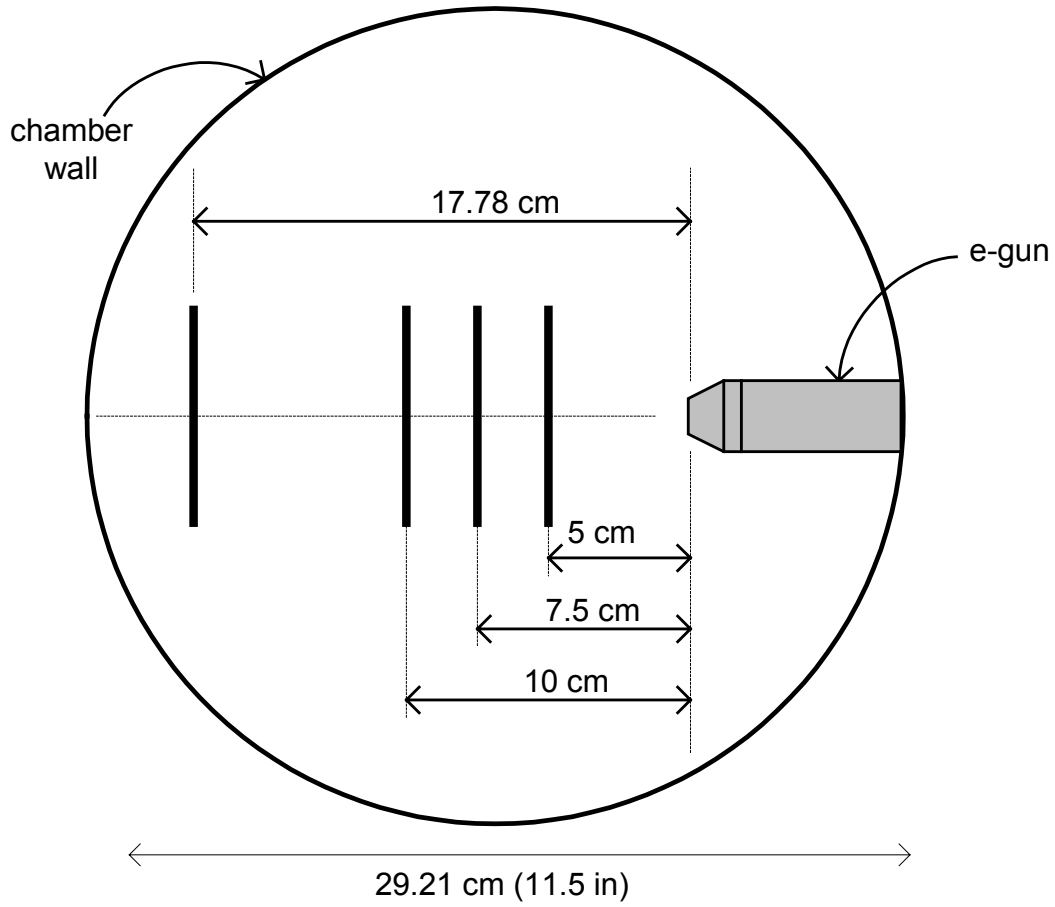

Figure 3.4. Various plate positions in vacuum chamber

The zero absolute state ascends to zero relative when the electron gun is fired at the charge-and-strain free plate as shown in Figure 3.5. The magnitudes of 7.5 and 17.8 cm appear to stabilize at approximately 6 microstrain. The magnitude of 5 cm tends to drift back to 0 microstrain. The magnitude of 10 cm tends to stabilize at approximately 9.5 microstrain. There does appear to be a dependence of position on the initial strain, but it does not seem to be simple.

The strain is plotted against the sinusoidal backpressure voltage to build a hysteresis plots, Figure 3.6. The calculated slope for each distance is obtained through linear regression method and is plotted in black. It shows that the slope becomes steeper as the distance increases, i.e. the strain becomes more sensitive to potential change. The calculated slopes are plotted together in Figure 3.7.

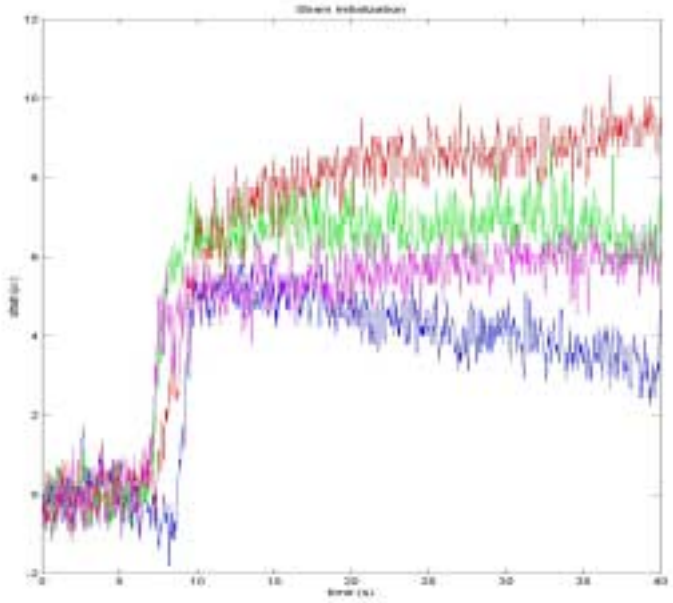

Figure 3.5. Initial strain increase from zero absolute to zero relative
Blue: 5 cm from the plate
Magenta: 7.5 cm from the plate
Red: 10 cm from the plate
Green: 17.78 from the plate

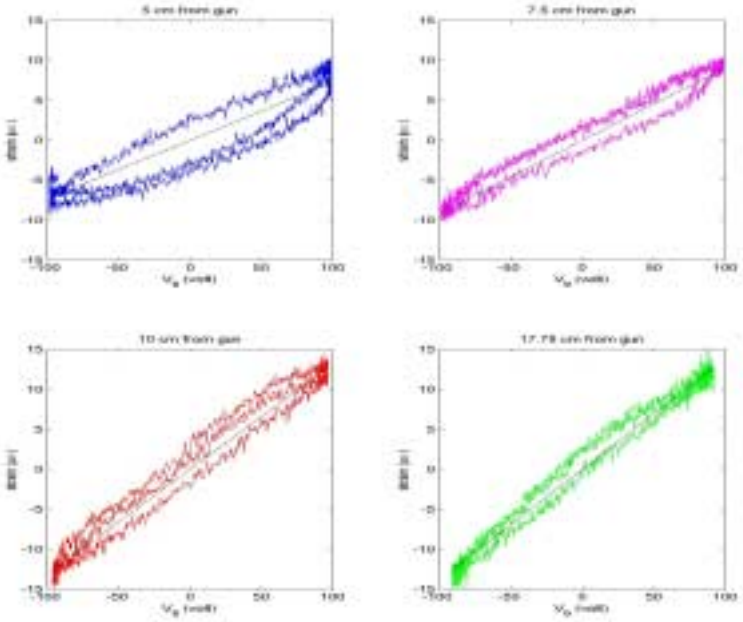

Figure 3.6. Hysteresis plots of various distance from the gun

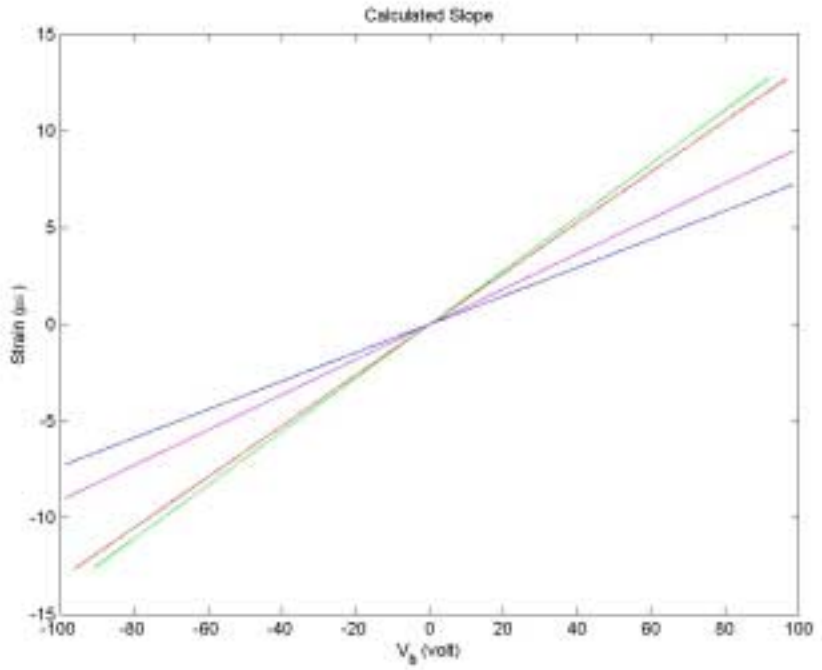

Figure 3.7. Calculated slope using linear regression method
Blue: 5 cm from the plate
Magenta: 7.5 cm from the plate
Red: 10 cm from the plate
Green: 17.78 from the plate

Table 3.1. Calculated Slope and Coefficient of Correlation for each Distance

	Distance from the Gun			
	5 cm	7.5 cm	10 cm	17.78 cm
Slope	1.4673	1.8124	2.6287	2.7707
Correlation (R)	0.9832	0.9832	0.9858	0.991

When the plate is 5 cm away from the gun, the secondary electrons are far from the chamber walls which act as the electron collector. This makes the strain development in the plate relatively difficult, as noted by the moderate slope and big phase lag on Figure 3.6, blue plot. As the plate is placed farther away from the gun, it becomes easier for the secondary electrons to reach the chamber wall. There is a better electron flow, so the plate becomes more sensitive (the slope becomes steeper and the phase lag decreases).

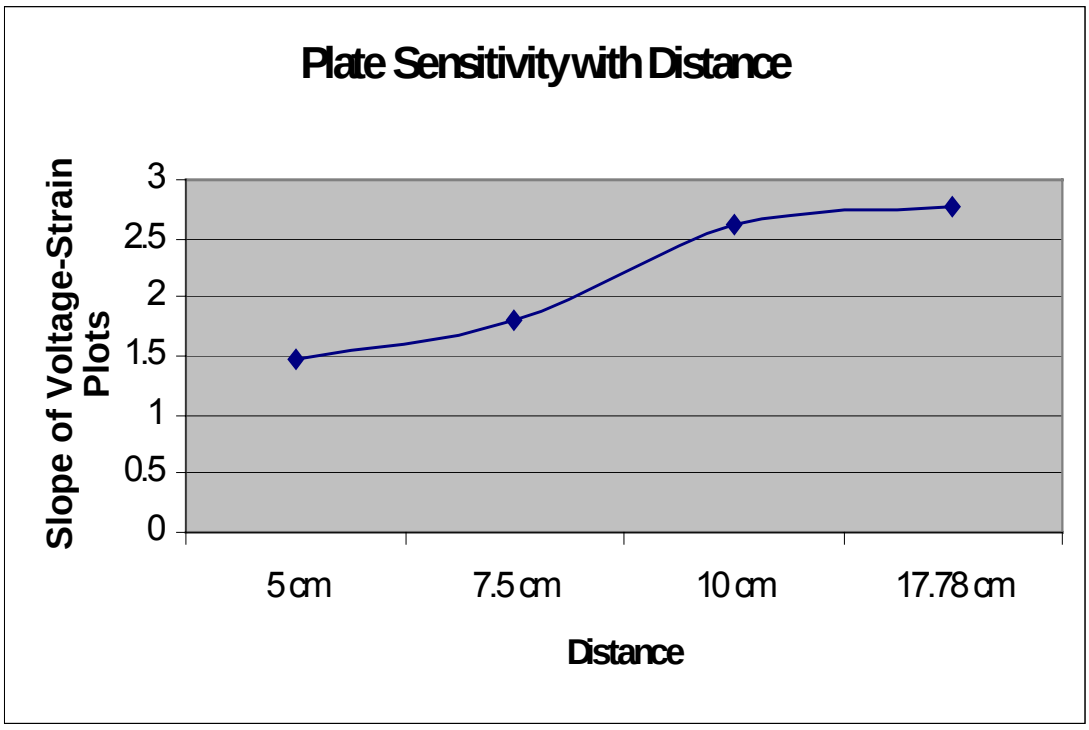

Figure 3.8. Plot of slope of hysteresis against distance of the plate from the gun

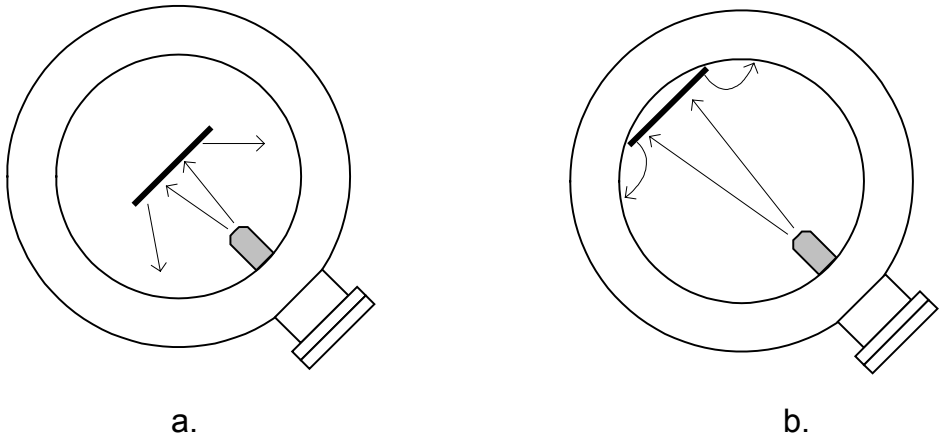

Figure 3.9. Electron flows in various distances:
a. Far from the walls (poor collector)
b. Close to the walls (better collector)

CHAPTER FOUR
INVESTIGATION OF ELECTRON CURRENT THROUGH PIEZOELECTRIC MATERIAL UNDER ELECTRON FLUX EXCITATION

This chapter describes an experiment developed to investigate the electron transport through piezoelectric materials subjected to an electron flux. Electron current on the positive side is provided by the electron gun, and electron current on the negative side is measured by the pico-ampere meter, as shown on the picture below.

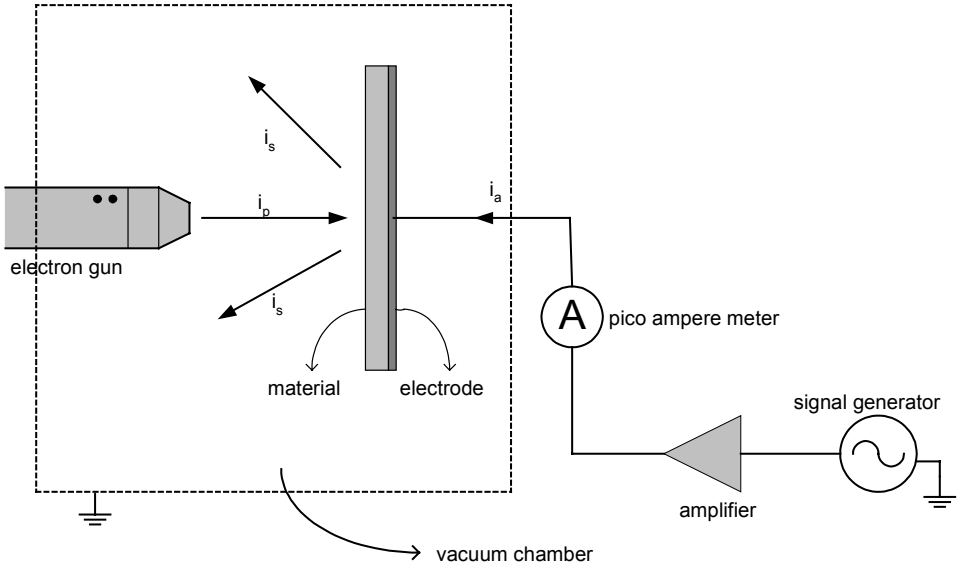

Figure 4.1. Experimental setup.

In Figure 4.1 i_p is the primary electron current, i_s is the secondary electron current, i_a is the electron current through the electrode lead. Charge conservation demands that the three currents are related by

$$i_a = i_s - i_p \tag{4.1}$$

when the system is at equilibrium.

The electron gun is used to control the potential at a given point on the bare ceramic surface, or positive surface (V_s). The power amplifier controls the potential on the negative surface (V_b). The electric field applied on the plate is given by the relationship

$$\bar{E} = \frac{V_b - V_p}{h} \tag{4.2}$$

where $\bar{E}$ = electric field across the plate,

V_p = potential on positive surface,

V_b = the potential on negative surface (backpressure voltage),

h = piezoelectric thickness.

In piezoelectric materials electric field is coupled to stress and strain ($\in$). The simple relationships

$$T = cS - e\bar{E} \tag{2.45}$$

and

$$D = \in \bar{E} + eS \tag{2.46}$$

result when the material is free to change dimensions under the influence of the electric field. In this relationship d_{31} is the piezoelectric constant, which is equal to -274 x 10^{-12} m/volt for PZT5h. Strains are controlled in piezoelectric materials using a power amplifier to control the potential of the single electrode on one side of the plate and the electron gun to control the potential at selected spots on the other side of the plate.

In this experiment the strain and current responses of a piezoelectric plate subjected to an electron flux are examined under a range of conditions. As before, strains were recorded at 16 locations using strain gages bonded to the single electrode. A 24-channel strain gage data acquisition system was used to record all of the strain signals simultaneously when the various inputs were applied to the plate.

The experimental apparatus enabled control of a variety of variables for this series of experiments. The electron gun emission current was kept constant at approximately 60 microampere and the beam electrons had energy of 400 eV. The relationship between emission current and beam current (ip) is illustrated in Figure 4.14. The electron gun used in these experiments is a Kimball Physics EFG-7. The current

flowing to or from the electrode was measured using Keithley 485 pico-ampere meter, which can measure currents from 2 nA to 2 mA. The sample is placed approximately 10 cm from the electron gun, referring to Chapter III. The positive output of the power amplifier is connected to the negative ground of pico-ampere meter. This means that a positive reading on the meter denotes an electron flow from the power amplifier to the plate, as shown in Figure 4.1. The pico-ampere meter was run on battery power and a high common-mode voltage rejection circuit [30] was placed between the ammeter and the data acquisition unit to allow the ammeter to function over the entire voltage range.

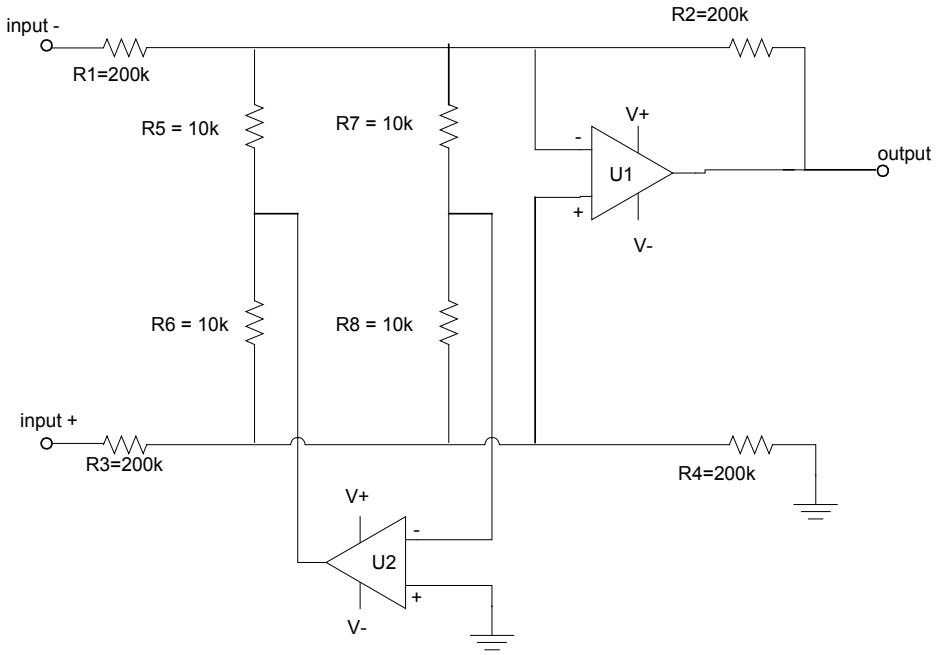

Figure 4.2. High common mode voltage rejection circuit.

The piezoelectric plate with all the strain gages was placed into a vacuum chamber, 10 cm from the tip of the electron gun. The air was then pumped out until the vacuum inside reached $3x10^{-7}$ torr (mm Hg). The first data taken measures the absolute zero. Setting the electrode potential, or backpressure voltage (V_b), as ground, the electron beam was applied to the entire plate. The resulting strain measurements show an initial ramp of strain from zero absolute to about 15 microstrain then a slow drift until it reaches 20 microstrain, as can be seen in Figure 4.3. The strain will not go down to

zero absolute until the air is allowed back into the chamber, so for the next experiments the zero condition is measured from this level new (zero relative).

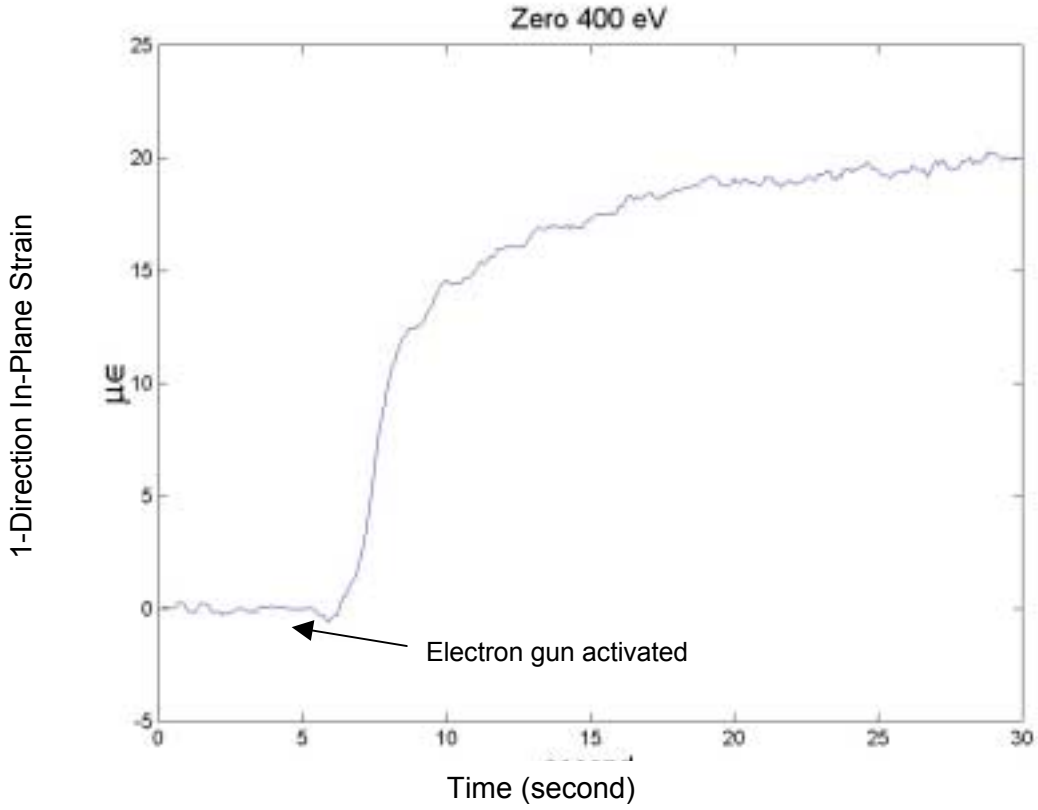

Figure 4.3. Zero absolute and zero relative strain.

During the process the electron current (i_a) is also measured. As can be seen from Figure 4.4, the amount of current that flows during this initial illumination is about -0.1 microampere. As the electrons hit the neutral plate, they quickly form 'hole-electron' pairs and reside on the plate as neutral charges. Thus only a small number of electrons flow through the plate to the ampere meter. When the gun is turned off, the strain drops only a couple of microstrain, but the electrode current goes back to zero.

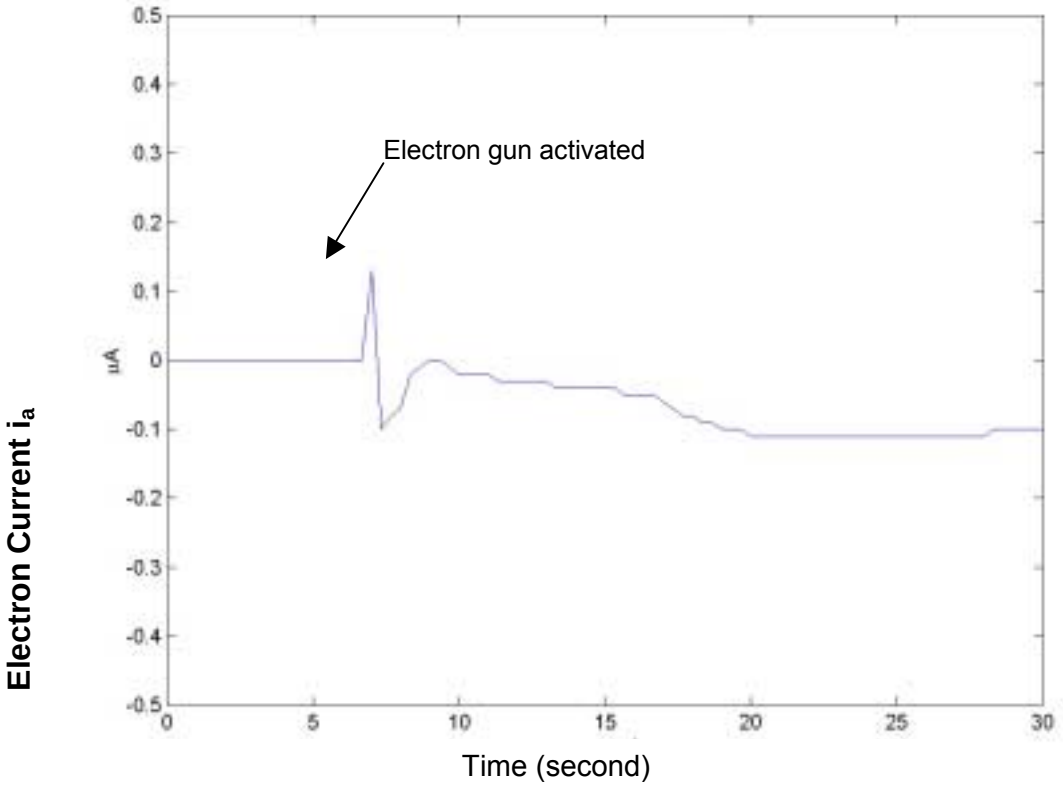

Figure 4.4. Electron current (i_a) at zero abolute and zero relative.

Quasi-Static Strain Response

Three sets of data are presented in the following figures. Only a single strain trace is shown in each figure since conditions are uniform at all locations on the plate: the electron beam floods the entire bare face of the piezoelectric and only single electrode covers the negative face. The strain traces were measured in-plane and the positive sign on the current traces indicates flow of conventional current from the electrode to the power amplifier. V_b was varied slowly using a sine wave with 20 mHz frequency and 200 volt peak-to-peak with various DC offsets to examine the strain and current response of the system.

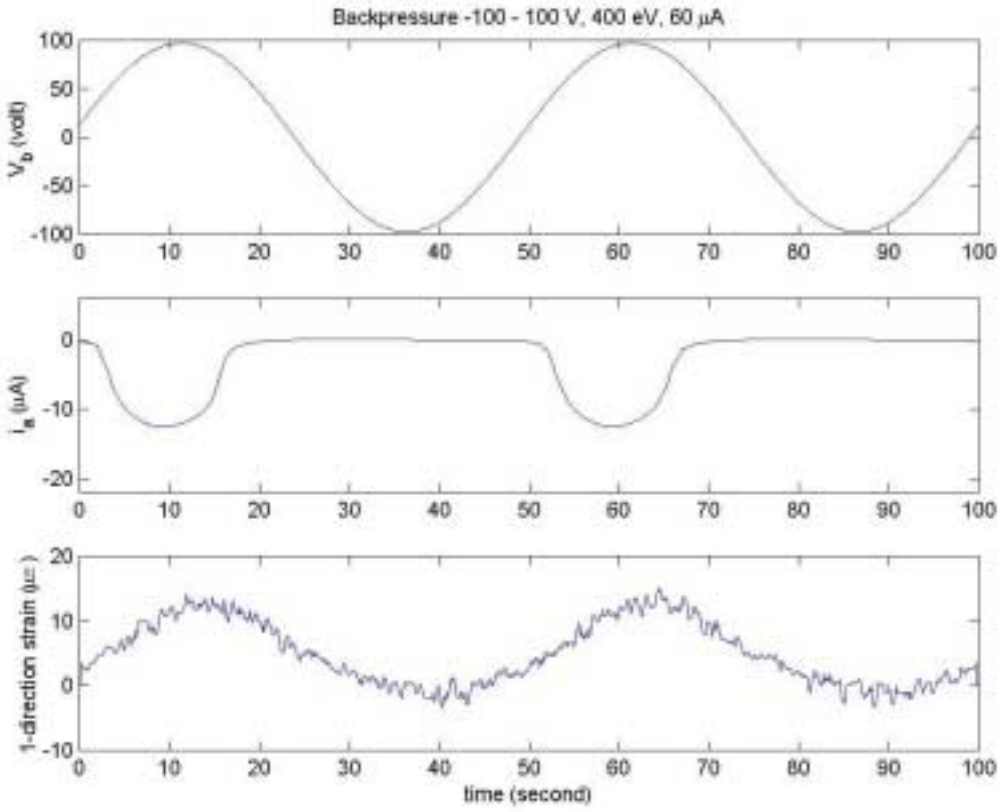

Figure 4.5. Time histories of strain and current output due to a 200V p-p, 0 DC volt offset V_b input.

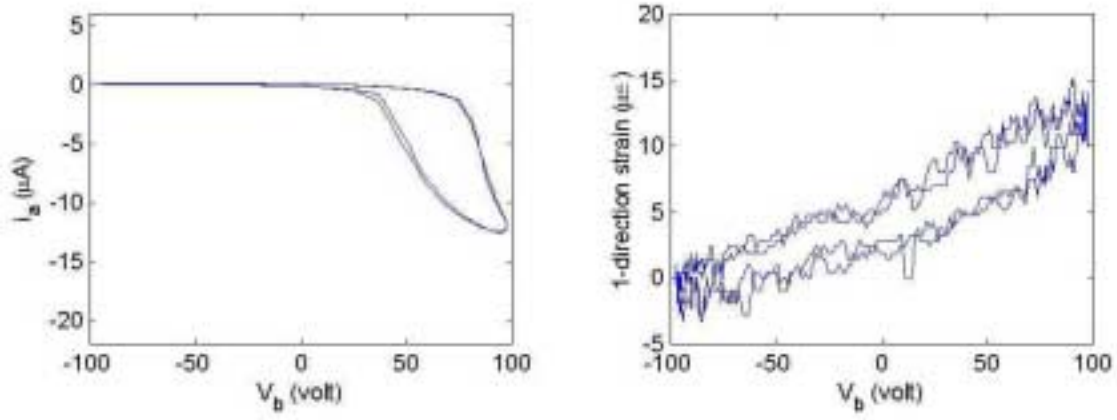

Figure 4.6. Strain and current hysteresis plot due to a 200V p-p, 0 DC volt offset V_b input.

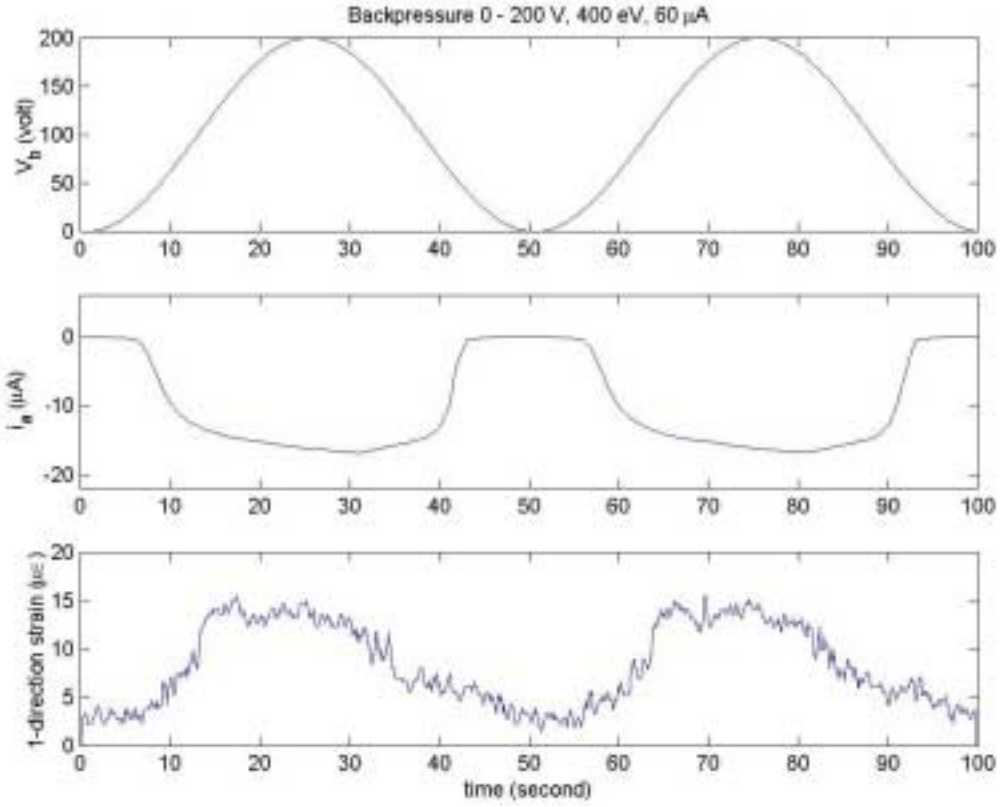

Figure 4.7. Time histories of strain and current output due to a 200V p-p, 100 DC volt offset V_b input.

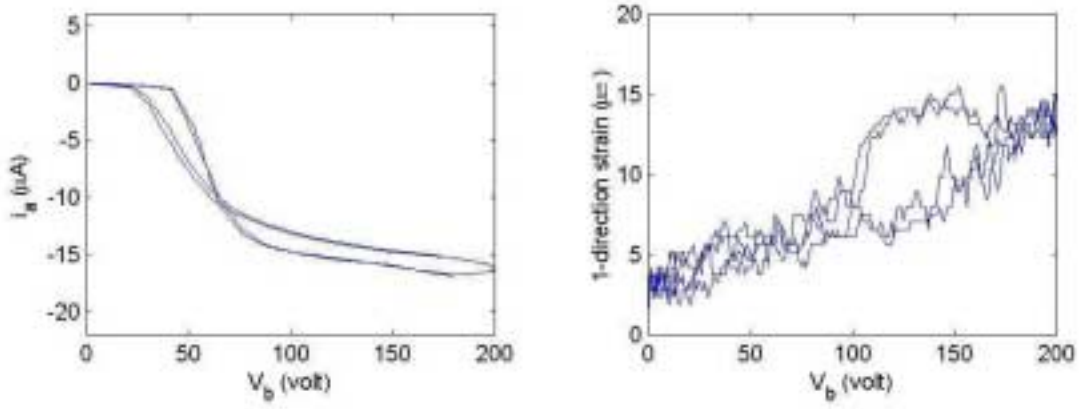

Figure 4.8. Strain and current hysteresis plot due to a 200V p-p, 100 DC volt offset V_b input.

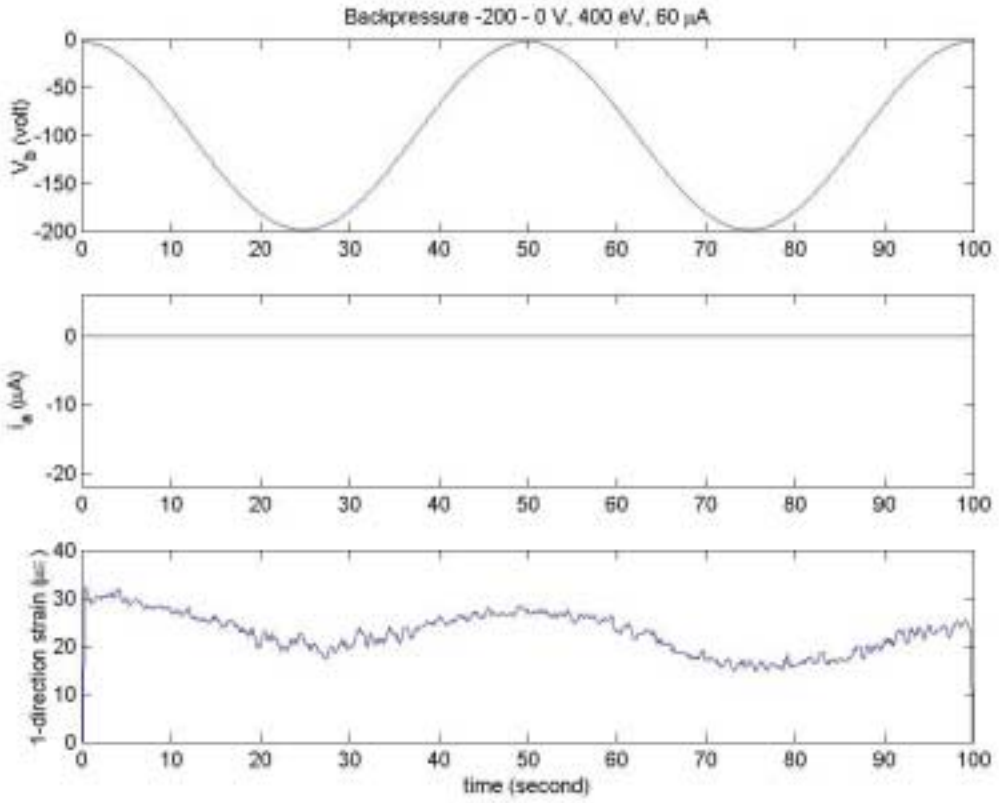

Figure 4.9. Time histories of strain and current output due to a 200V p-p, -100 DC volt offset V_b input.

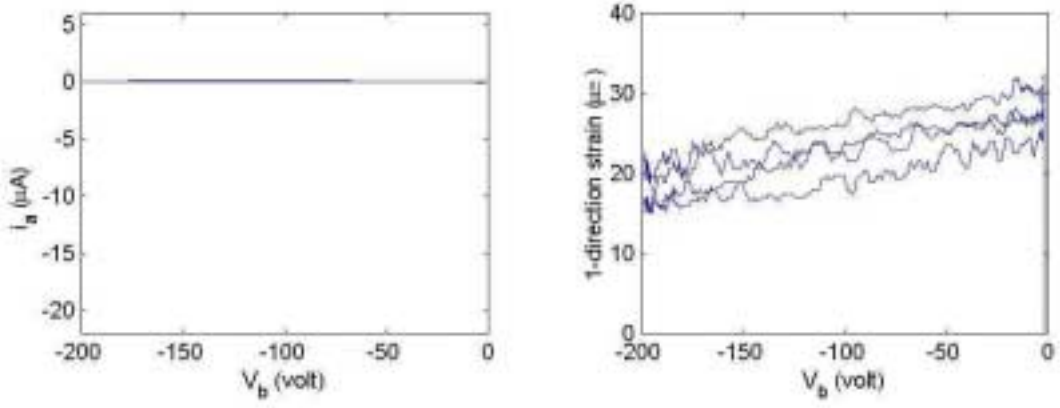

Figure 4.10. Strain and current hysteresis plot due to a 200V p-p, -100 DC volt offset V_b input

Since strain control is the ultimate goal of this investigation, the impact of various conditions on the strain trace will be discussed first. Note that in the strain traces where the backpressure potential (V_b) remains predominantly positive, the strain output is very stable and dependent upon V_b (Figure 4.6.b). In the tests with predominantly negative V_b, the strain still responds as a function of V_b, but significant drift is evident (Figure 4.10.b).

The current results also show a sharp contrast between actuation with positive and negative V_b. In all of the tests the current remained at extremely low levels (approximately 10^{-7} ampere or less) when V_b was below 40 volts. As V_b transitions to greater than 40 volts the current flow through the material suddenly decreases to approximately –12 microampere, as can be seen in Figure 4.5 and 4.6. Further increases above 40 volts lead to a slight gradual decrease in the current until approximately –18 microampere as can be seen in Figure 4.7. One possible explanation for this phenomenon is outlined in the next section.

Discussion Using Quantum Physics Theory

DeBroglie and Einstein [31] made a suggestion that a particle (in this case electron) can be represented as a wave with wavelength

$$\lambda = \frac{h}{p} \text{ and } \nu = \frac{E_p}{h} \tag{4.3}$$

λ = wavelength of the wave function

ν = frequency of the wave function

$$E_p = \frac{p^2}{2m} + U \text{ = energy of particle (in this case: electron)} \tag{4.4}$$

U = potential energy

h = Planck constant = 6.6×10^{-34} Js

p = particle momentum

m = electron mass

v = the speed of electron

Using these postulates, Schrödinger [31] derived the equation of wave function as

$$-\frac{\hbar^2}{2m}\frac{d^2\Psi}{dx^2}+U\Psi=E_p\Psi \tag{4.5}$$

$$\hbar = \frac{h}{2\pi} \tag{4.6}$$

k = wave number

$$= \frac{2\pi}{\lambda}$$

The wave function can be used to describe the electrons travelling through vacuum and impacting the plate. This can be represented by an electron stumbling upon an energy barrier, as can be seen in Figure 4.11.

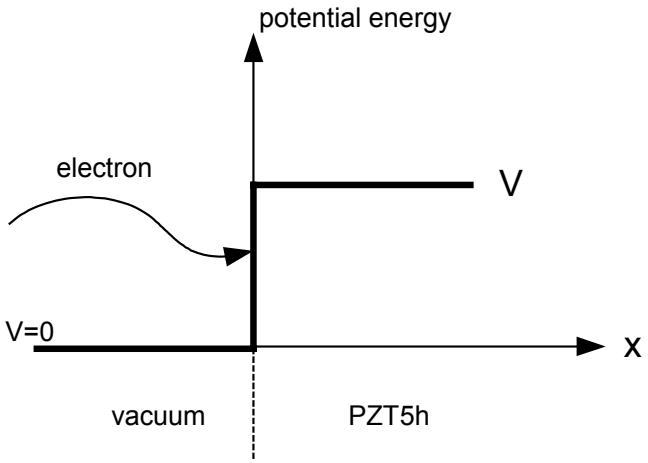

Figure 4.11. Energy representation of an electron impacting the PZT plate

In vacuum the electron has no potential energy, so Equation (4.5) becomes

$$-\frac{\hbar^2}{2m}\frac{d^2\Psi}{dx^2}=E_p\Psi \tag{4.7}$$

The solution of Equation (4.7) is

$$\Psi_1 = Y_1 e^{i\alpha x} + Y_2 e^{-i\alpha x} \tag{4.8}$$

where $$\alpha = \sqrt{\frac{2mE_p}{\hbar^2}} \tag{4.9}$$

which can be represented as a sinusoidal wave equation. An acceptable solution for Schrödinger equation (generally a wave equation) is required that the solution and its derivative are finite, single valued, and continuous. These requirements are imposed in order to ensure that the function be a mathematically "well-behaved" function so that measurable quantities will also be well behaved.

When the electron strikes the plate it is exposed to the potential barrier U. Equation (4.5) again holds, but now the electron can give up some energy to the plate and increase the plate potential. The solution inside the plate is therefore

$$\Psi_2 = Z_1 e^{i\beta x} + Z_2 e^{-i\beta x} \tag{4.10}$$

where $$\beta = \sqrt{\frac{2m(E_p - U)}{\hbar^2}} \tag{4.11}$$

This is, too, a sinusoidal wave equation.

These currents are all electron currents and their positive directions are shown in Figure 4.12. The first term in Equation (4.8) describes the incoming electron current (primary electron, i_p), while the second term describes the secondary electron current (i_s). The first factor of Equation (4.10) is the electron current from PZT to amplifier (i_{a1}), and the second factor denotes the electron current in the opposite direction (i_{a2}). The electron current i_a denoted on Equation (4.1) is the combination of these two factors:

$$i_a = i_{a1} + i_{a2}$$

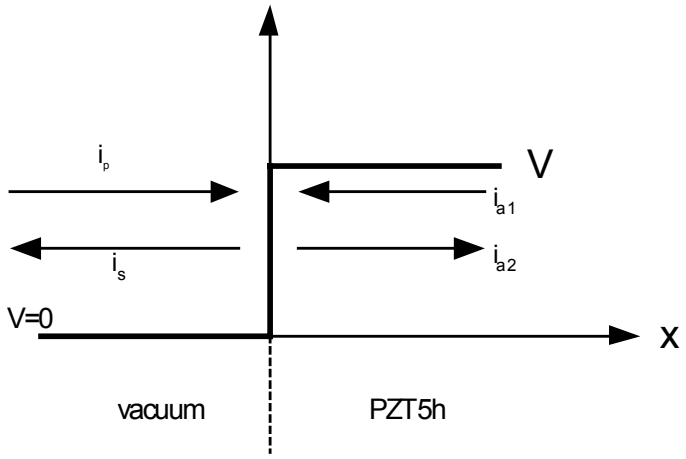

Figure 4.12. Electron current directions at the energy barrier.

The kinetic energy of electron can be represented as a function of surface potential [10]

$$K=\frac{1}{2}mv^2 = e\,V_p \tag{4.12}$$

e = electron charge

V_p = the potential at the surface of the ceramic surface (front surface, exposed to electron beam)

So the kinetic energy of electron varies linearly with the potential of the bare surface of the plate. The PZT can be considered as a capacitor with potential energy [32]

$$U=\frac{1}{2}C\left(V_p - V_b\right)^2 \tag{4.13}$$

C = material capacitance

V_b = backpressure potential

V_p = positive-side potential

So the potential energy of PZT varies quadratically with the potentials on the front and back of the plate.

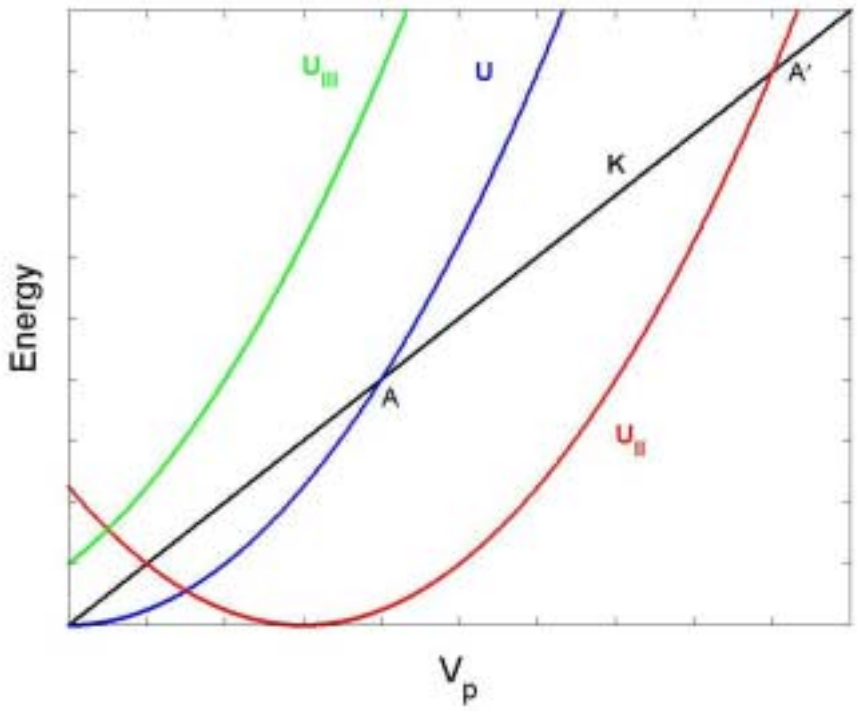

Figure 4.13. Electron kinetic energy and PZT potential energy chart

The energy balance is shown conceptually in Figure 4.13. If V_b is initially set to zero, then the potential energy of the plate as a function of the plate positive surface potential (V_p) is a parabola with the vertex at the origin (Curve U). The kinetic energy of the incoming electron (Eq. 4.12) is represented by a line. If an electron flux with initial energy in the positive yield range strikes the plate then the surface will become increasingly positive until a balance is achieved between the kinetic energy of the incoming electron and the potential energy of the plate. This system state is therefore at point A and the plate surface potential is given by the location of point A on the horizontal axis. The driving force behind the current is the electric field in the material, $(V_p-V_b)/h$.

Increasing V_b moves the potential energy curve to the right, represented by U_{II}, and the stable state moves from point A to A'. A new equilibrium state is achievable under these circumstances. Increasing V_b will reduce the secondary electron emission yield. More primary electrons stick to the plate, so the excess electrons will flow towards

the power amplifier. The negative readings on the pico-ampere meter in the positive V_b region support this phenomenon, Figure 4.5, 4.6, 4.7, and 4.8. The very stable V_b-strain behavior experienced at V_b values above 40 volts supports the conclusion that the system is in a very stable regime in this V_b range and the increase in the electric field in the material supports the increase in the leakage current.

Reducing V_b means making the plate surface more negative, so the next incoming electron comes with slower speed. The potential energy curve moves to the left, represented by U_{III}, and eventually no balance between the incoming kinetic energy and the plate potential energy is possible. This lack of a stable equilibrium is demonstrated by the drift in the strain output seen in Figure 4.9 and Figure 4.10.

Effect of Emission Current to Electrode Current and Strain

The next experiment was developed to see how the beam current (or emission current) affects the strain or electrode current. The same apparatus is illuminated with electron beam with V_b at ground to get zero-relative strain. Then suddenly V_b is stepped up to 200 V. The strain and electrode current are measured. This procedure is repeated with various emission currents: 10, 20, 40, 60, 80, and 100 microampere. The correspondence to beam current is shown in Figure 4.14, provided by Kimball Physics.

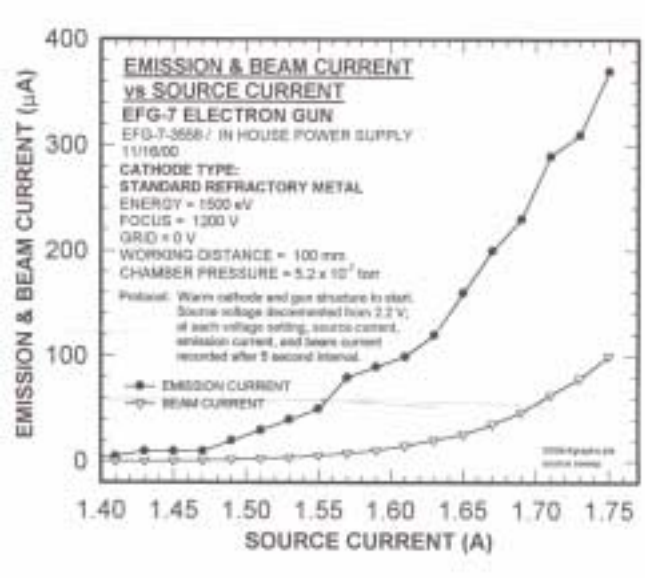

Figure 4.14. Calibration chart of source, emission and beam currents

Plotting both i_a and V_b versus time, it can be seen that i_a is linearly related to emission current. This can be explained directly using Equation (4.1). The secondary electron yield remains constant throughout the emission variation because the energy used remains constant (400 eV). So bigger i_p yields to bigger i_a.

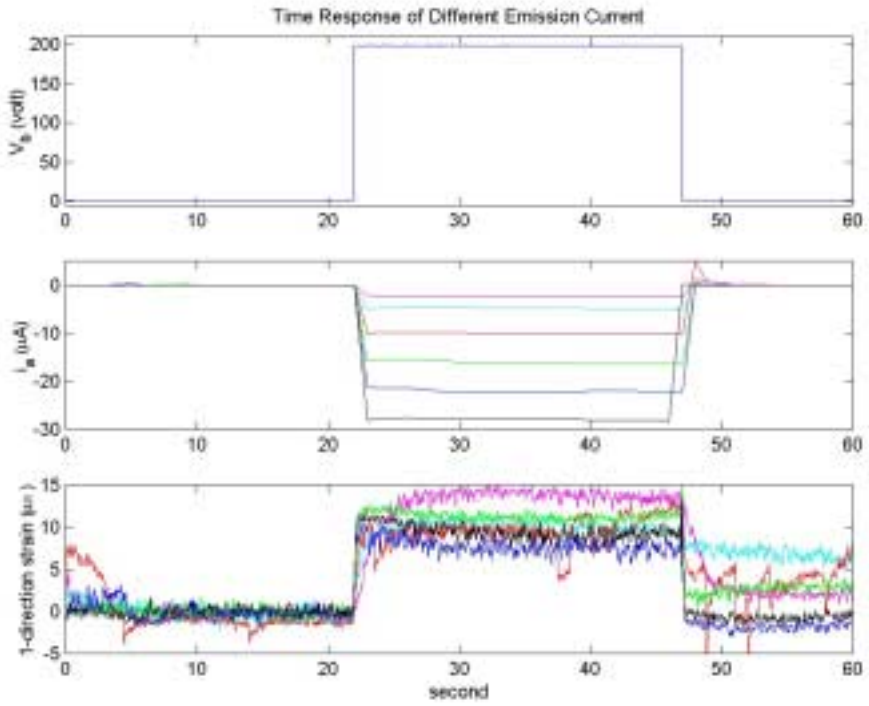

Figure 4.15. Plot of material time response with various emission currents
Magenta: 10 microampere
Cyan: 20 microampere
Red: 40 microampere
Green: 60 microampere
Blue: 80 microampere
Black: 100 microampere

The interesting part is the strain. The rate of change for the strain to reach steady state position is also a function of the magnitude of emission current. Larger emission current leads to a smaller time. This happens due to the fact that the piezoelectric material acts like a capacitor. Considering a slight resistance in the material, the time constant is modeled by using an R-C series circuit

$$t_c = RC \tag{4.14}$$

where t_c = time constant

R = material resistance

C = material capacitance

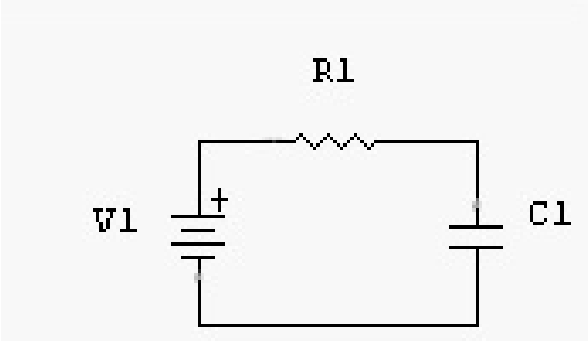

Figure 4.16. R-C Circuit

Changing V_b abruptly is analogous to connecting an R-C circuit to a power supply (V_1 in Figure 4.16.), thus the charge stored in the material is given by

$$Q = Q_f (1 - e^{-t/RC}) \tag{4.15}$$

where Q = the charge at time t

Q_f = the charge at initial time

Rearranging the equation

$$(Q-Q_f) = Q_f e^{-t/RC}$$

Taking derivative with respect to time

$$\frac{dQ}{dt} = -Q_f RC e^{-t/RC} \tag{4.16}$$

The first term is current, so

$$i = -Q_f RC e^{-t/RC}$$

The bigger the current, the smaller the time needed to reach steady state, meaning the plate will respond faster. From Figure 4.17 it is clear that for 10 microampere emission

current the strain needs about 2.5 seconds to reach steady state position. The material needs less than half a second to level off using 100 microampere.

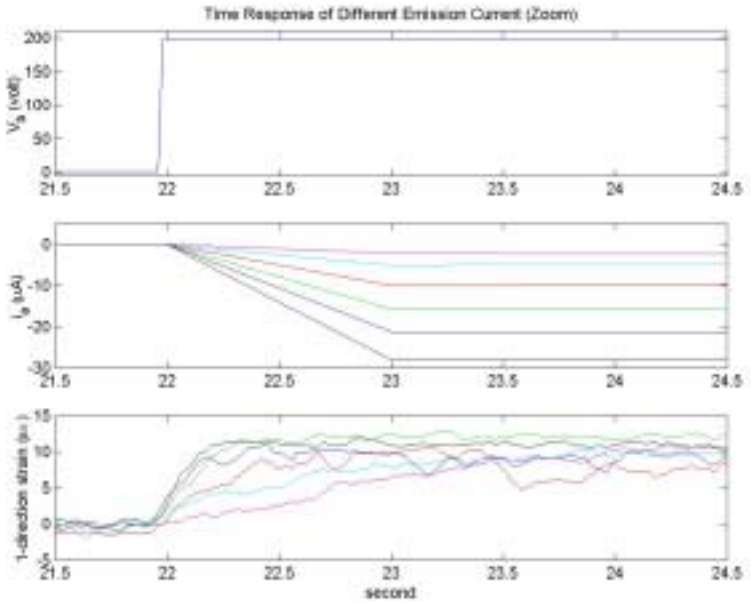

Figure 4.17. Plot of material time response with various emission currents

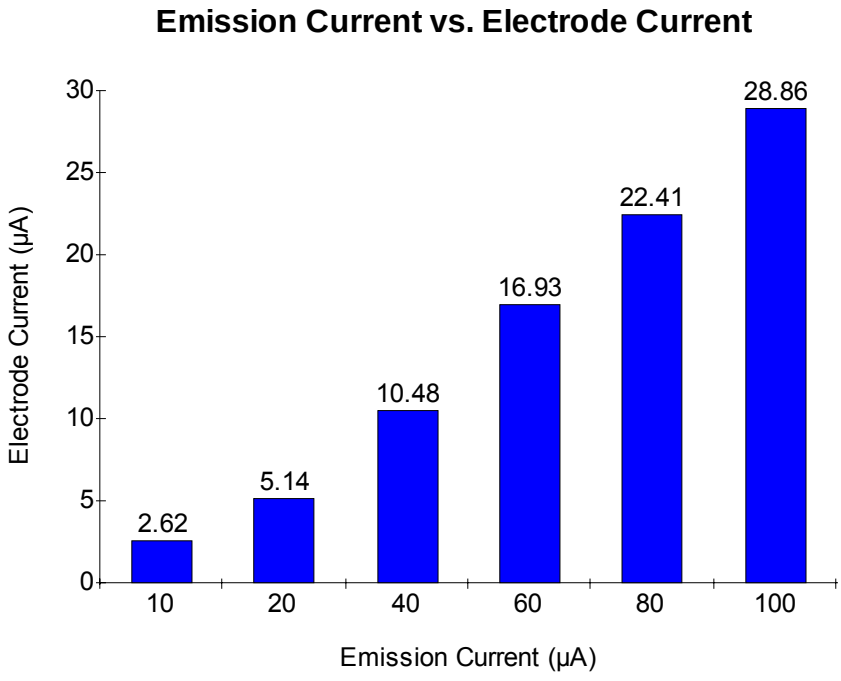

Figure 4.18. Plot of Emission Current versus Electrode Current

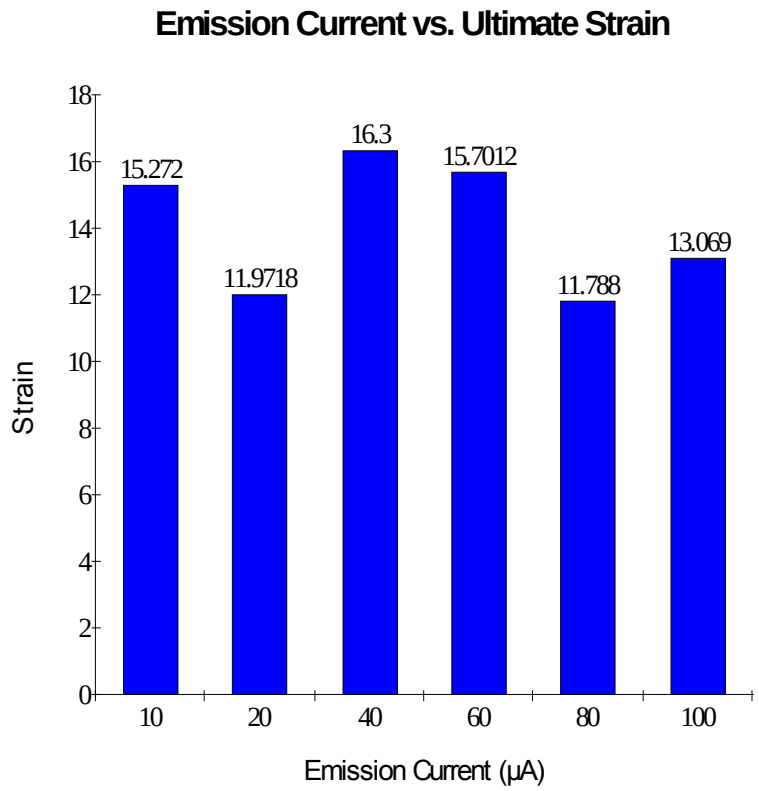

Figure 4.19: Plot of Emission Current versus Ultimate Strain

CHAPTER FIVE
STRAIN DEVELOPMENT

Development of strain is the primary interest in this chapter. There are two subjects: the time response of the material and the blooming of the strained area. Each will be investigated and discussed thoroughly in separate sub chapters.

Time Response of Piezoelectric under Electron Beam Influence

The positive (stripped) side of piezoelectric plate is exposed to a Kimball Physics EFG-7 electron gun. The specimen is placed 10 centimeter from the electron gun. As an early experiment, only nine strain gages are attached on the negative (electroded) side. It is then connected to a power amplifier to allow the potential of the electrode to be controlled (V_b). The experimental protocol required the experiment to be enclosed in a vacuum chamber and exposed to a vacuum condition, $5x10^{-7}$ torr (mm Hg). The bare side is subjected to the electron flux, which is kept constant at emission current 60 microampere and the beam energy of 400 eV. A sketch of the experimental setup is included as Figure 5.1.

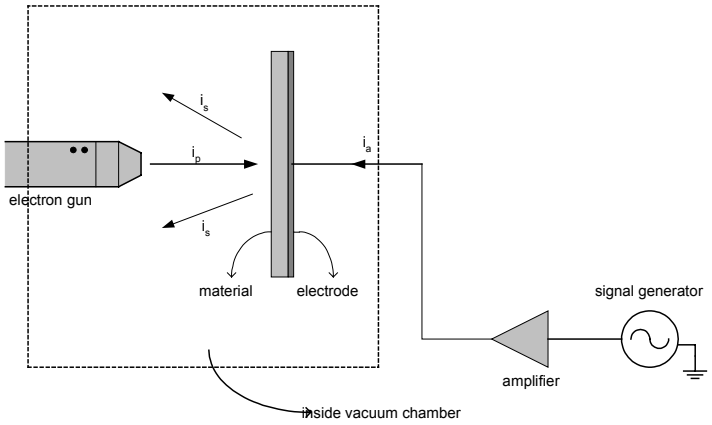

Figure 5.1. Experiment setup

The backpressure voltage (V_b), electron beam diameter, beam position, and beam motion (constant position or raster) were all varied to some degree in these experiments. Note that the electron gun used in these experiments is a flood gun, thus even when small spot sizes are achieved with this gun, electron current is still distributed over a large area surrounding the target spot. The strains were recorded by the 9 strain gages atop the remaining electrode. The strain gages were single direction gages, measuring strain in the base-tip direction. A 24-channel strain gage data acquisition system was used to record all of the strain signals simultaneously when the various inputs were applied to the plate. The matrix outlining all of the tests is included as Table 5.1.

Various beam types were used and are illustrated in Figure 5.2. Static, nonmoving beams were applied at three different locations. The “Center” location refers to a spot on the piezoelectric plate which is opposite strain gage #5. The “Corner” location refers to a location opposite strain gage #1 and the “Base” location refers to a target on the plate opposite strain gage #5. The first section of Table 1 lists all of the experiments run using static beams irradiating these locations. The table notations indicate the step voltage applied to the electrode to stimulate the strain change and the diameter of the beam as it appeared on a phosphor screen mounted near the piezoelectric sample. Note that because a flood gun was used in these tests the diameters are only useful when compared to each other and have no absolute meaning. For example, the focus is set to be as small as 1 mm in diameter, the beam is still dispersed, as is seen from the beam profile in Figure 5.3.

Six different rastering beams were also used and strain results recorded. The electron beam was set to scan across the locations of strain gages #1, 2, and 3 (Vert 2); 4, 5, and 6 (Vert 1); and 7, 8, and 9 (Vert 3). Tests were also run with the beam scanning across strain gages #1, 4, and 7 (Horz 2); 2, 5, and 8 (Horz 1); and 3, 6, and 9 (Horz 3). The second and third sections of Table 2 list all of the experiments run using the beam rastering. Table notations indicate the electrode step voltage, the beam diameter as measured on a phosphor screen, and the rate of the raster scan.

Table 5.1. Matrix of Test Conditions

Center (step, diameter of beam)	Corner (step, diameter of beam)	Base (step, diameter of beam)
0-100 V,1mm	0-100 V , 1mm	0-100 V , 1mm
0-100 V,10mm	0-100 V , 10mm	0-100 V , 10mm
0-(-100)V , 1mm	0-(-100)V , 1mm	0-(-100)V , 1mm
0-(-100)V , 10mm	0-(-100)V , 10mm	0-(-100)V , 10mm

Vert 1 (step, diameter of beam, raster rate)	Vert 2 (step, diameter of beam, raster rate)	Vert3 (step, diameter of beam, raster rate)
0-100 V , 1mm 1Hz	0-100 V , 1mm 1Hz	0-100 V , 1mm 1Hz
0-100 V , 10mm 1Hz	0-100 V , 10mm 1Hz	0-100 V , 10mm 1Hz
0-(-100)V , 1mm 1Hz	0-(-100)V , 1mm 1Hz	0-(-100)V , 1mm 1Hz
0-(-100)V , 10mm 1Hz	0-(-100)V , 10mm 1Hz	0-(-100)V , 10mm 1Hz
0-100 V , 1mm 10Hz	0-100 V , 1mm 10Hz	0-100 V , 1mm 10Hz
0-100 V , 10mm 10Hz	0-100 V , 10mm 10Hz	0-100 V , 10mm 10Hz
0-(-100)V , 1mm 10Hz	0-(-100)V , 1mm 10Hz	0-(-100)V , 1mm 10Hz
0-(-100)V , 10mm 10Hz	0-(-100)V , 10mm 10Hz	0-(-100)V , 10mm 10Hz

Horz 1 (step, diameter of beam, raster rate)	Horz 2 (step, diameter of beam, raster rate)	Horz 3 (step, diameter of beam, raster rate)
0-100 V , 1mm 1Hz	0-100 V , 1mm 1Hz	0-100 V , 1mm 1Hz
0-100 V , 10mm 1Hz	0-100 V , 10mm 1Hz	0-100 V , 10mm 1Hz
0-(-100)V , 1mm 1Hz	0-(-100)V , 1mm 1Hz	0-(-100)V , 1mm 1Hz
0-(-100)V , 10mm 1Hz	0-(-100)V , 10mm 1Hz	0-(-100)V , 10mm 1Hz
0-100 V , 1mm 10Hz	0-100 V , 1mm 10Hz	0-100 V , 1mm 10Hz
0-100 V , 10mm 10Hz	0-100 V , 10mm 10Hz	0-100 V , 10mm 10Hz
0-(-100)V , 1mm 10Hz	0-(-100)V , 1mm 10Hz	0-(-100)V , 1mm 10Hz
0-(-100)V , 10mm 10Hz	0-(-100)V , 10mm 10Hz	0-(-100)V , 10mm 10Hz

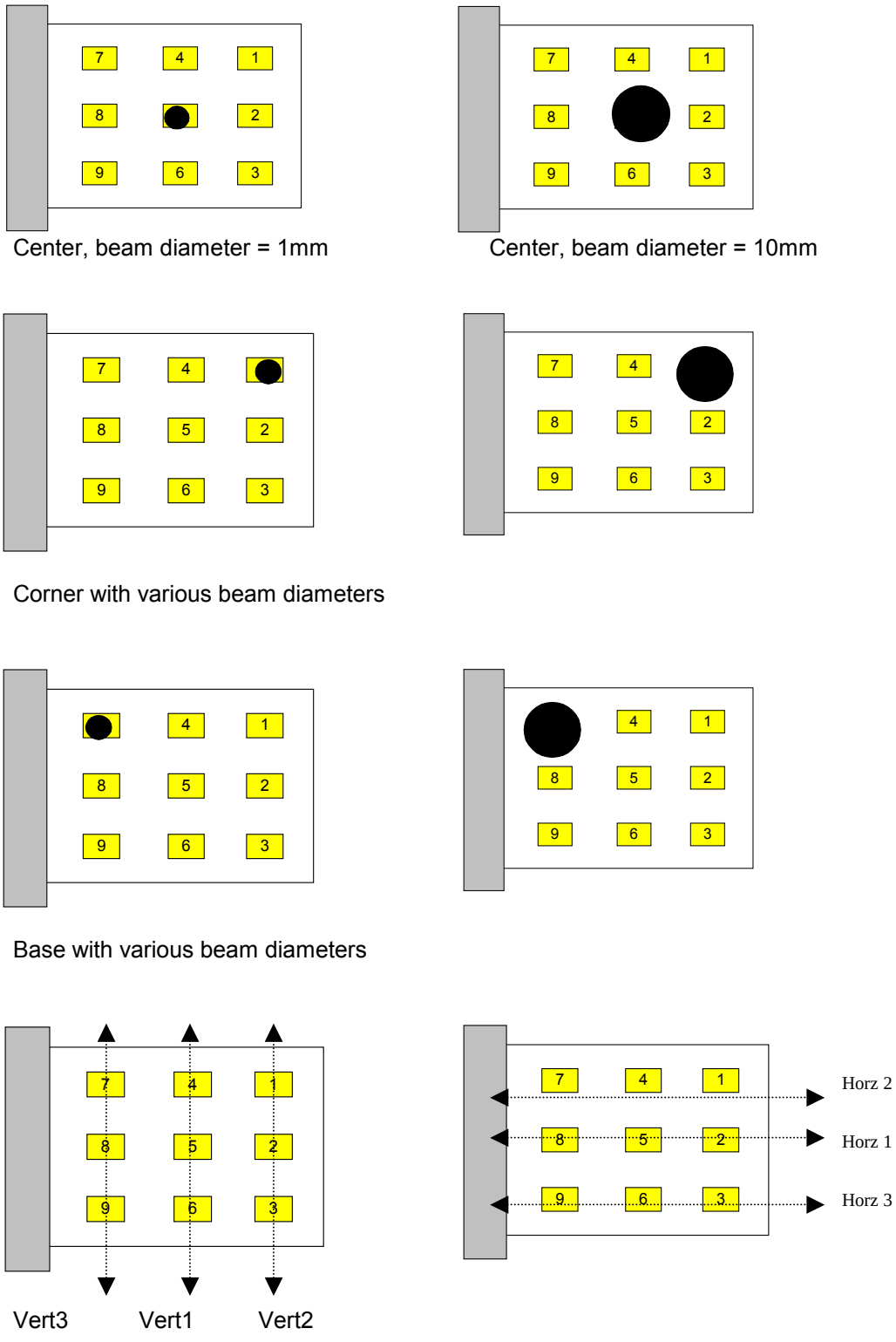

Figure 5.2. Sketches of beam inputs used in experiments.

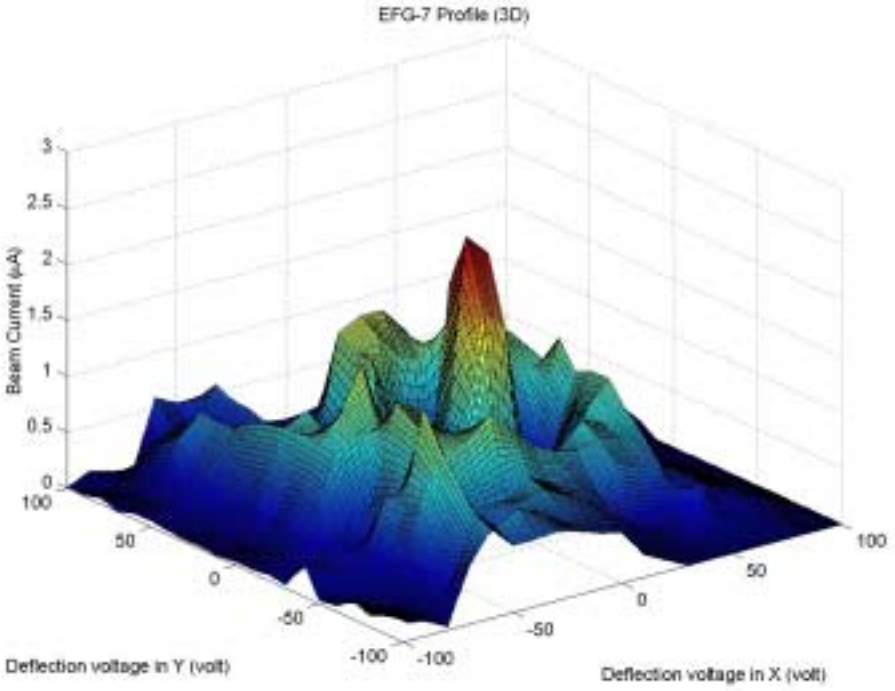

a.

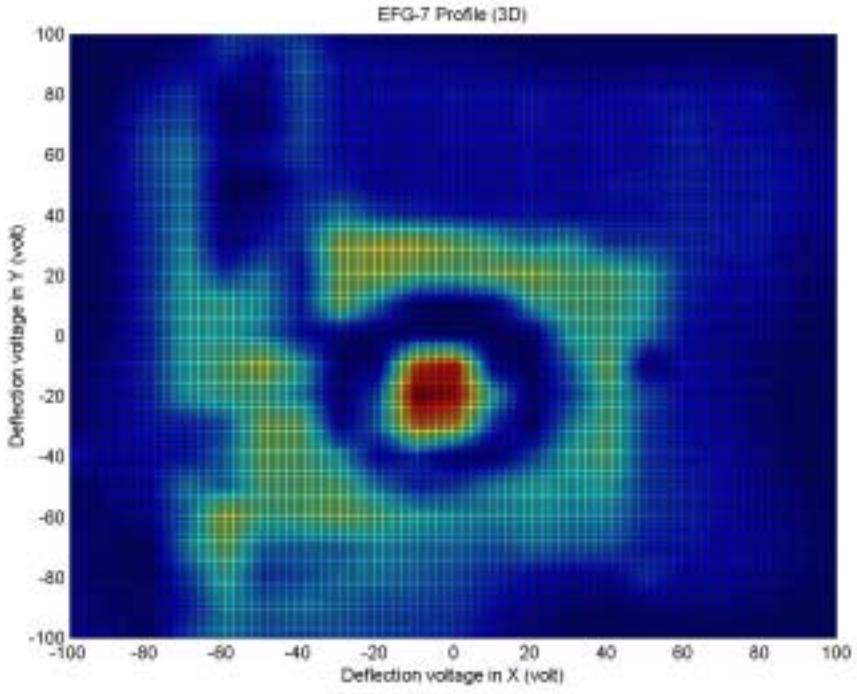

b.

Figure 5.3. EFG-7 electron beam profile: a. in 3D, b. in 2D

There are 60 sets of data (by Table 5.1.), but for brevity only 6 of them are presented here. Other results are presented in Appendix D. Results from two static beam locations, Center and Corner, and one raster location, Vert1, are presented. In all cases the results from the small beam spot (1mm) are used. The strain responses are due to two step changes in electrode potential, a 0-100 V step and a 0- -100 step. The captions on Figures 5.4 - 5.8 indicate the beam type and electrode (V_p) potential change that stimulated the illustrated strain changes.

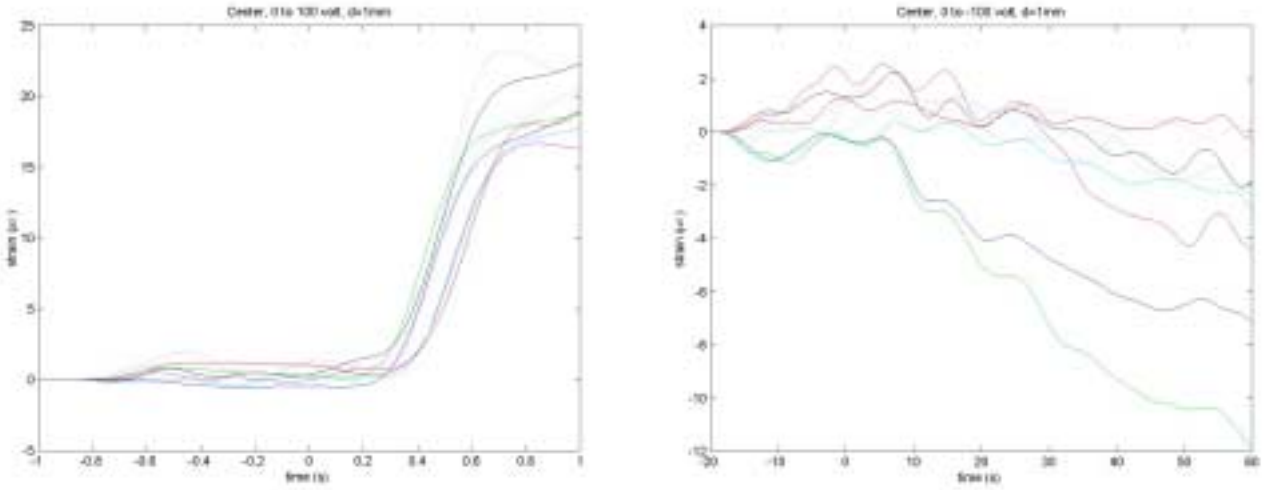

Figure 5.4. Step up and step down response for center beam experiments.

magenta — : strain gage 1
cyan —: strain gage 2
red —: strain gage 3
green —: strain gage 4
blue —: strain gage 5
black —: strain gage 6
magenta … : strain gage 7
cyan … : strain gage 8
red … : strain gage 9

A clear trend is the faster rate of strain change in response to the positive V_b steps relative to the negative steps. In fact, there appear to be two distinct time constants. If V_b is stepped up (from 0 to 100V) the time constant is about 1 second. That means the charge in the plate changes from the initial value to the final value in approximately 1 second. But if V_b is stepped down, the time constant is nearly 60 seconds. This means the charge in the plate takes significantly more time to change from the initial value to the final value. As can be see in the previous pictures, the strain needs almost one minute to reach steady state value.

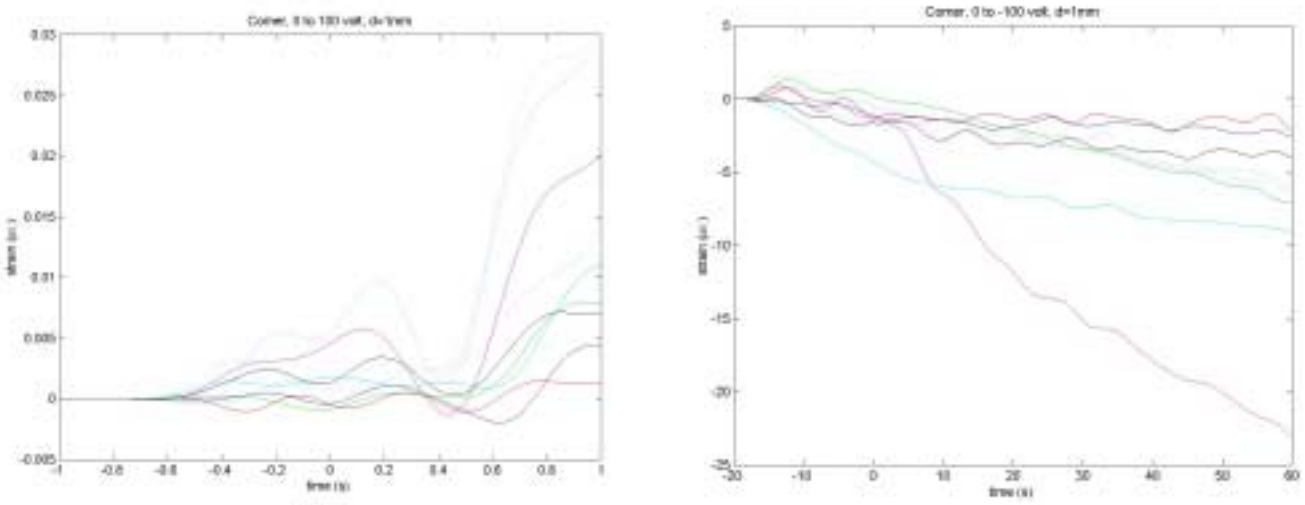

Figure 5.5. Step up and step down response for corner beam experiments.

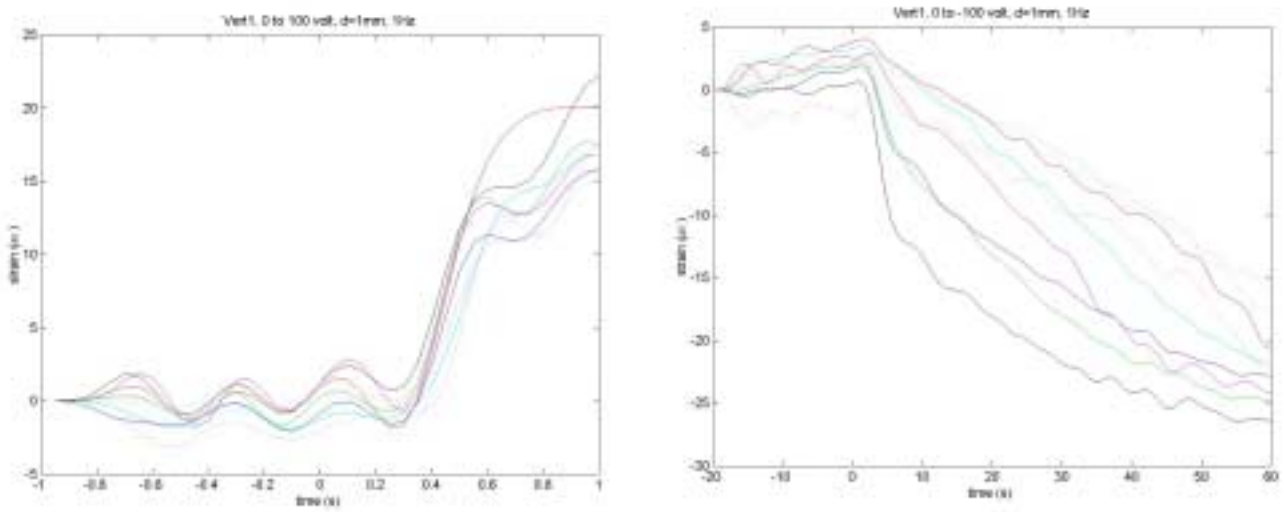

Figure 5.6. Step up and step down response for vertical beam experiments.

A number of conclusions can be drawn from this data. First, the fastest strain changes are typically seen in the location of the electron flux. In Figure 5.4 the fastest change in the strain response corresponds to gages #4 and 5 when the electron beam is aimed at strain gage #5. In Figure 5.5 the fastest response is in strain gage #1, again when the electron flux is aimed in this location (referring to Figure 5.2.). And finally, when the beam is rastered across strain gages #4, 5, and 6 (Figure 5.6.) the most rapid strain responses were observed in these gages. This phenomenon will be discussed more thoroughly on the next subchapter.

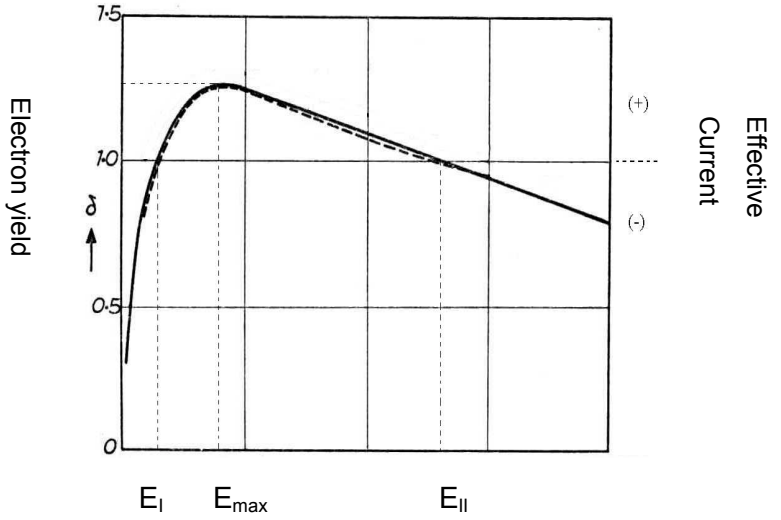

Figure 1.4. Plot of secondary electron yield against incoming energy

The difference in time constant mentioned before also occurred here. To explain this time difference phenomenon, Figure 1.4. is redrawn above. If the primary electron has energy less than E_I, the secondary electron yield is less than 1. That means the primary electron is absorbed, and a net negative charge is immediately resident on the plate surface. This will induce a bigger pushing force for the next incoming primary electron, which in turn travels with slower speed. The primary electron energy will drop until at some point the whole system will be shut down. If the primary electron energy lies between E_{max} and E_{II}, the primary electron will push more electron out from the plate (due to the secondary electron yield greater than 1). The next electron will travel with

greater speed and energy, until the energy reaches E_{II}. As soon as the energy is greater than E_{II}, the same phenomenon happens when the energy is less than E_I. So E_{II} is a stable point.

When an electron strikes the plate, there are a number of interactions that can take place [2,3], and energy is transferred to the electrons in the plate. Recall that energy of electron lies in discrete levels, as shown in Figure 5.7. If an electron receives some amount of energy, it will be excited to a higher level. If the energy is big enough, it will be excited to vacuum, thus positive and negative charges (i.e. holes and electrons) are released.

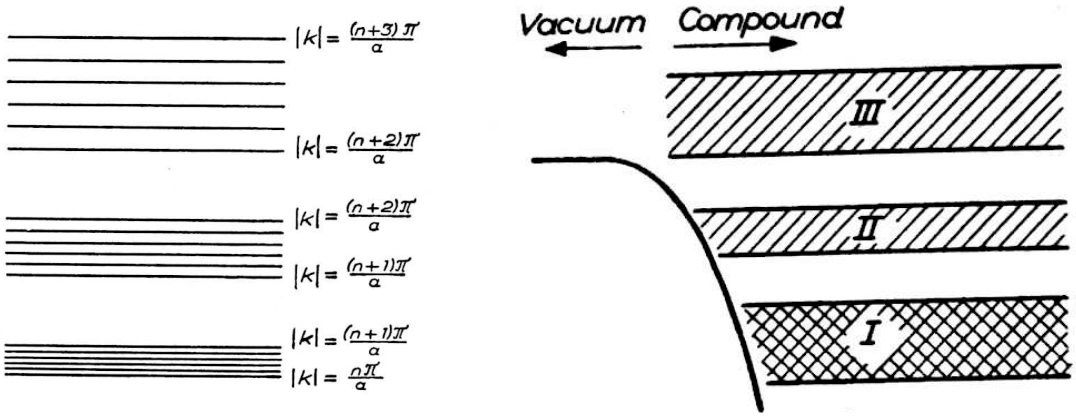

Figure 5.7. Electron levels of energy

The constant electron beam can be considered as an excitation to the plate. Its presence quickly changes the energy equilibrium of the whole system, until it resides on E_{II} point on Figure 1.3. When the backpressure voltage is increased, the plate becomes more positive. The primary electron energy will increase due to the faster velocity of the electrons. The secondary electron yield will fall below 1. This means the primary electrons are absorbed, and their energy is not enough to eject electrons residing on the plate.

On the other hand, when the backpressure voltage is reduced, primary electrons of an energy less than E_{II} strike the plate, and their energy is transferred to eject slightly more electrons than that of the incident. This energy exchange and electron excitation process takes time, so the result is a slower strain change when the electrode is

stepped down, which decelerates the incident electrons, than when it is stepped up. These processes manifest themselves in the secondary yield curve, where electrons with energies greater than E_{II} generate negative charges on a dielectric surface, and those with energies less than E_{II} stimulate positive surface charges.

Blooming Effect

These experiments show that the fastest and largest changes in strain take place where the electron flux strikes the surface. The results from the experiments show a slight difference, i.e. the rest of the area also responds to the electron flux, although with much slower rate. The following experiment was conducted to investigate this phenomenon in more detail. The same specimen as in Chapter III and IV (with 16 strain gages on the electroded side) is subjected to backpressure V_b = 0 when illuminated by electron beam. This sets the zero point for the test. Then the electron gun is turned off and V_b is increased to 200 volt. The next step is to shoot the plate with 400 eV energy, 60 microampere emission current, approximately 1 cm in diameter for 2 seconds, as is denoted in Figure 5.8.

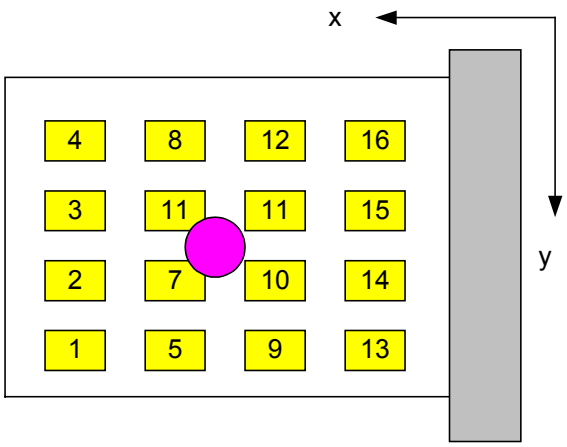

Figure 5.8. Electron flux is activated at the center of the plate with V_b = 200 V

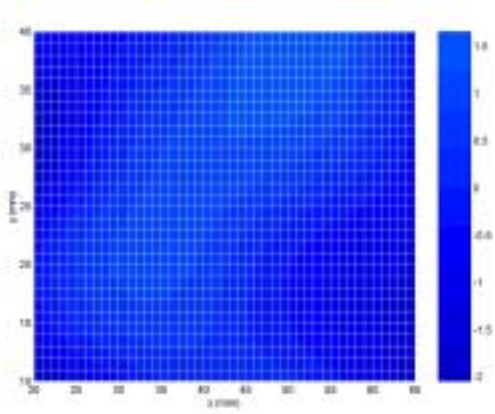

a.

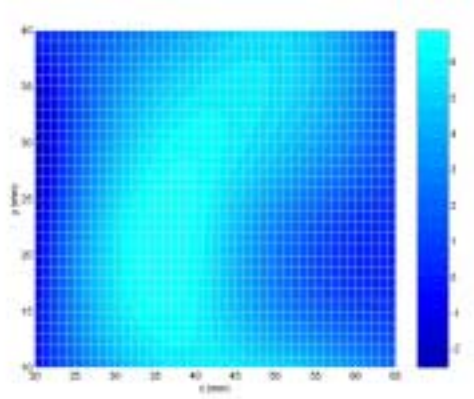

b.

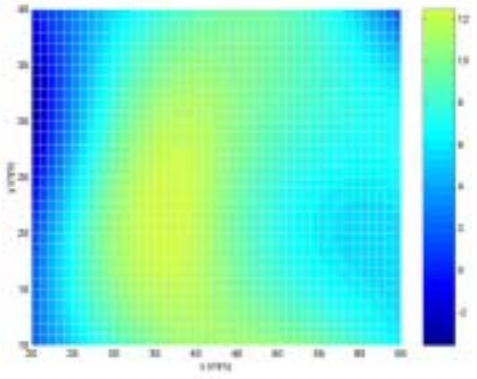

c.

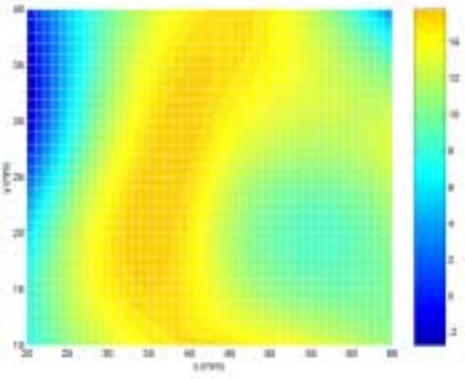

d.

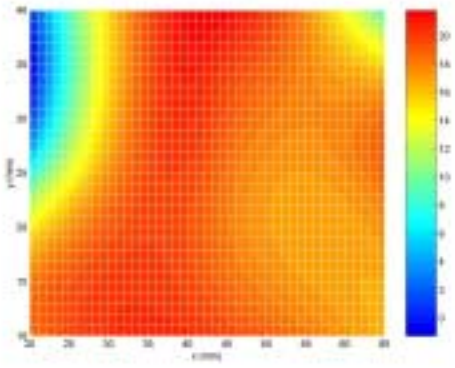

e.

Figure 5.9. Strain distribution sequence with electron beam in the middle:

a. t = -0.4 s, b. t = 0.4 s, c. t = 0.6 s, d. t = 0.8 s, e. t = 1 s

The strain distribution sequence is presented in Figure 5.9. At first only the area under illumination responds to the electron flux, denoted by high strain on the center. Then the strain distributes along the plate until the whole surface has high strain. This is slightly different from what is suggested by analytical and numerical solutions provided in Chapter II. A clearer view of how the charge (and strain) distributes along the material is provided by placing the electron flux on the edge of the material, as depicted in Figure 5.9. The results are presented in Figure 5.10. Again, it is clearly seen that the area under illumination (i.e. strain gage no 1 or the left lower corner of the plate) developed the strain first. Then the rest of the area follows. This phenomenon is called 'blooming'.

The next experiment is to place the electron beam on the edge. The beam is placed at the edge of the plate, as presented in Figure 5.10. The results are presented in time sequence in Figure 5.11.

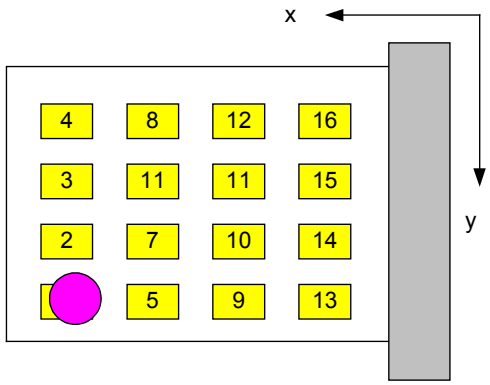

Figure 5.10. Electron flux is activated at the center of the plate with V_b = 200 V

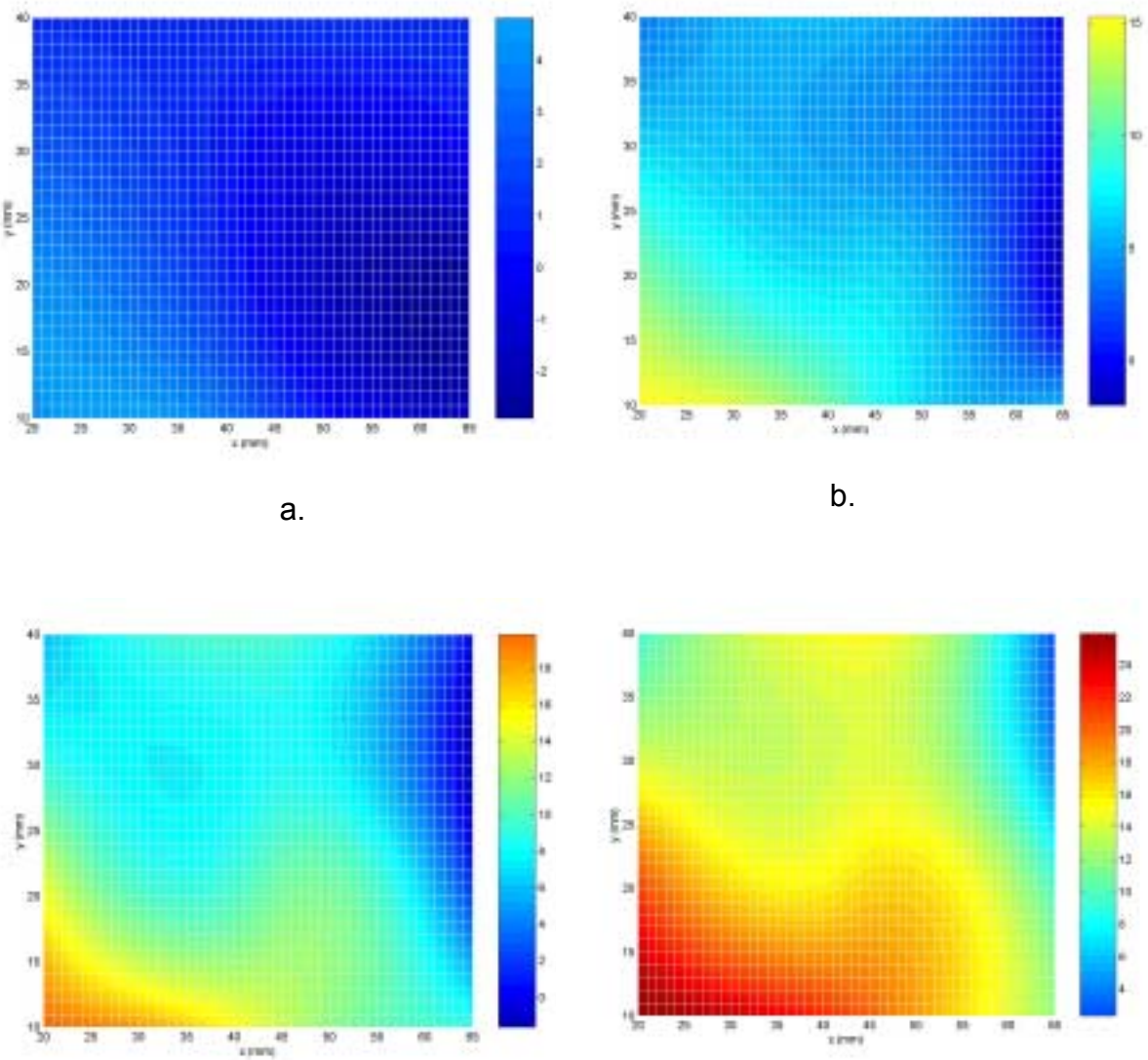

a. b.

c. d.

Figure 5.11. Strain distribution sequence with electron beam on the edge:
a. t = 0.4 s, b. t = 0.6 s, c. t = 0.8 s, d. t = 1 s

Note that the expansion of the strain as a function of time is similar to the surface charge blooming predicted by Attard and Ganachaud [5]

CHAPTER SIX
CONCLUSIONS AND FUTURE WORK

Conclusions

The static and quasi-static state of a piezoelectric material under electron flux influence is the primary interest in this research. Two sets of mathematical analysis are presented, one is qualitative analysis from piezoelectric electro-mechanical set of equations developed by Love and Tzou, the other one is numerical analysis using piezoelectric constitutive equations. Several sets of experiments are carried out to investigate the behavior of the material under electron influence, i.e. material's sensitivity to distance from the source of excitation (electron gun), electron flow (secondary electron and electrode current), time response, and distribution of charge and strain in the material. A complete analysis of the experimental results is conducted based on the mathematical analysis.

The electro-mechanical equations need a lot of simplification for a thin, rectangular piece of material. The solution is obtained by considering that the material is a simply-simply supported thin rectangular structure, thus the effect of the clamps holding the material in place is not considered. The effect of temperature is also not considered, assuming that the temperature is always steady at room temperature (27^{o}C or 80^{o}F). The result shows that only the surface area under electron influence changes in strain, while the rest of the surface virtually does not change from initial condition.

The constitutive equations are only discussed briefly, and the material properties are inputted into Ansys program. Again, a simply-simply supported model is used, and the result shows the same thing as the electro-mechanical solution.

From the first experiment it is shown that the sensitivity of piezoelectric strain to electron beam excitation depends on the distance between the specimen and the source of excitation (i.e. the electron gun). The farther the specimen is from the gun, the more sensitive it is to the change in backpressure voltage. It is likely that the vacuum

chamber wall acts as an electron collector, so when the specimen is close to the wall, the secondary electrons are attracted to the wall, making the electron flow better.

The secondary electron flow is dependent to the polarity of the backpressure voltage. If the backpressure voltage is positive, primary electrons come with greater speed, thus their energy increases. Referring to Figure 1.4, the secondary electron yield drops below 1, so the excess electrons flow through the ampere meter, hence the negative current. If, on the other hand, the backpressure voltage is set negative, the primary electrons come with slower speed, thus increasing the secondary electron yield greater than 1. Excess electrons in the plate are thrown out through the secondary electron emission. At this state almost no current is detected through the ampere meter.

The magnitude of electrode current is linearly related to the emission current, which is obvious from Kirchoff's Law. The magnitude of the strain is barely affected by the magnitude of emission current, but the strain time constant drops when the emission current rises. This phenomenon can be considered as a classic R-C series circuit problem, when the charging time of the capacitor is related exponentially with the magnitude of the current flowing through the circuit.

A set of experiments were conducted to explore the charging rate of the piezoelectric material. There is a significant difference between the time response of the material when the backpressure is increased (approximately 1 second) and that when the backpressure is decreased (approximately 60 seconds). This difference is due to the fact that increasing the backpressure voltage will reduce the secondary electron flow. There are more primary electrons that reside in the material than local electrons expelled from the material. There is still energy transfer from the primary electrons to the locals, but it is not enough to exit the electrons into secondary electrons. If the backpressure is reduced, the secondary electron yield will increase above 1. The primary electrons will transfer their energy to the electrons in the plate so they can be exited into vacuum. This transfer process, along with the lack of moving charge in the material, slows down the material response to change in backpressure.

The highest magnitude in strain responses is due to the location of the electron flux, but after some time, most of the surface has the same strain magnitude with that directly under electron flux influence. This is called blooming effect. Blooming happens

because the primary electrons transfer their energy to local electrons so they have enough energy to pass the energy barrier and be exited as free electron. The trajectories of these electrons are denoted by Boltzmann transport theory.

Future Work

As implied in the conclusion part, a more complete mathematical analysis needs to be conducted that takes into account the temperature effect and initial strain. The specimen can be considered as a cantilever plate, or one side of the rectangle can be constrained to a specific strain, instead of a simply-simply-supported model. The excitation (i.e. electron beam) can also be modeled closer to the actual beam profile presented in Figure 5.3.

The dynamic aspects of piezoelectric material under electron flux influence can be investigated. Instead of feeding a step or quasi-static signal to backpressure voltage, wide variety of rapid-changing signals can be used, such as ramp, impulse, sinusoidal with different frequencies or even white noise. These signals can also be fed into the electron beam power supply to vary the energy and current of the electron beam.

Different kinds of material can be investigated, such as PVDF, to find out the most suitable material under certain condition. Also, an electron collector can be installed to catch the secondary electrons to see the effect of better electron flow from the system.

In computational analysis, the results of this research can be put into a Monte Carlo simulation to model electron movement in piezoelectric material in a certain condition. Another simulation using Ansys can also be carried out to predict how the material will react given a certain condition and excitation. This simulations will give some ideas about the shape, magnitude, intensity or energy of the excitation (electron beam and/or backpressure voltage) needed to control a certain shape and type of material.

Appendix A: Vacuum Chamber Specification

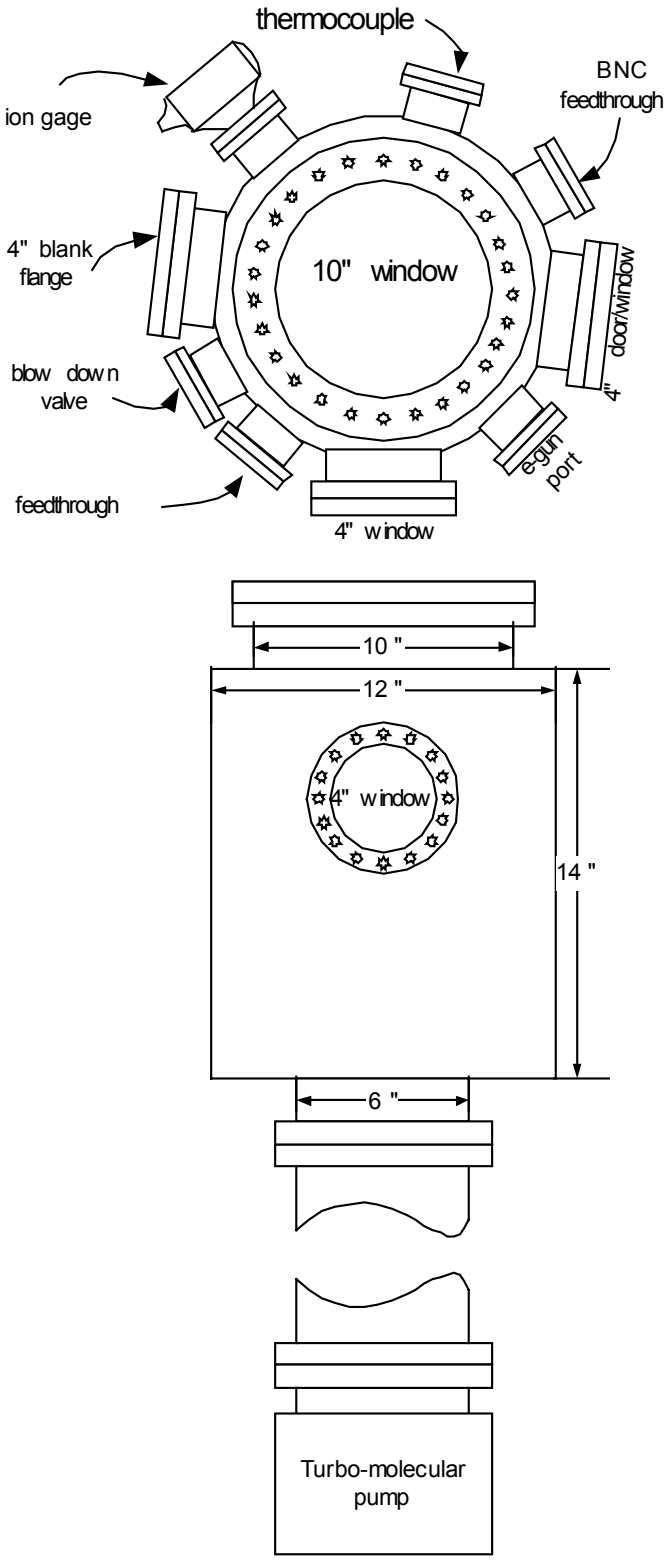

Appendix B: Ansys56 Codes

```
/filename,pzt5h
/prep7

! Element type definition, material property definitions

et,1,solid5
mp,ex,1,6.2e10
mp,ey,1,6.2e10
mp,ez,1,4.8e10
mp,nuxy,1,.24
mp,nuxz,1,.31
mp,nuyz,1,.31
mp,gxy,1,2.5e10
mp,gyz,1,2.0049e10
mp,gxz,1,2.0049e10
mp,kxx,1,43
mp,perx,1,3.84e14
mp,pery,1,3.84e14
mp,perz,1,3.84e14


! Define PIEZ and ANEL Data Tables

tb,piez,1,,,,
tbmodif,1,3,-13.3576
tbmodif,2,3,-13.3576
tbmodif,3,3,22.0524
tbmodif,5,2,14.8559
tbmodif,5,2,14.8559

tb,anel,1,,,,
tbmodif,2,1,7.572e10
tbmodif,3,1,2.572e10
tbmodif,4,1,2.4346e10
tbmodif,8,1,7.572e10
tbmodif,9,1,2.4346e10
tbmodif,13,1,5.9686e10
tbmodif,17,1,2.5e10
tbmodif,20,1,2.0049e10
tbmodif,22,1,2.0049e10

! Define keypoints to define geometry

k,1,0,0,0
k,2,.075,0,0
k,3,.075,.05,0
k,4,0,.05,0
```

```
k,5,0,0,2e-3
k,6,.075,0,2e-3
k,7,.075,.05,2e-3
k,8,0,.05,2e-3


! Define lines based on keypoints

l,1,2
l,2,3
l,3,4
l,4,1
l,5,6
l,6,7
l,7,8
l,8,5
l,1,5
l,2,6
l,3,7
l,4,8


! Define areas based on keypoints

a,1,2,3,4
a,5,6,7,8
a,1,2,6,5
a,2,3,7,6
a,3,4,8,7
a,1,4,8,5


! Define volume

ksel,s,,,1,8,1
lslk,,1
asll,,1
va,all


! Mesh geometry

vmesh,all

save
finish


! Apply BC's

/solu
```

```
! Constrain areas

ksel,s,,,1
ksel,a,,,4
ksel,a,,,8
ksel,a,,,5
lslk,,1
asll,,1
nsla,,1
d,all,all,0
allsel


! Apply 100-V to area 1

ksel,s,,,1,4
lslk,,1
asll,,1
da,all,volt,100
allsel


! Apply 0-V to area 2

ksel,s,,,5,8
lslk,,1
asll,,1
nsla,,1
nsel,u,,,422,423,1

nsel,u,,,436,437,1
d,all,volt,0
allsel

! Apply -50-V to some particular nodes

nsel,s,,,422
nsel,a,,,423
nsel,a,,,437
nsel,a,,,436
f,all,amps,+25e-6
allsel

! Run solution for given conditions

solve

save
finish
```

Appendix C: Matlab Codes

C.1. Matlab Simulation of Piezoelectric Material Response to Electron Flux

```
%Initialization of the plate
clear;
clf reset;

a=0.075;
b=0.05;
rho=7500;
h=0.001975;

x=0:0.001:0.075;
y=0:0.001:0.05;
D=544.9;
P=5e6;

for r=0:0.002:0.01,
for theta=0:(2*pi/10):2*pi,

xs=0.035+(r*cos(theta));
ys=0.025+(r*sin(theta));

%Defining the Mode Shape of the Plate
lamdax=25;
lamday=0;
uk=0;
for m=1:50,
        for n=1:50,
        U3k=(sin((m*pi*x/a)))'*(sin(n*pi*y/b));
                U3k2=U3k.*U3k;

                Nk1=trapz(x,U3k2);
                Nk=trapz(y,Nk1);

                U3ks=(sin((m*pi*xs/a)))'*(sin(n*pi*ys/b));
                Fk=(P/(rho*h*Nk))*U3ks;

                ohm=(lamdax^4)*(D/(rho*h));
                ohmk=ohm.*ohm;
                nk=Fk/(ohmk);
                uk=uk+(nk.*U3k);
        end
end

end
```

```
end

mesh(uk);
xlabel('x (mm)');
ylabel('y (mm)');
zlabel('Strain');
```

C.2. Matlab Code for Generating Blooming Sequence, by Haiping Song

Exp3dm.m

```
%
%  To plot some experiments solution
%

fid=fopen('CS10s.txt','r');
Sdate=fscanf(fid,'%12f');
Time=[0:1/16:899/16];
PXX=[0 20 35 50 65 75];
PYY=[0 10 20 30 40 50];
for j=2:17
%   PZ_EX(:,j-1)=Sdate(j:17:(959*17+j));
   PZ_EX(:,j-1)=Sdate(j:17:(959*17+j))-Sdate(j);
   PZ_EX1(1,j-1)=PZ_EX(1,j-1);PZ_EX1(2)=PZ_EX(2,j-1);
end
%
delt=50;nframes=12;
MM=moviein(nframes);
imm=[80:10:300];

%This is the fraction of picture to be displayed;
iss=size(imm);
for jm=1:iss(2)
itim=imm(jm);
PZ_ALL(1:6,1:6)=0.0;PZ_ALL(2,2:5)=PZ_EX(itim,13:16);PZ_ALL(3,2:5)=PZ_EX(itim,9:12);
PZ_ALL(4,2:5)=PZ_EX(itim,5:8);PZ_ALL(5,2:5)=PZ_EX(itim,1:4);%PZ_ALL(3,4)=0.0;

%
%  To smooth meshes by cubic smoothling spline method
%

%PZ_ALL
for icc=2:5
   if icc~=3
      valuey=csaps([10 20 30 40],PZ_ALL(icc,2:5),0.4,[0:10:50]);
   else
```

```
      PPIN=[PZ_ALL(icc,2:3),PZ_ALL(icc,5)];
      valuey=csaps([10 20 40],PPIN,0.4,[0:10:50]);
   end
   PZ_ALL(icc,:)=valuey;
end
%PZ_ALL
for jcc=1:6
   valuex=csaps([0 20 35 50 65],PZ_ALL(1:5,jcc),0.4,[0 20 35 50 65 75]);
   PZ_ALL(2:6,jcc)=valuex(2:6).';
end
%PZ_ALL
%
%
%mesh(PXX,PYY,PZ_ALL.');VIEW(150,50);
%
%
%pause
ky=3;knotsy=augknt([0 16.7 33.4 50],ky);
sp=spap2(knotsy,ky,PYY,PZ_ALL);
yy=[-2:2:52]; vals=fnval(sp,yy);
%mesh(PXX,yy,vals.');VIEW(150,50);
%
coefsy=fnbrk(sp,'c');
kx=3; knotsx=augknt([0 20 50 75],kx);
sp2=spap2(knotsx,kx,PXX,coefsy.');
coefs=fnbrk(sp2,'c').';
xv=[0:1.5:75]; yv=[0:1:50];
values=spcol(knotsx,kx,xv)*coefs*spcol(knotsy,ky,yv).';
%mesh(xv,yv,values.');
%[cs,h]=contour(xv,yv,values.',20);;
h=surf(xv,yv,values.'); view(0,90);colorbar;%axis([0 80 0 50 -20 50]);
%set(h,'FaceColor','interp','EdgeColor','none','FaceLighting','phong');
MM(:,jm)=getframe;
end
movie(MM,5,2);
```

Appendix D: Results for Experiments on Time Response

All data have the same format:

— : strain gage 1	— : strain gage 4	··· : strain gage 7
— : strain gage 2	— : strain gage 5	··· : strain gage 8
— : strain gage 3	— : strain gage 6	··· : strain gage 9

Refer to table 5.1 for the location, movement and focus of the electron beam

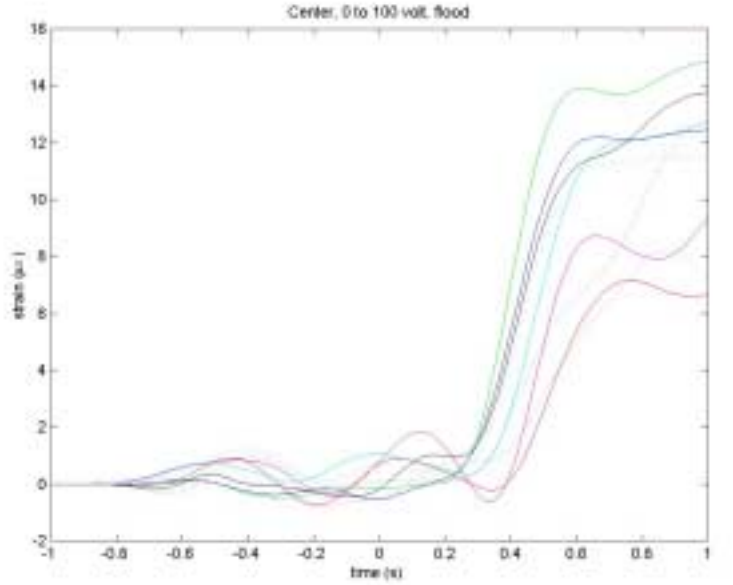

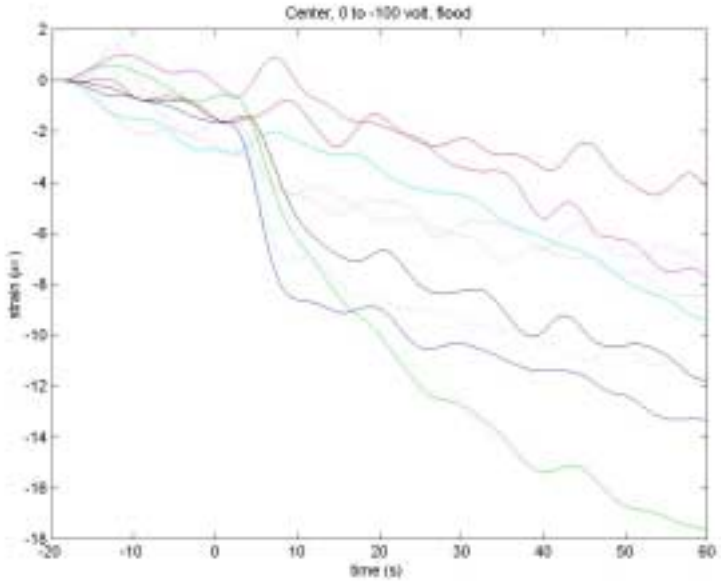

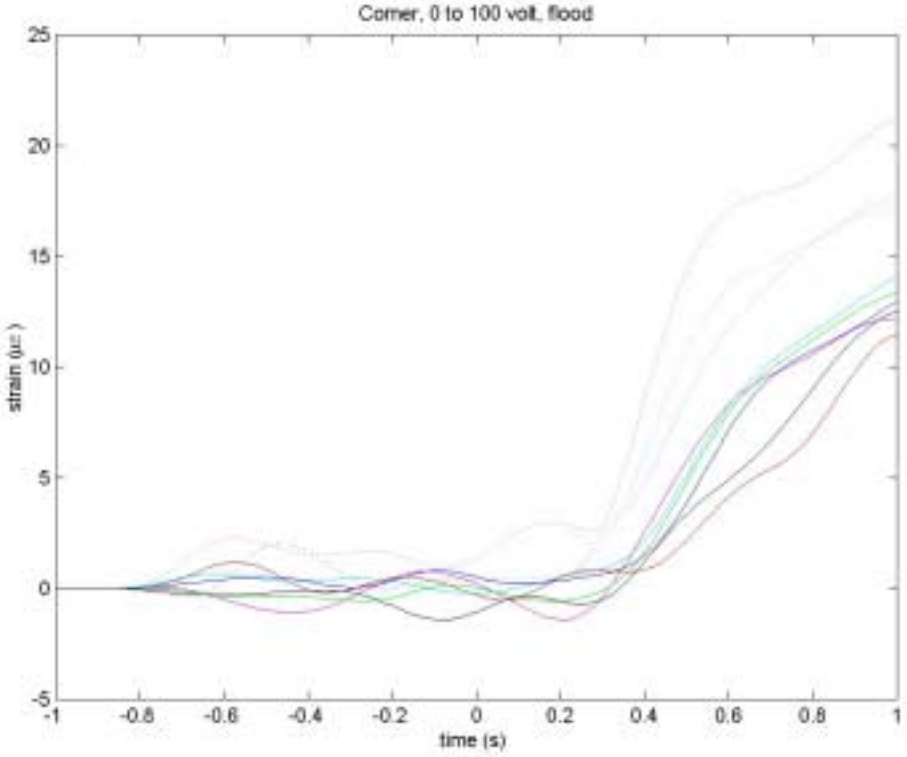
Corner, 0 to 100 volt, flood
strain (με)
time (s)
25
20
15
10
5
0
-5
-1
-0.8
-0.6
-0.4
-0.2
0
0.2
0.4
0.6
0.8
1

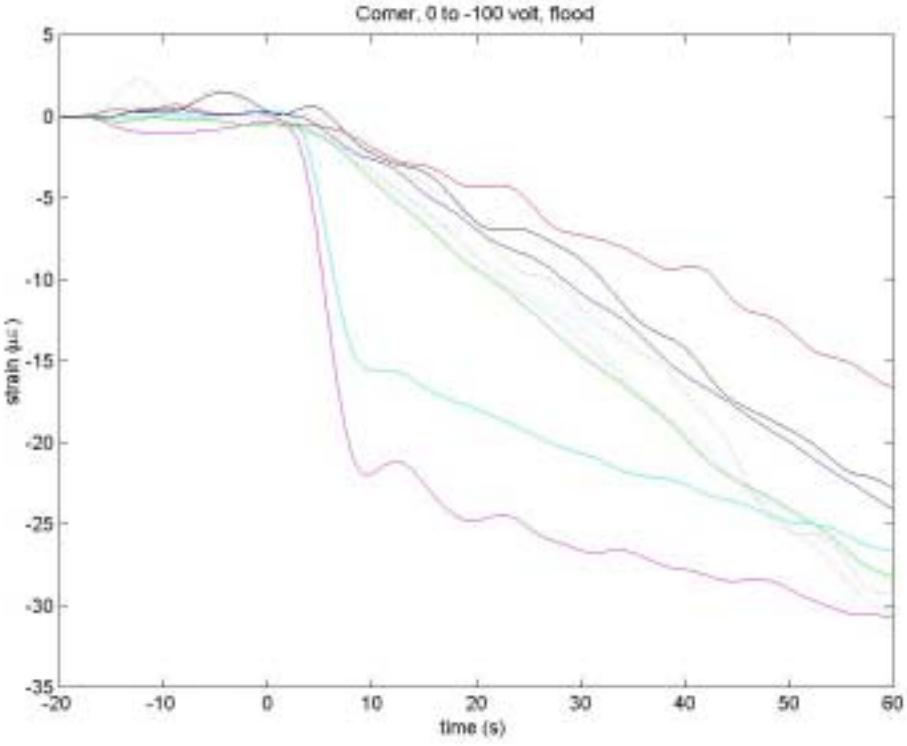
Corner, 0 to -100 volt, flood
strain (με)
time (s)
5
0
-5
-10
-15
-20
-25
-30
-35
-20
-10
0
10
20
30
40
50
60

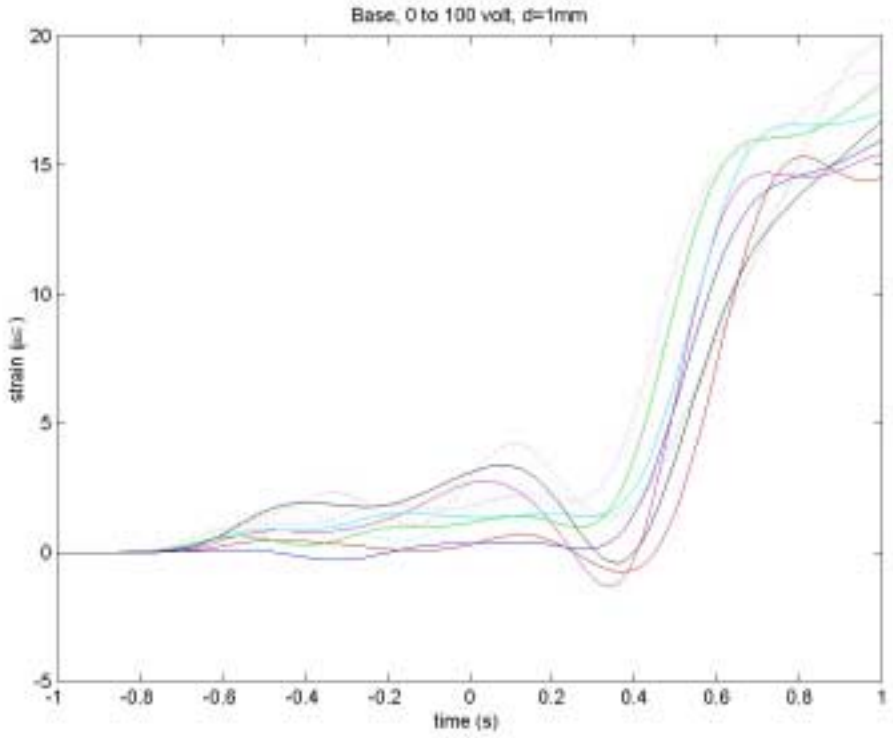
Base, 0 to 100 volt, d=1mm
strain (με)
time (s)
20
15
10
5
0
-5
-1
-0.8
-0.6
-0.4
-0.2
0
0.2
0.4
0.6
0.8
1

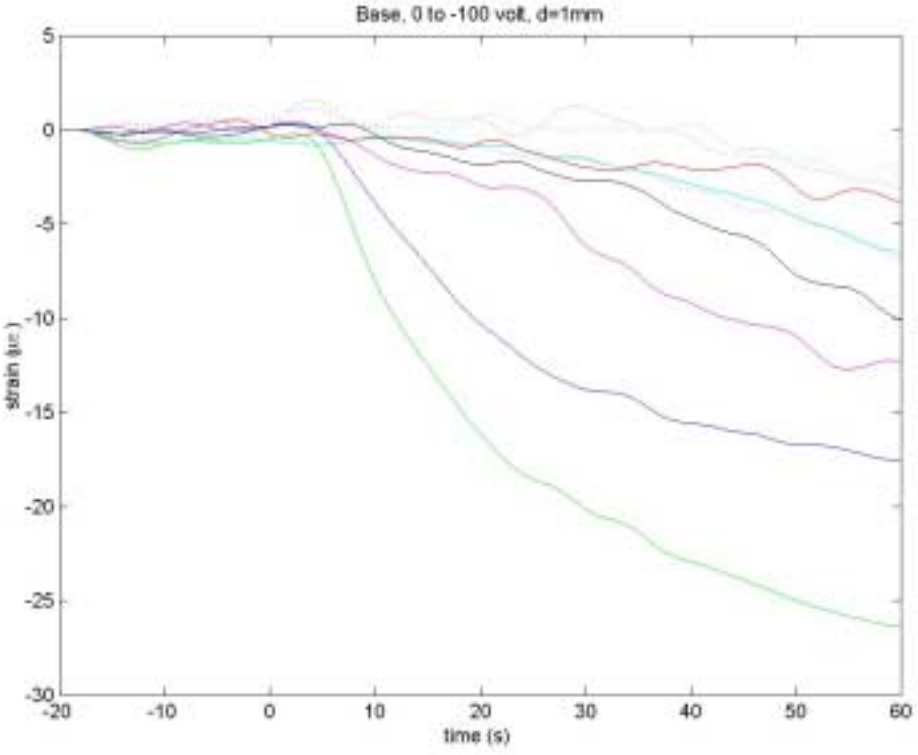
Base, 0 to -100 volt, d=1mm
strain (με)
time (s)
5
0
-5
-10
-15
-20
-25
-30
-20
-10
0
10
20
30
40
50
60

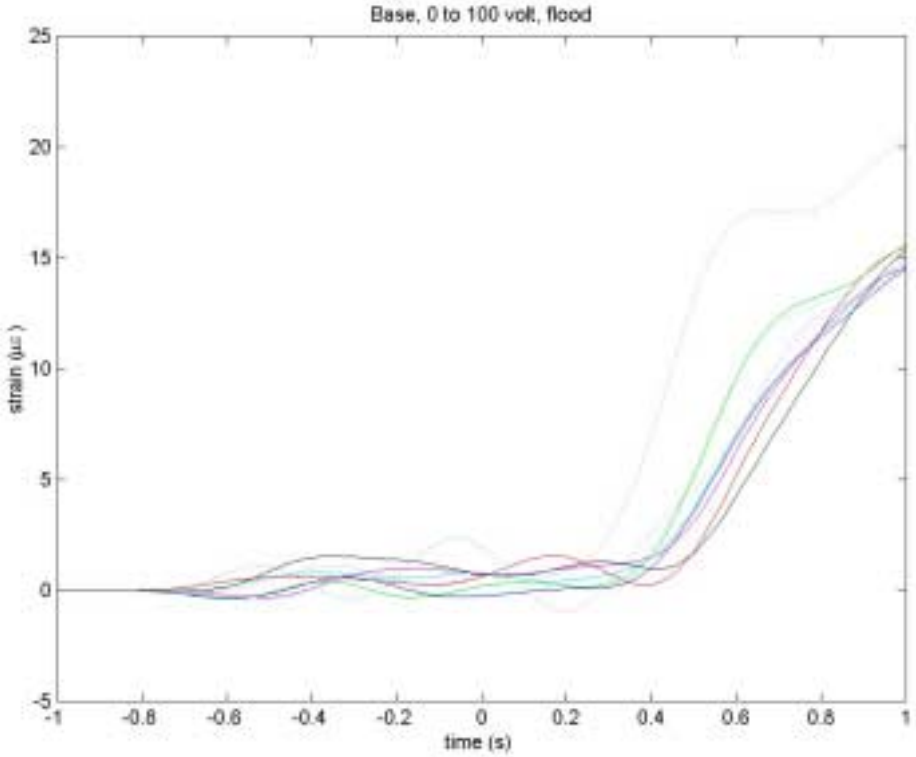
Base, 0 to 100 volt, flood
strain (με)
time (s)

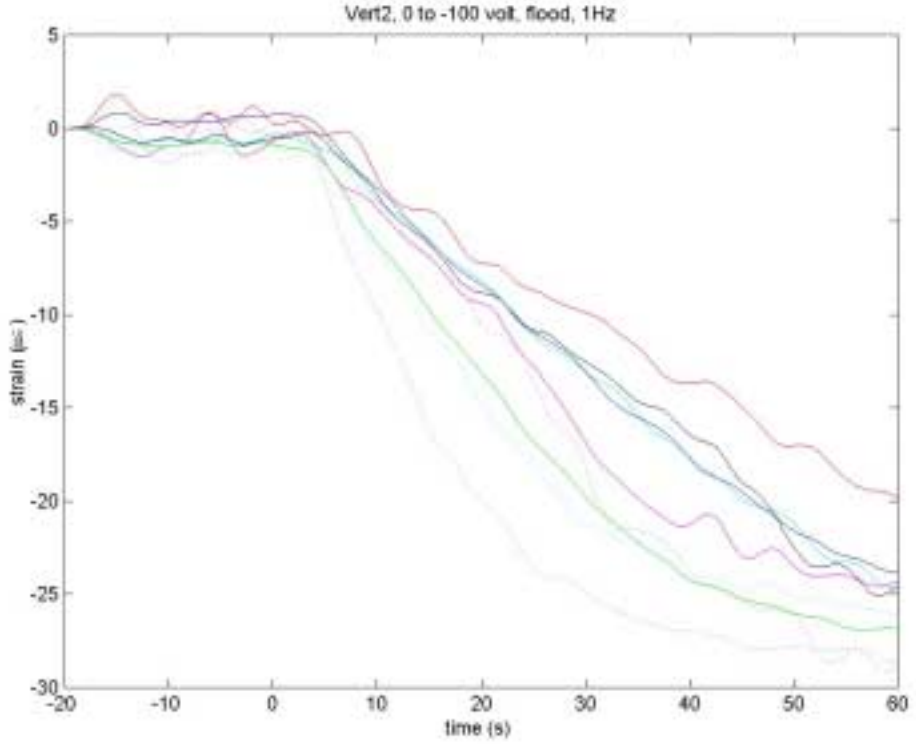
Vert2, 0 to -100 volt, flood, 1Hz
strain (με)
time (s)

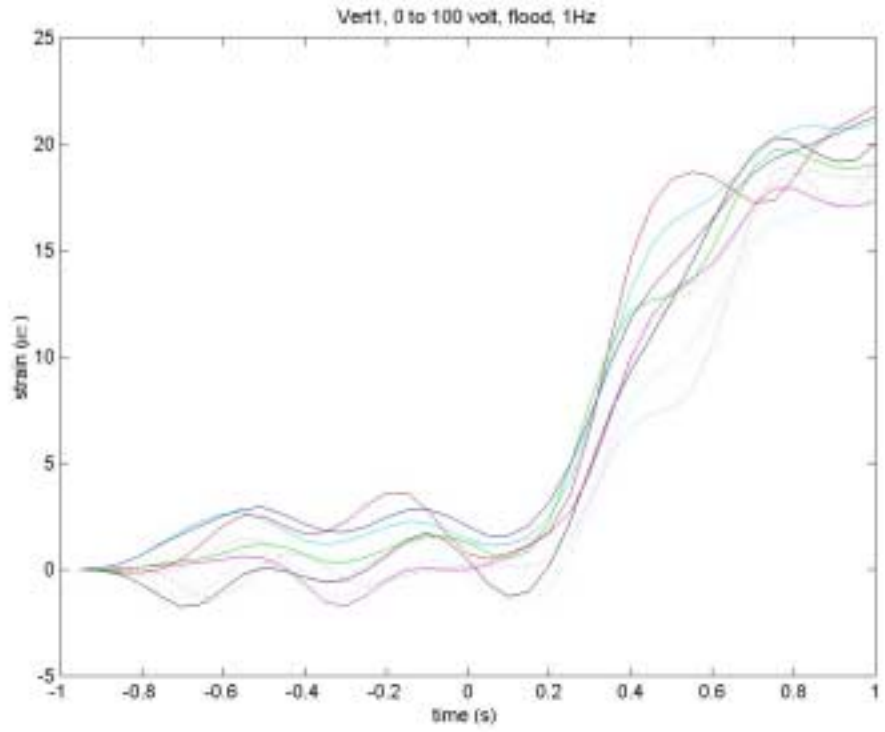
Vert1, 0 to 100 volt, flood, 1Hz
strain (με)
time (s)
25
20
15
10
5
0
-5
-1
-0.8
-0.6
-0.4
-0.2
0
0.2
0.4
0.6
0.8
1

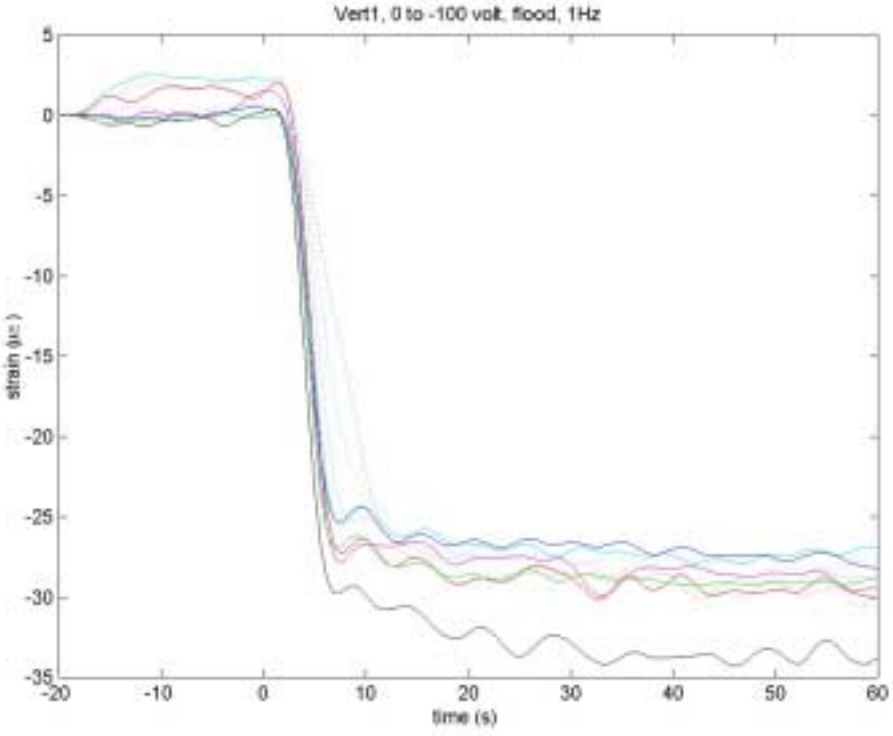
Vert1, 0 to -100 volt, flood, 1Hz
strain (με)
time (s)
5
0
-5
-10
-15
-20
-25
-30
-35
-20
-10
0
10
20
30
40
50
60

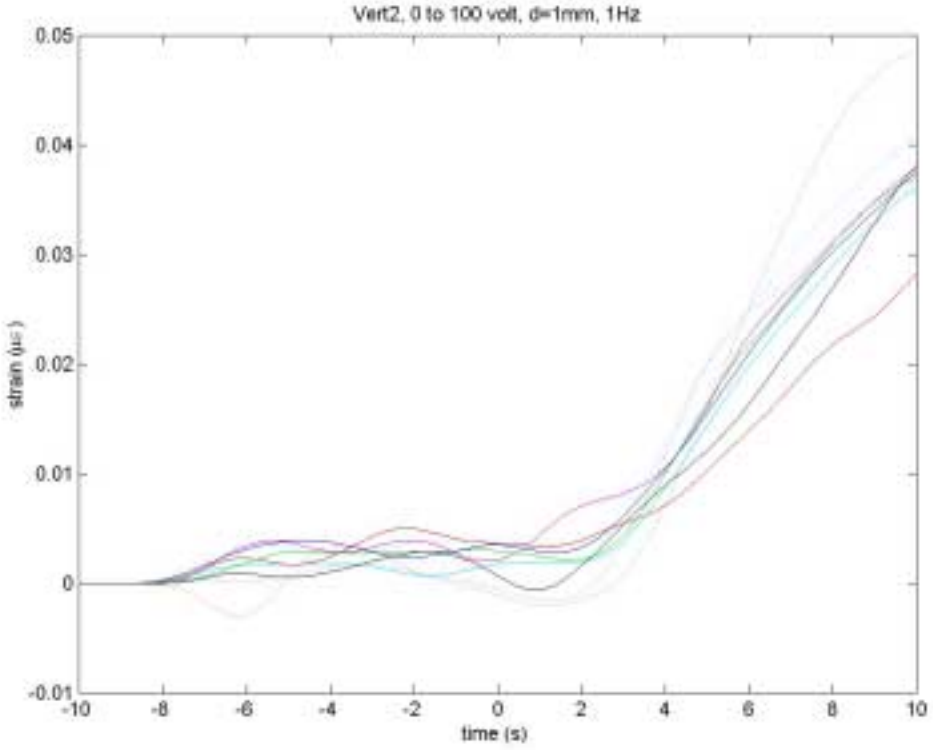
Vert2, 0 to 100 volt, d=1mm, 1Hz
strain (με)
time (s)
0.05
0.04
0.03
0.02
0.01
0
-0.01
-10
-8
-6
-4
-2
0
2
4
6
8
10

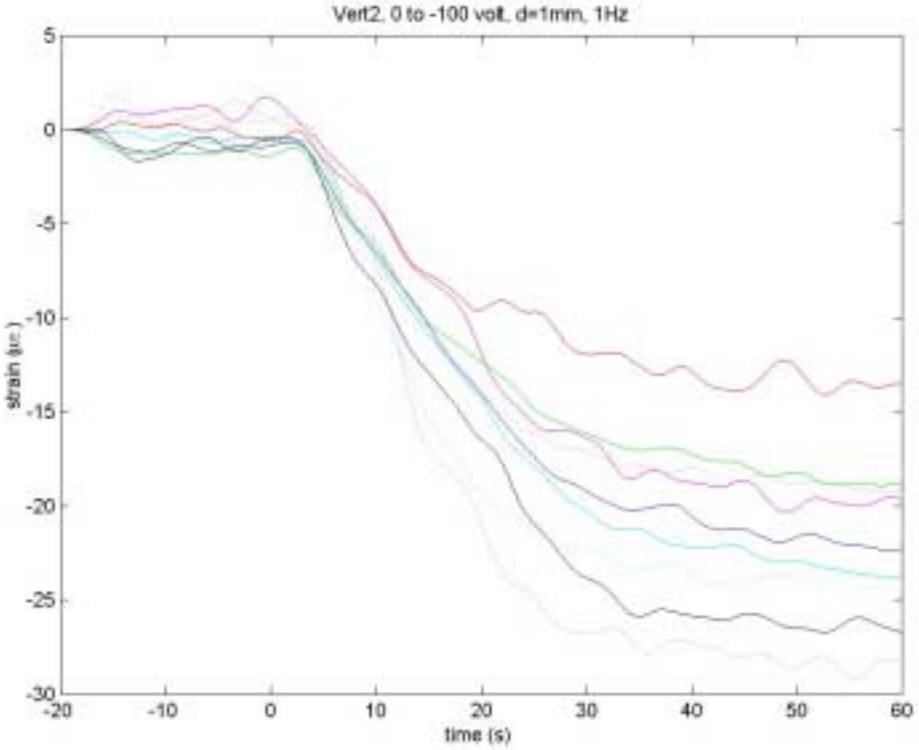
Vert2, 0 to -100 volt, d=1mm, 1Hz
strain (με)
time (s)
5
0
-5
-10
-15
-20
-25
-30
-20
-10
0
10
20
30
40
50
60

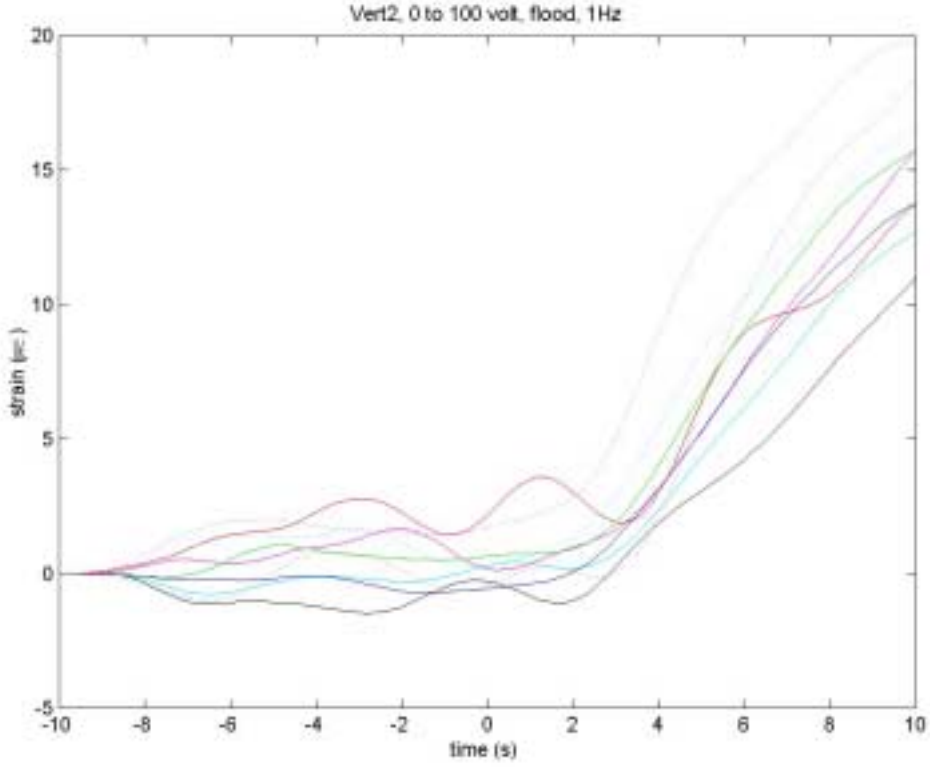
Vert2, 0 to 100 volt, flood, 1Hz
strain (με)
time (s)
20
15
10
5
0
-5
-10
-8
-6
-4
-2
0
2
4
6
8
10

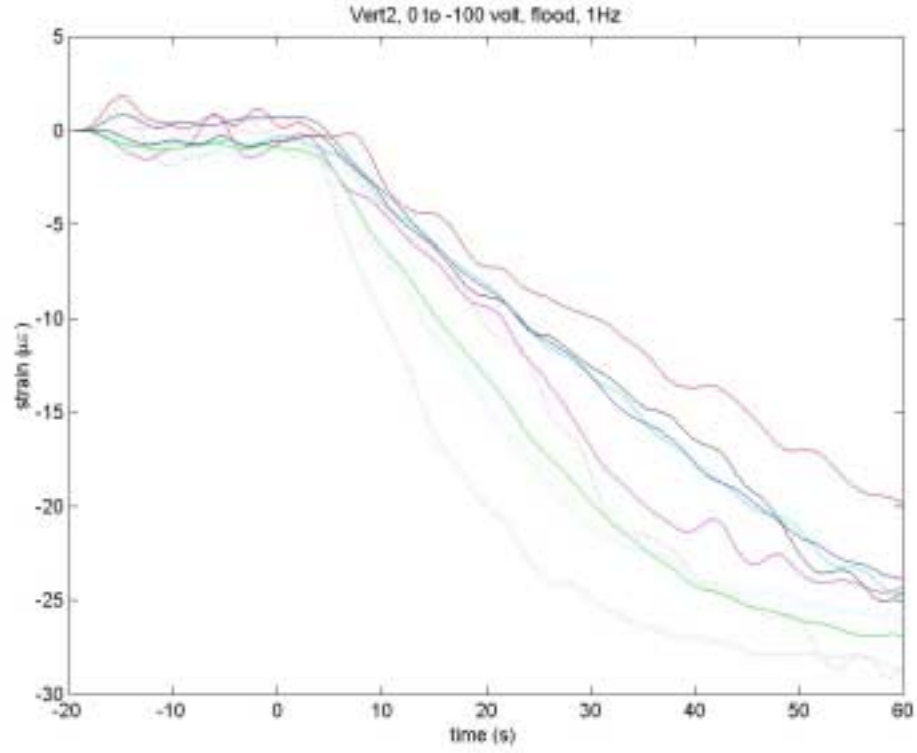
Vert2, 0 to -100 volt, flood, 1Hz
strain (με)
time (s)
5
0
-5
-10
-15
-20
-25
-30
-20
-10
0
10
20
30
40
50
60

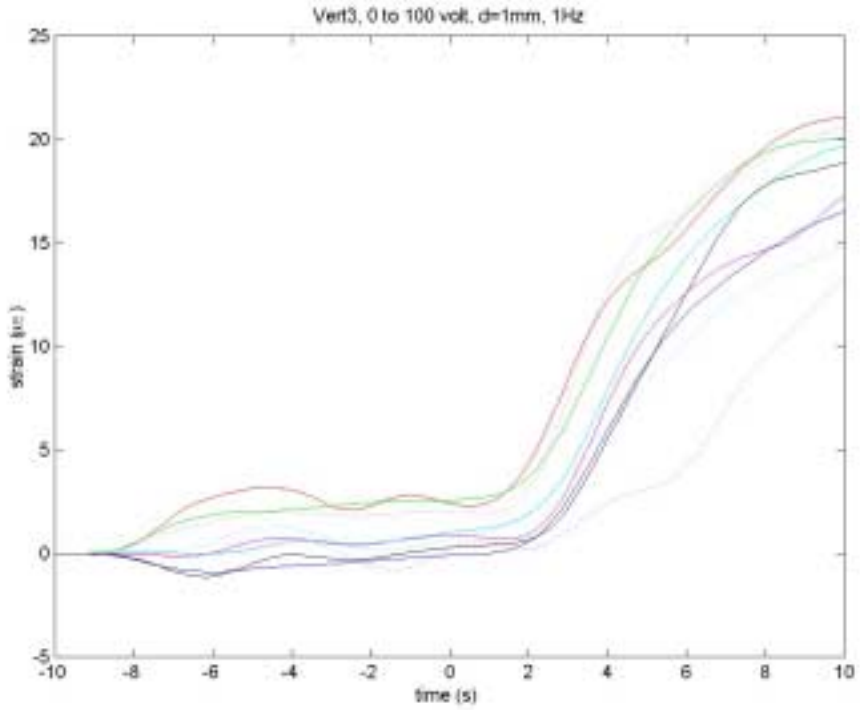
Vert3, 0 to 100 volt, d=1mm, 1Hz
strain (με)
time (s)

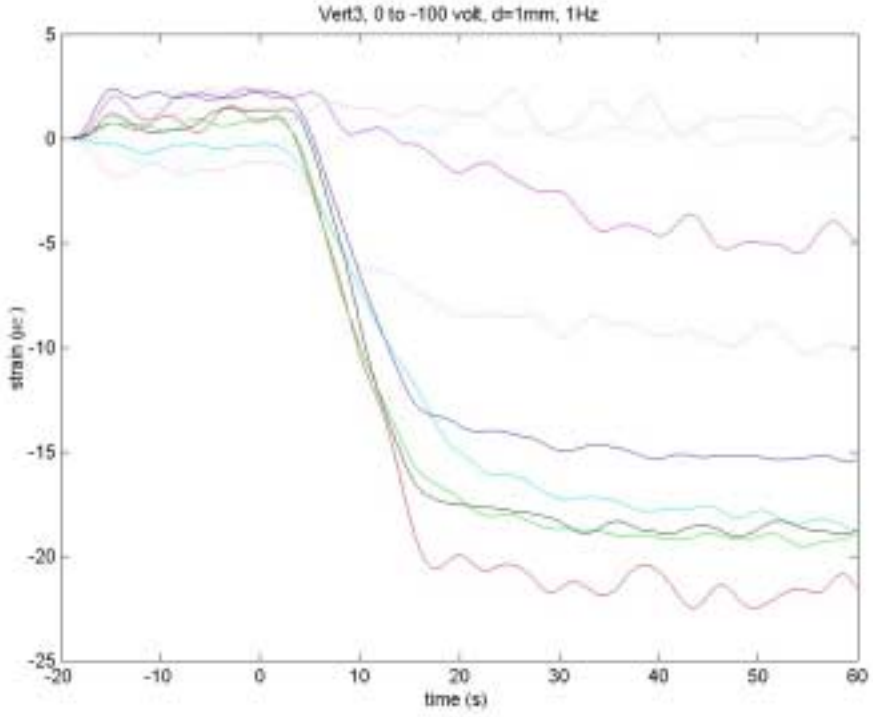
Vert3, 0 to -100 volt, d=1mm, 1Hz
strain (με)
time (s)

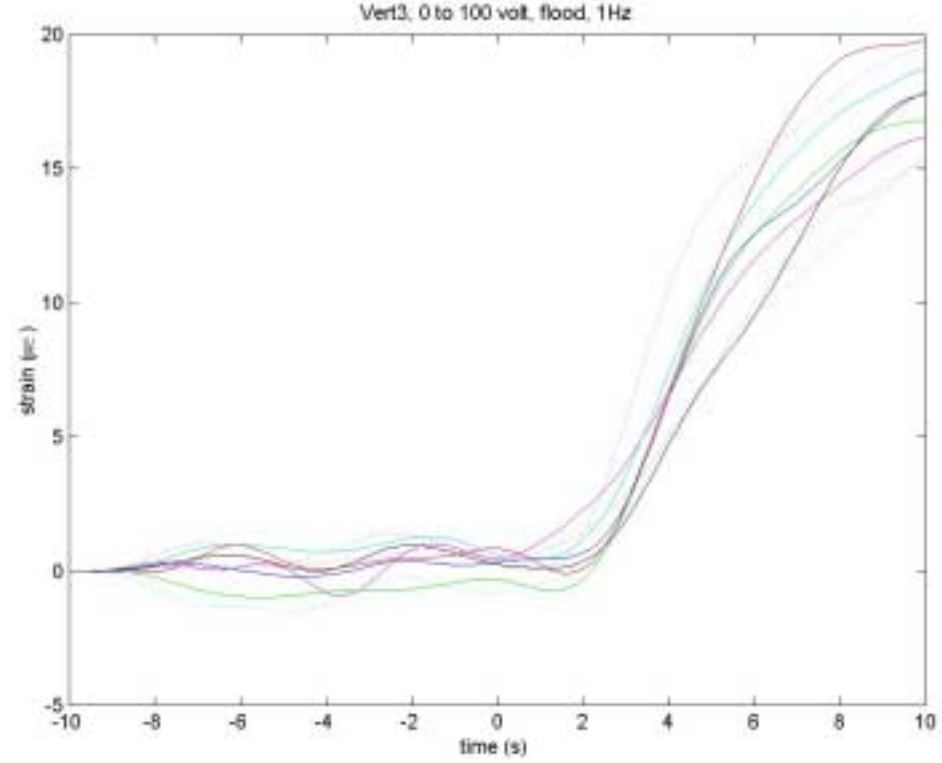
Vert3, 0 to 100 volt, flood, 1Hz
strain (με)
time (s)
20
15
10
5
0
-5
-10
-8
-6
-4
-2
0
2
4
6
8
10

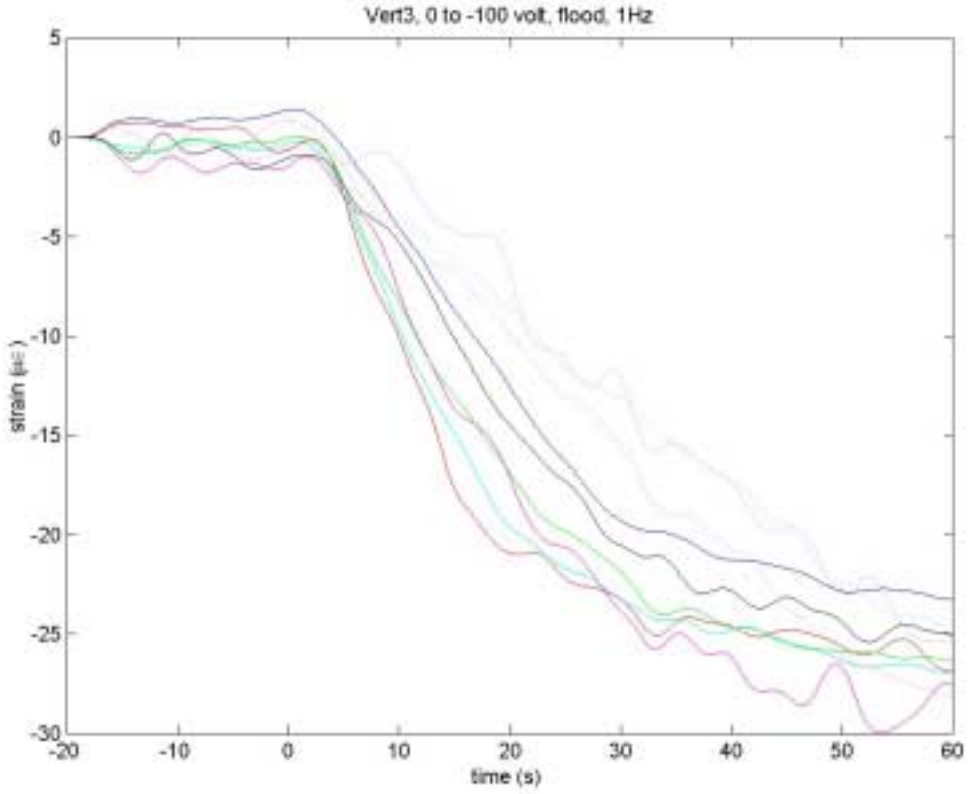
Vert3, 0 to -100 volt, flood, 1Hz
strain (με)
time (s)
5
0
-5
-10
-15
-20
-25
-30
-20
-10
0
10
20
30
40
50
60

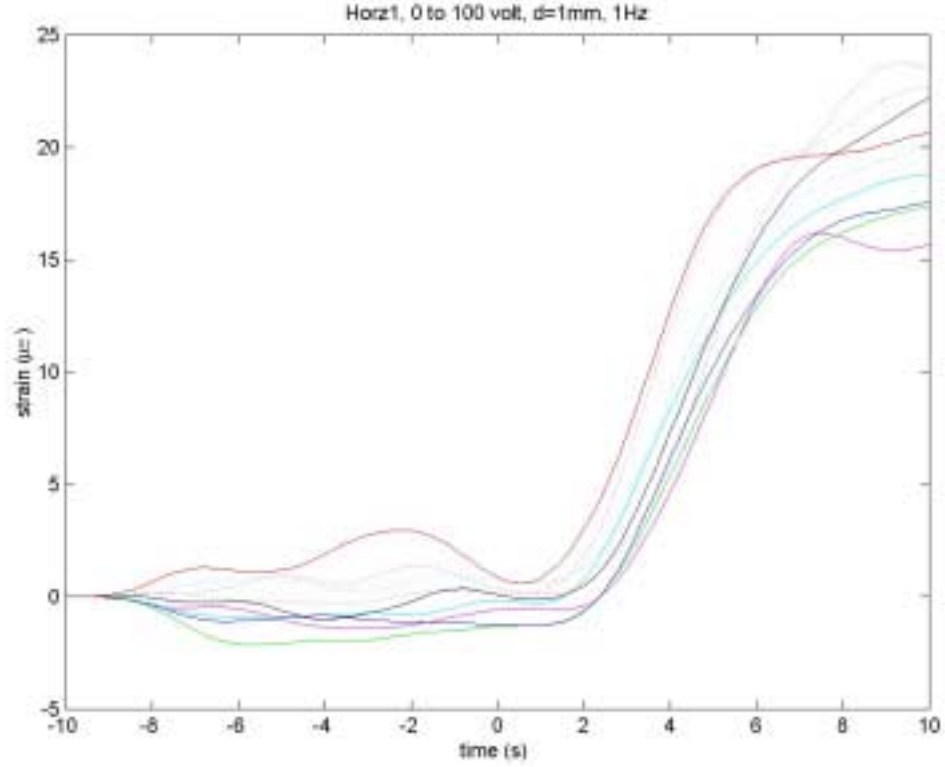
Horz1, 0 to 100 volt, d=1mm, 1Hz
strain (με)
time (s)
25
20
15
10
5
0
-5
-10
-8
-6
-4
-2
0
2
4
6
8
10

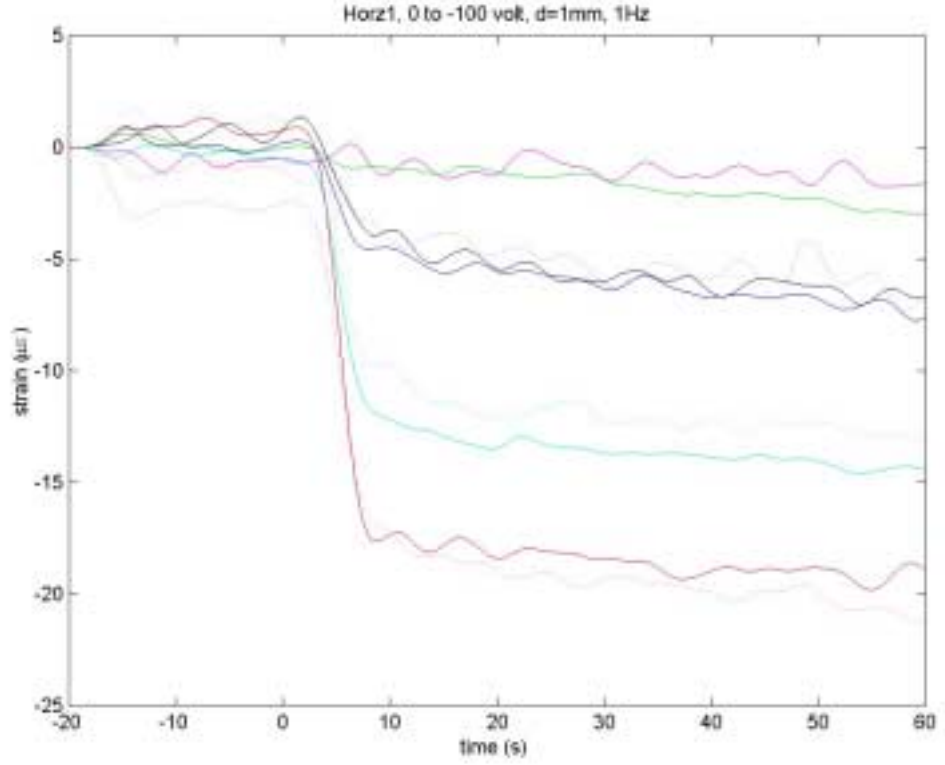
Horz1, 0 to -100 volt, d=1mm, 1Hz
strain (με)
time (s)
5
0
-5
-10
-15
-20
-25
-20
-10
0
10
20
30
40
50
60

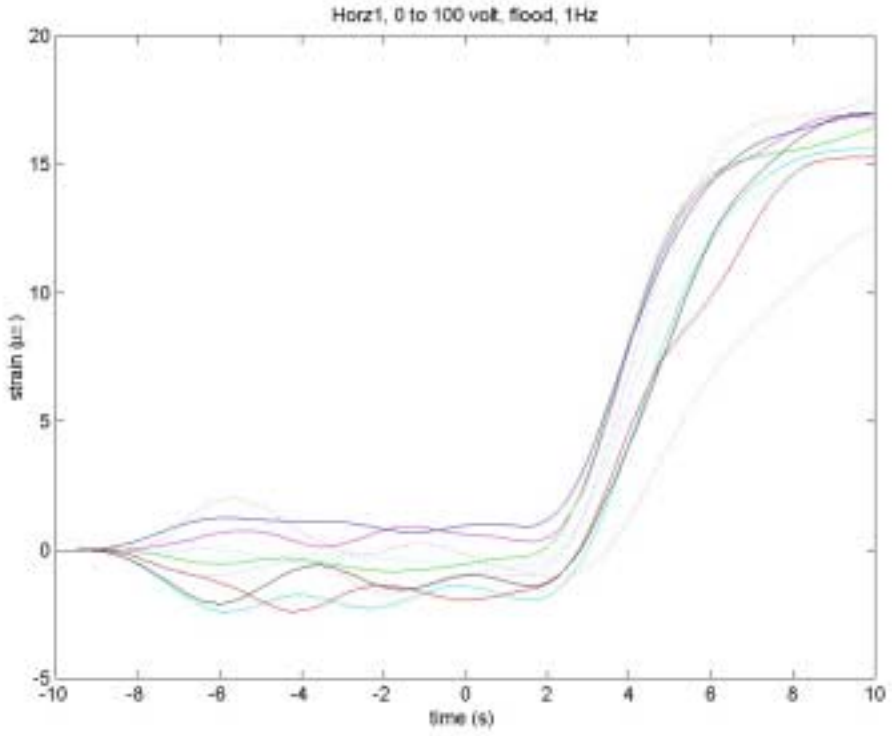
Horz1, 0 to 100 volt, flood, 1Hz
strain (με)
time (s)
20
15
10
5
0
-5
-10
-8
-6
-4
-2
0
2
4
6
8
10

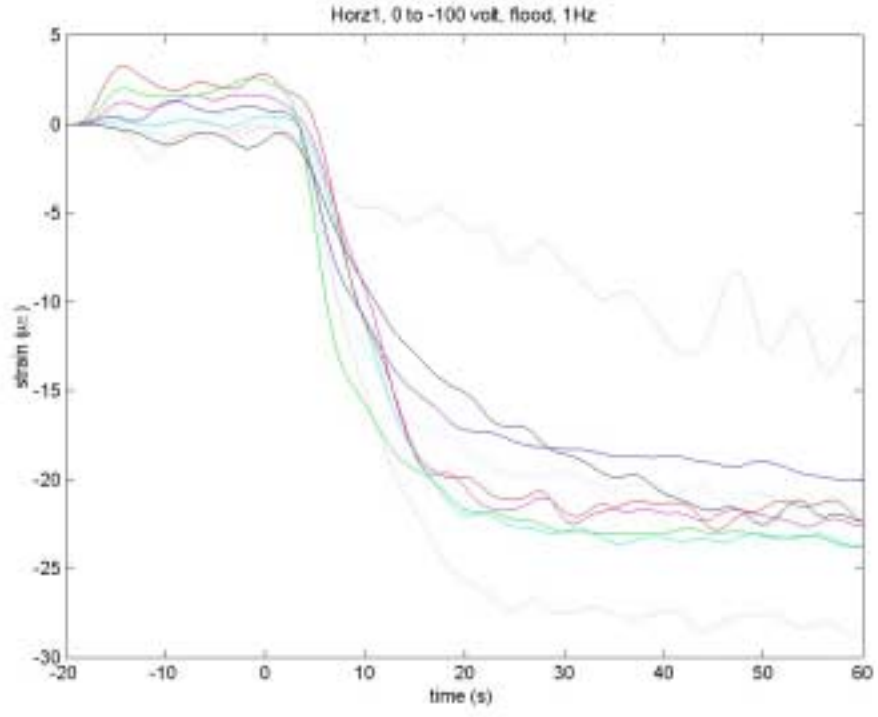
Horz1, 0 to -100 volt, flood, 1Hz
strain (με)
time (s)
5
0
-5
-10
-15
-20
-25
-30
-20
-10
0
10
20
30
40
50
60

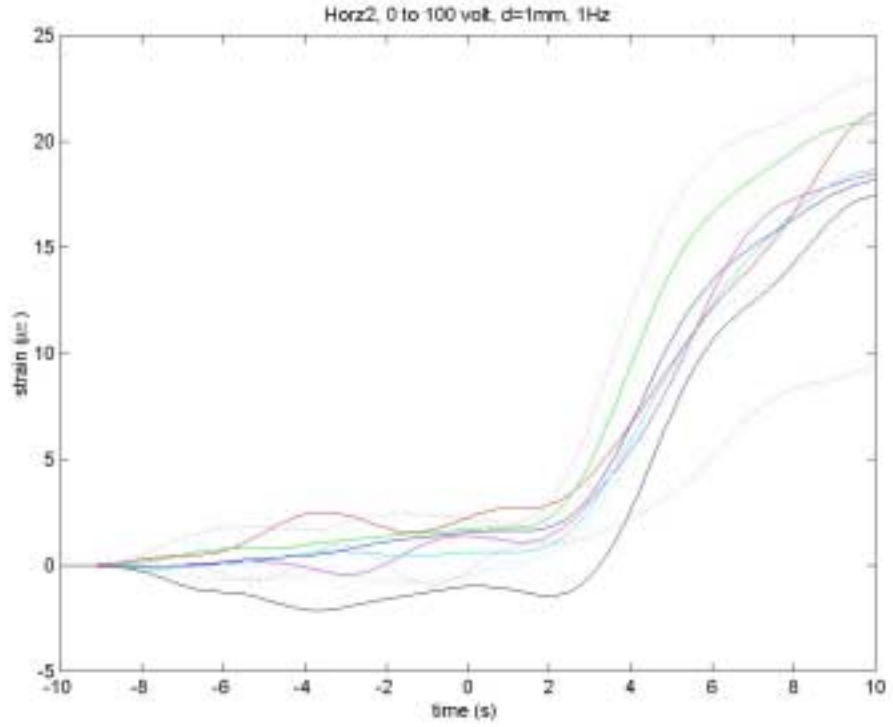
Horz2, 0 to 100 volt, d=1mm, 1Hz
strain (με)
time (s)
25
20
15
10
5
0
-5
-10
-8
-6
-4
-2
0
2
4
6
8
10

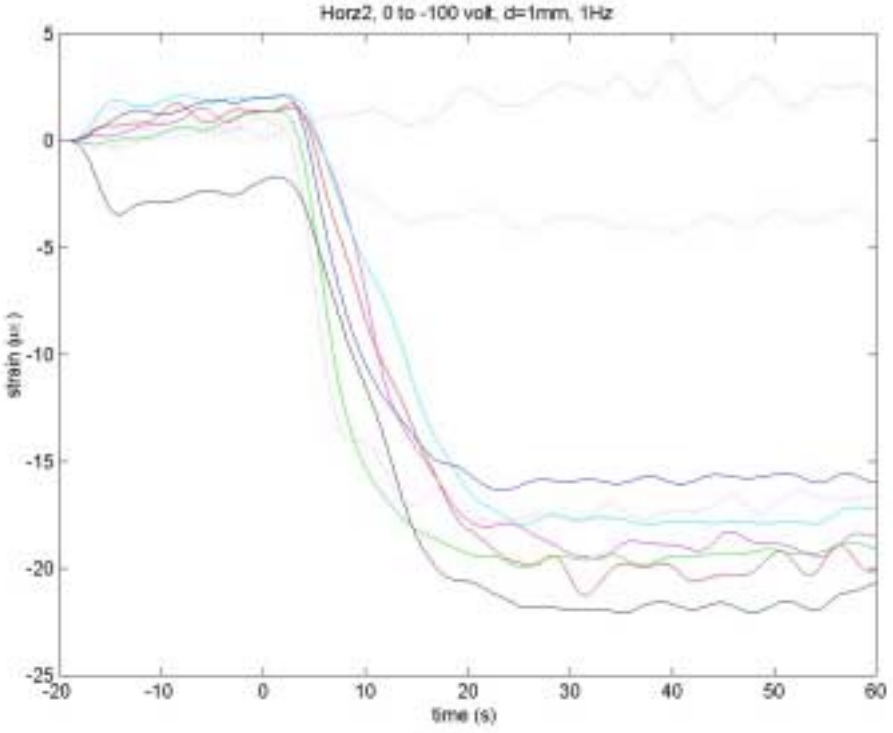
Horz2, 0 to -100 volt, d=1mm, 1Hz
strain (με)
time (s)
5
0
-5
-10
-15
-20
-25
-20
-10
0
10
20
30
40
50
60

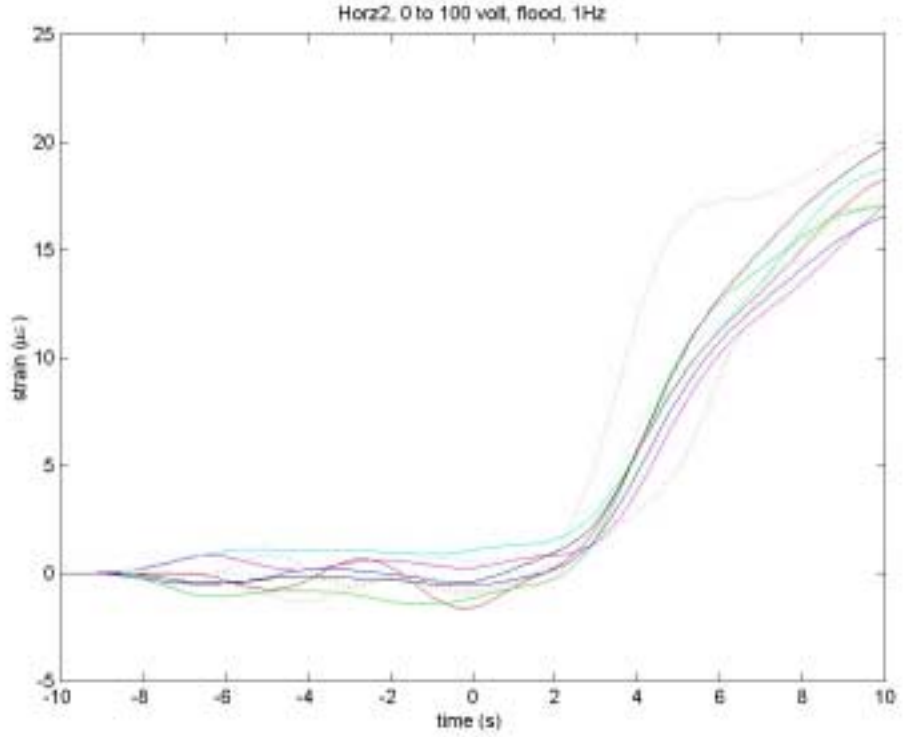
Horz2, 0 to 100 volt, flood, 1Hz
strain (με)
time (s)

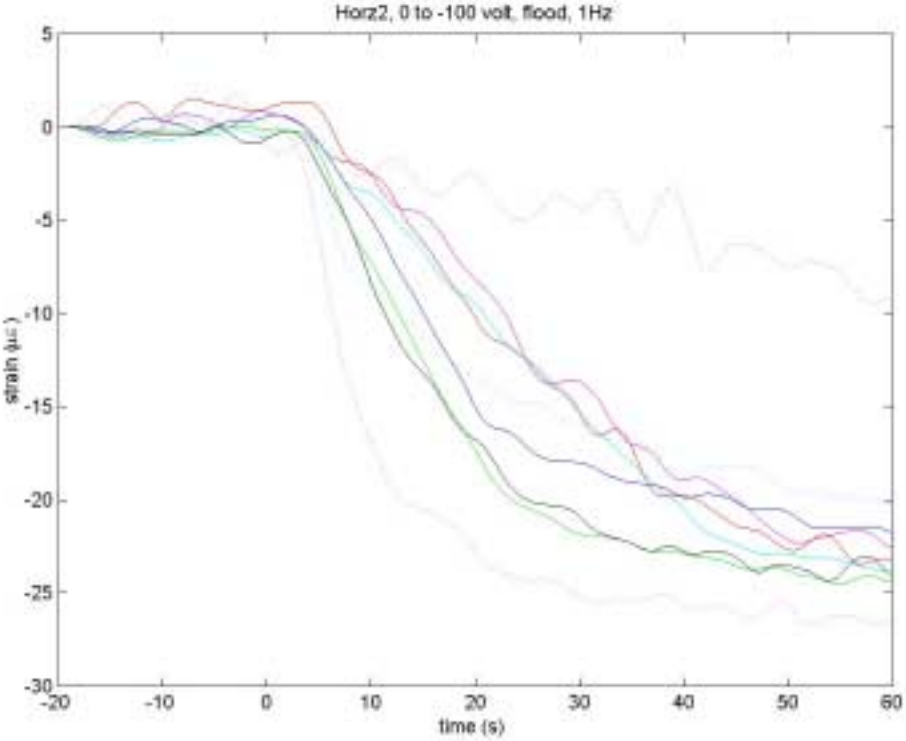
Horz2, 0 to -100 volt, flood, 1Hz
strain (με)
time (s)

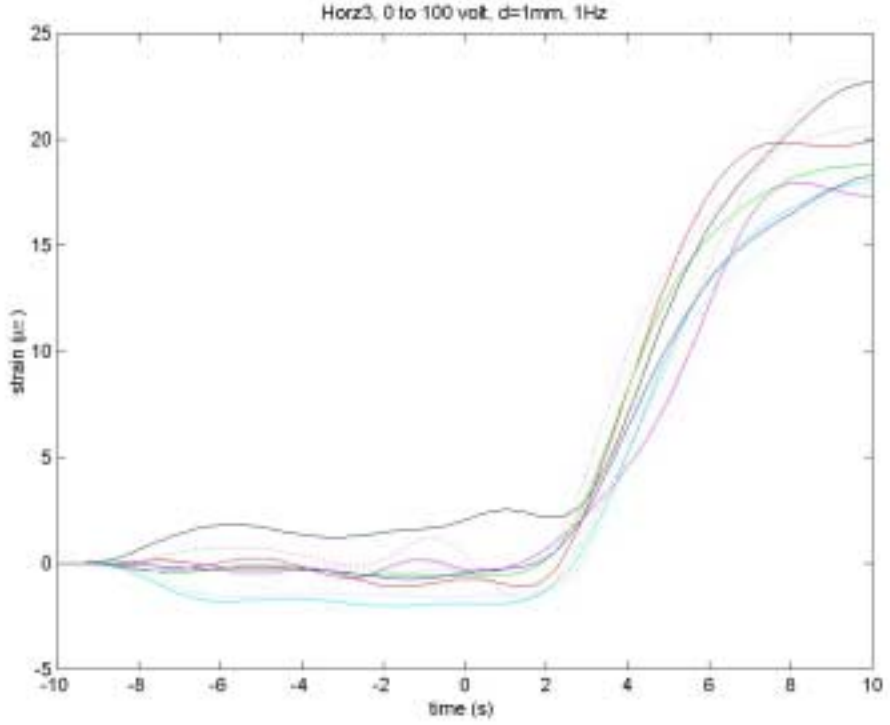
Horz3, 0 to 100 volt, d=1mm, 1Hz
strain (με)
time (s)
25
20
15
10
5
0
-5
-10
-8
-6
-4
-2
0
2
4
6
8
10

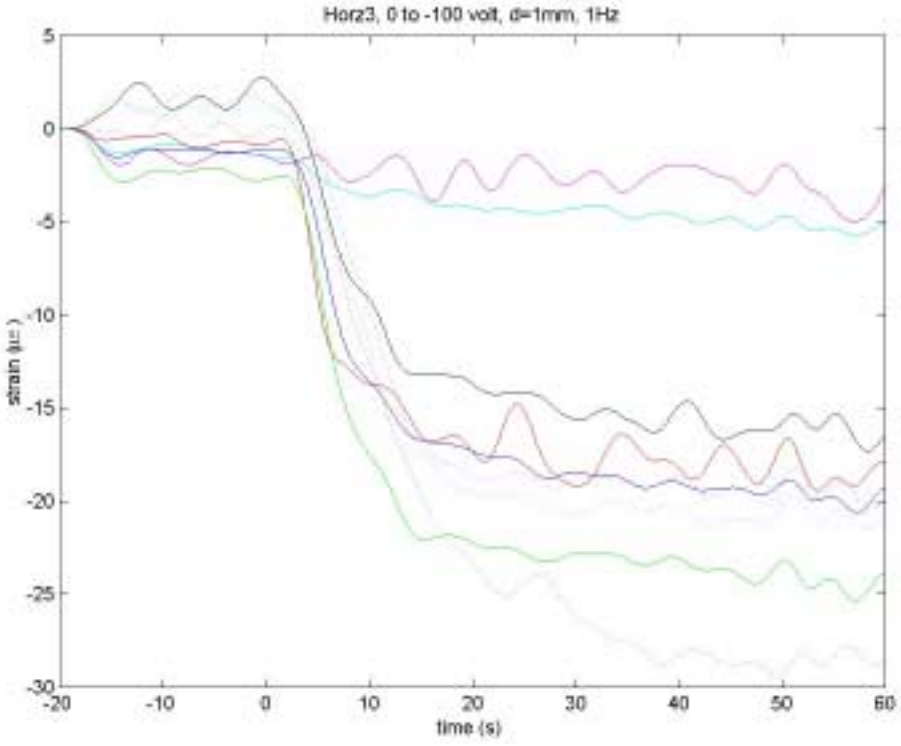
Horz3, 0 to -100 volt, d=1mm, 1Hz
strain (με)
time (s)
5
0
-5
-10
-15
-20
-25
-30
-20
-10
0
10
20
30
40
50
60

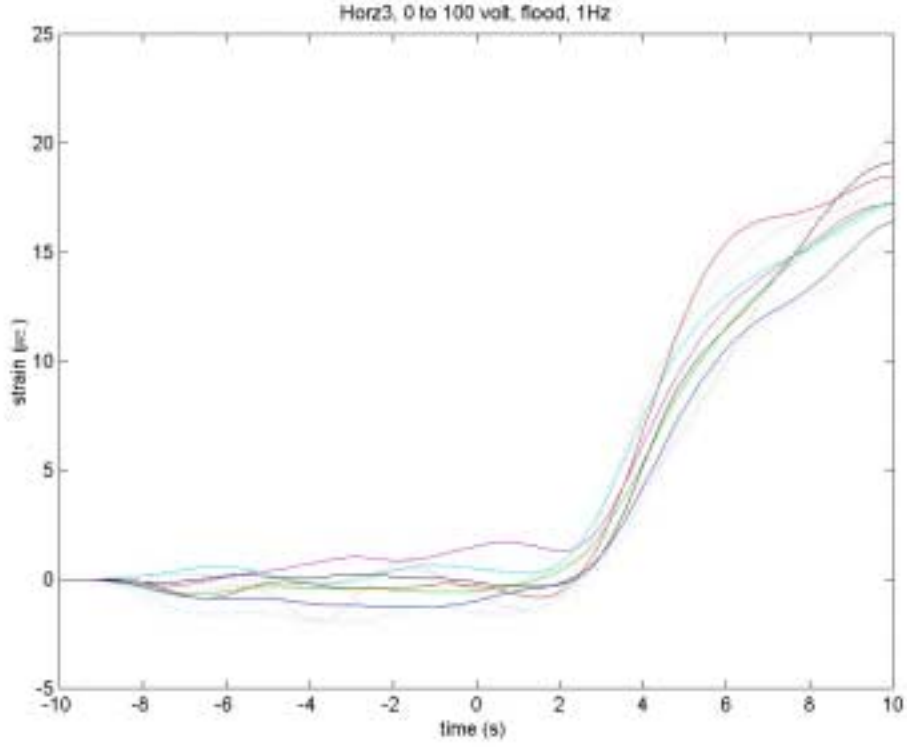
Horz3, 0 to 100 volt, flood, 1Hz
strain (με)
time (s)
25
20
15
10
5
0
-5
-10
-8
-6
-4
-2
0
2
4
6
8
10

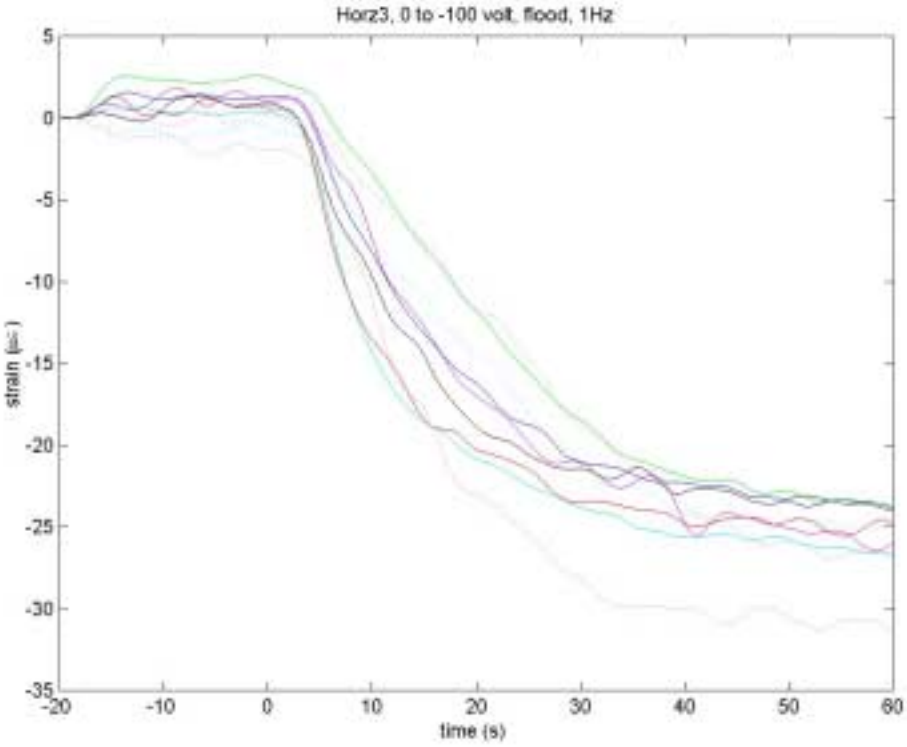
Horz3, 0 to -100 volt, flood, 1Hz
strain (με)
time (s)
5
0
-5
-10
-15
-20
-25
-30
-35
-20
-10
0
10
20
30
40
50
60

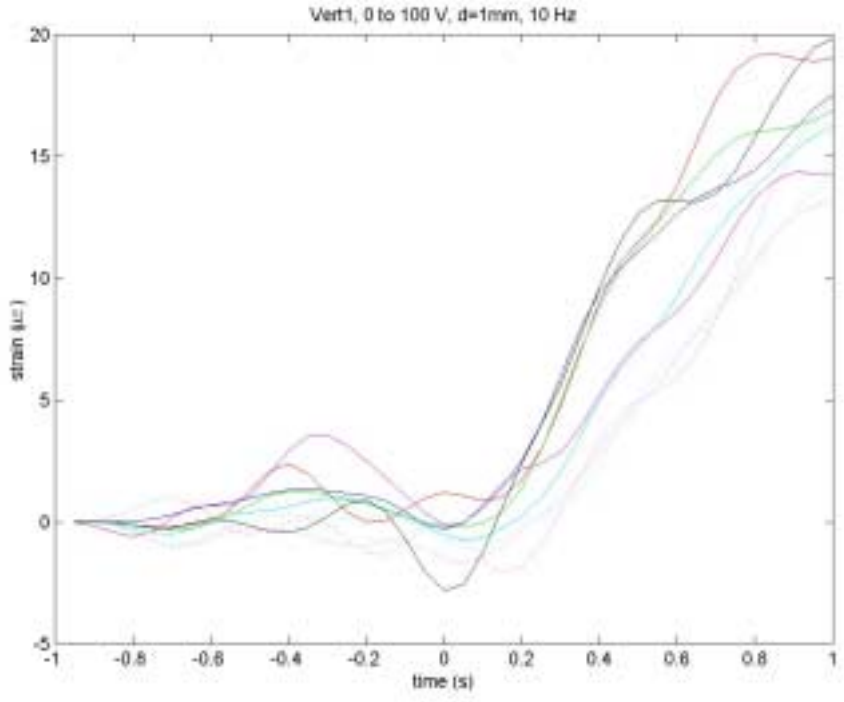
Vert1, 0 to 100 V, d=1mm, 10 Hz
strain (με)
time (s)
20
15
10
5
0
-5
-1
-0.8
-0.6
-0.4
-0.2
0
0.2
0.4
0.6
0.8
1

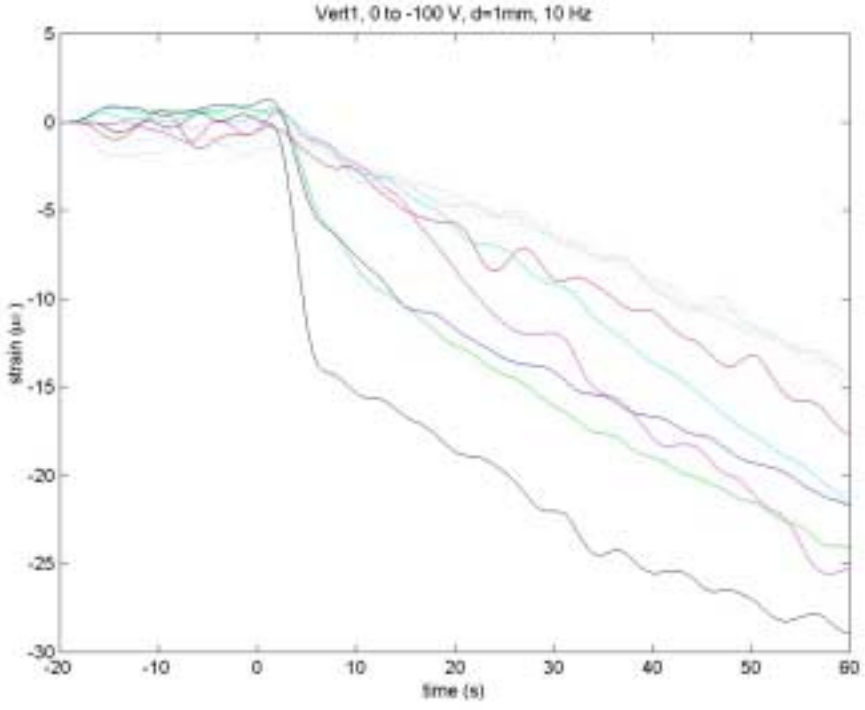
Vert1, 0 to -100 V, d=1mm, 10 Hz
strain (με)
time (s)
5
0
-5
-10
-15
-20
-25
-30
-20
-10
0
10
20
30
40
50
60

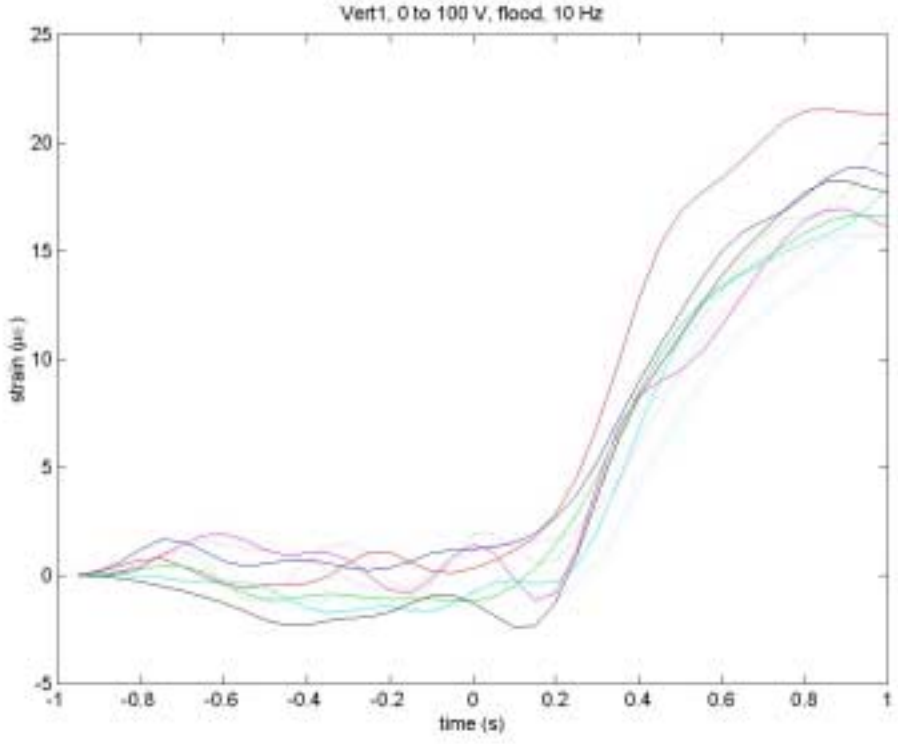
Vert1, 0 to 100 V, flood, 10 Hz
strain (με)
time (s)
25
20
15
10
5
0
-5
-1
-0.8
-0.6
-0.4
-0.2
0
0.2
0.4
0.6
0.8
1

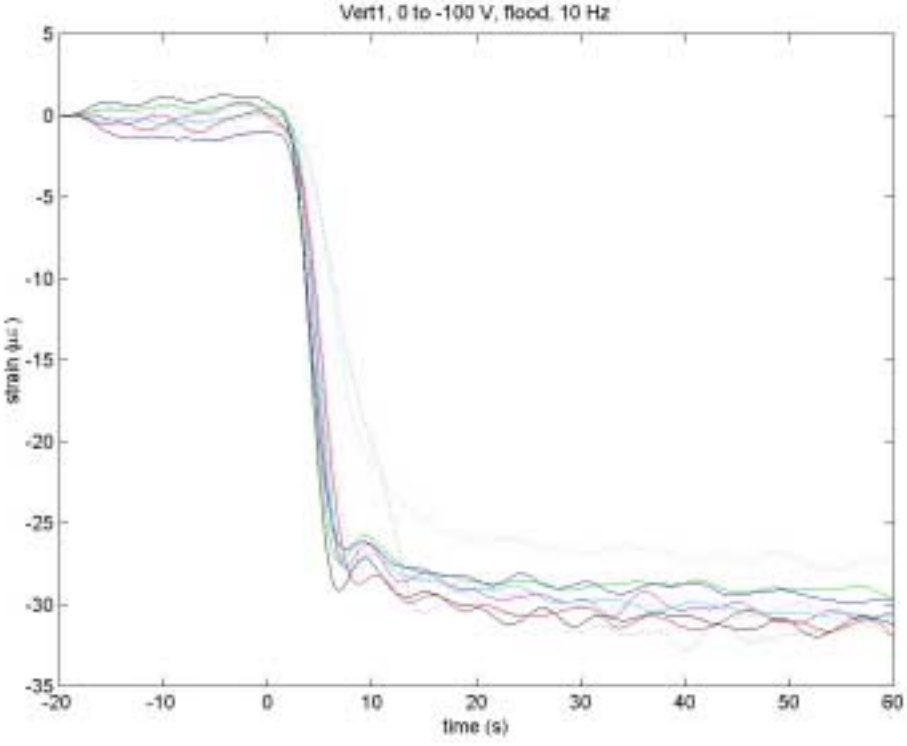
Vert1, 0 to -100 V, flood, 10 Hz
strain (με)
time (s)
5
0
-5
-10
-15
-20
-25
-30
-35
-20
-10
0
10
20
30
40
50
60

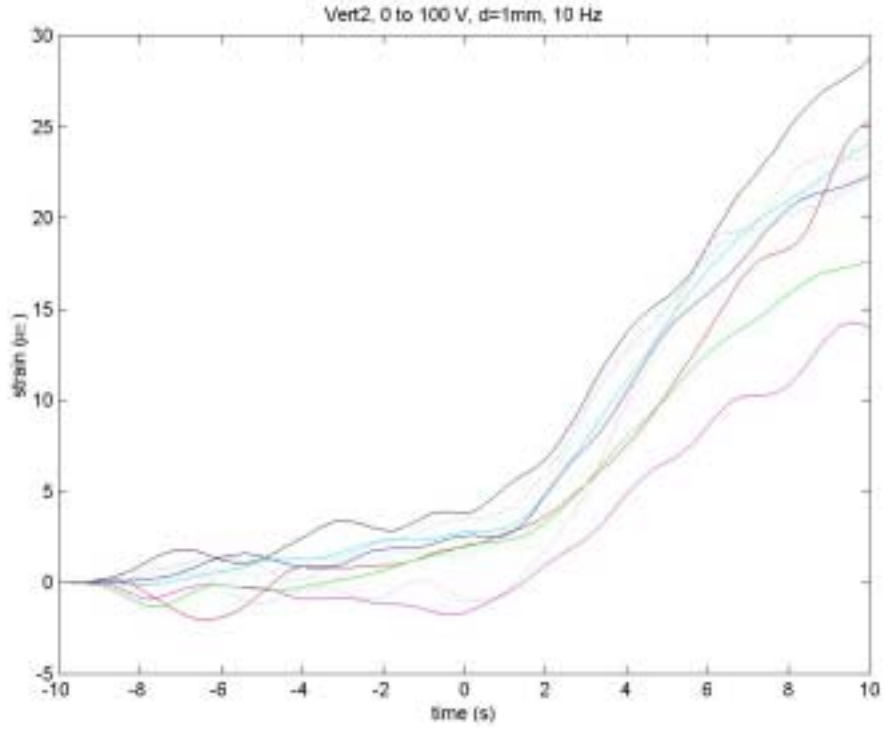
Vert2, 0 to 100 V, d=1mm, 10 Hz
strain (με)
time (s)

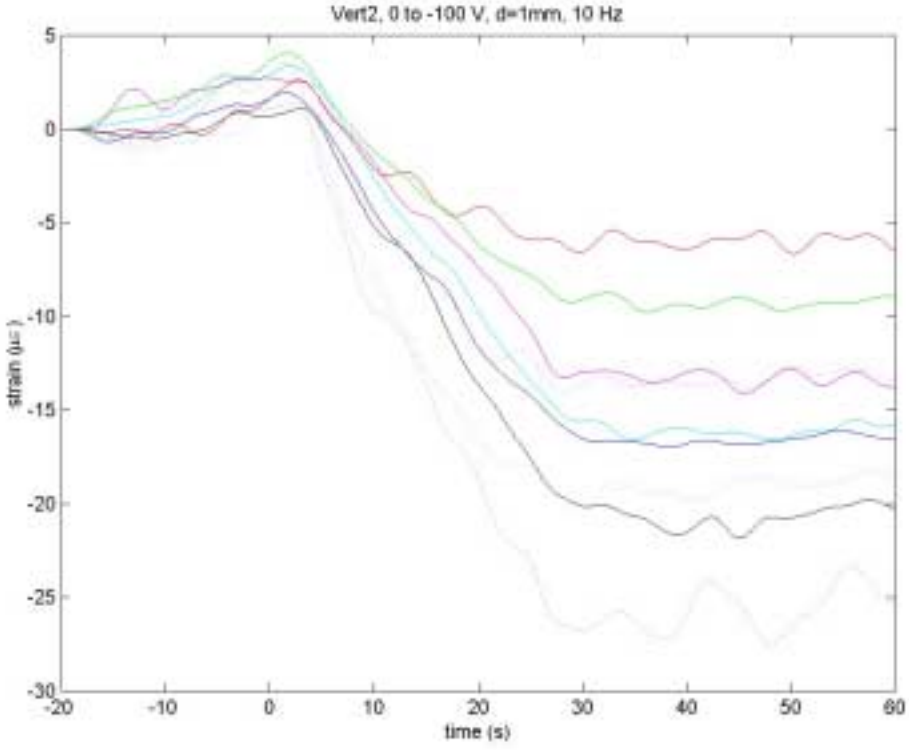
Vert2, 0 to -100 V, d=1mm, 10 Hz
strain (με)
time (s)

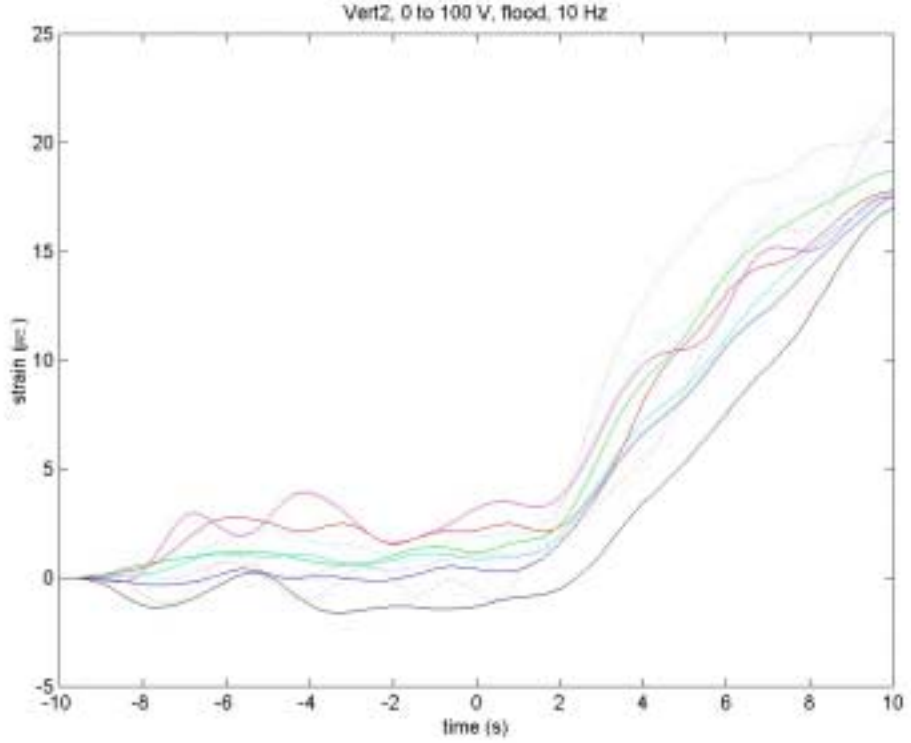
Vert2, 0 to 100 V, flood, 10 Hz
strain (με)
time (s)

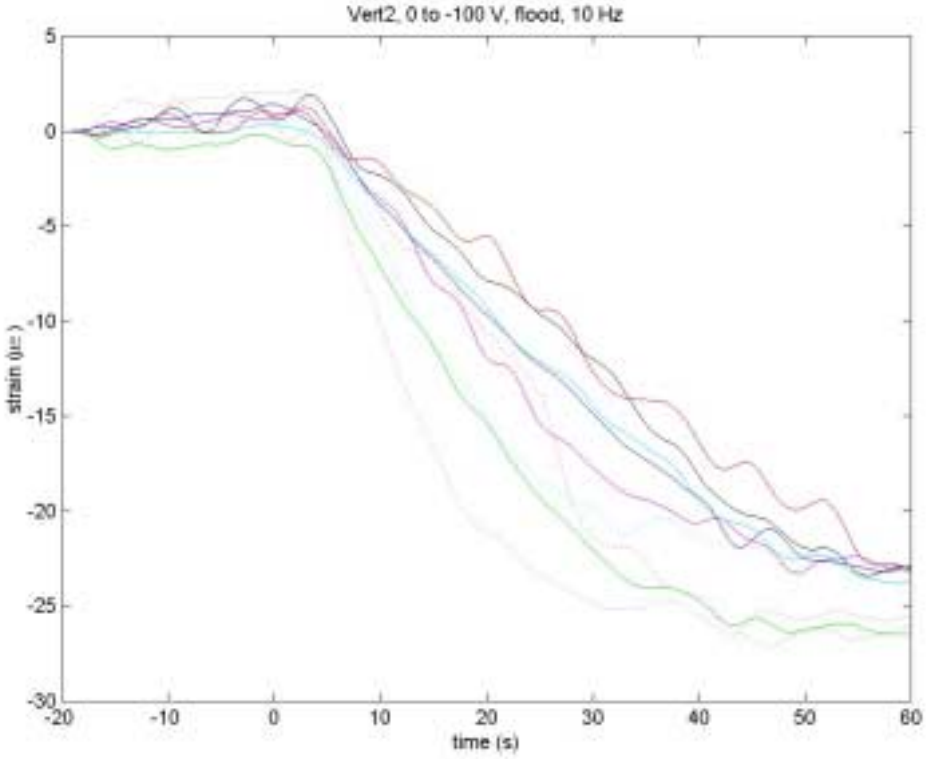
Vert2, 0 to -100 V, flood, 10 Hz
strain (με)
time (s)

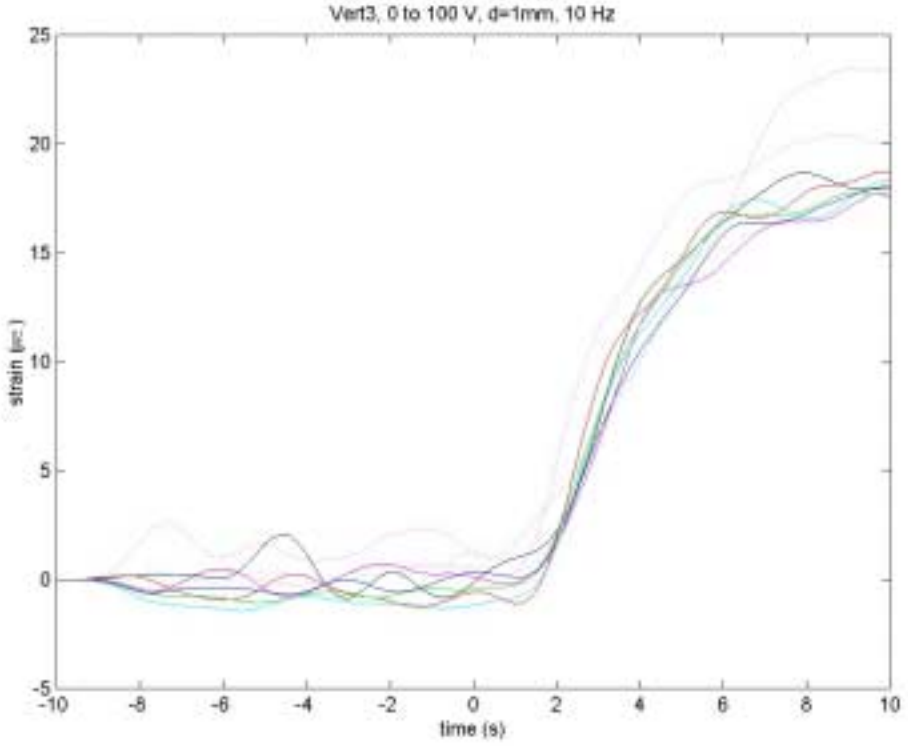
Vert3, 0 to 100 V, d=1mm, 10 Hz
strain (με)
time (s)

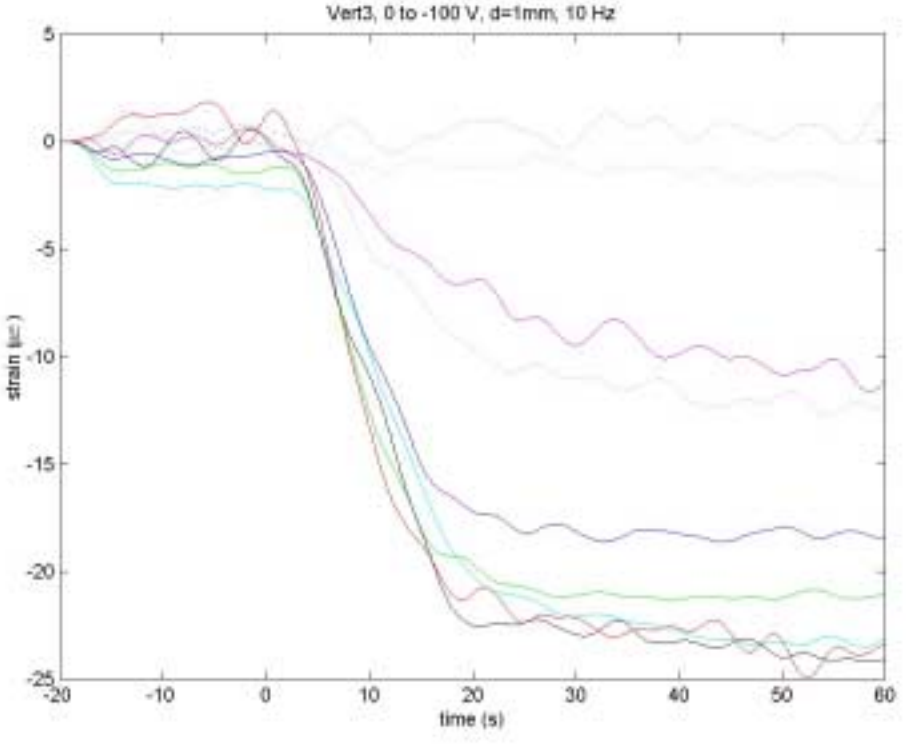
Vert3, 0 to -100 V, d=1mm, 10 Hz
strain (με)
time (s)

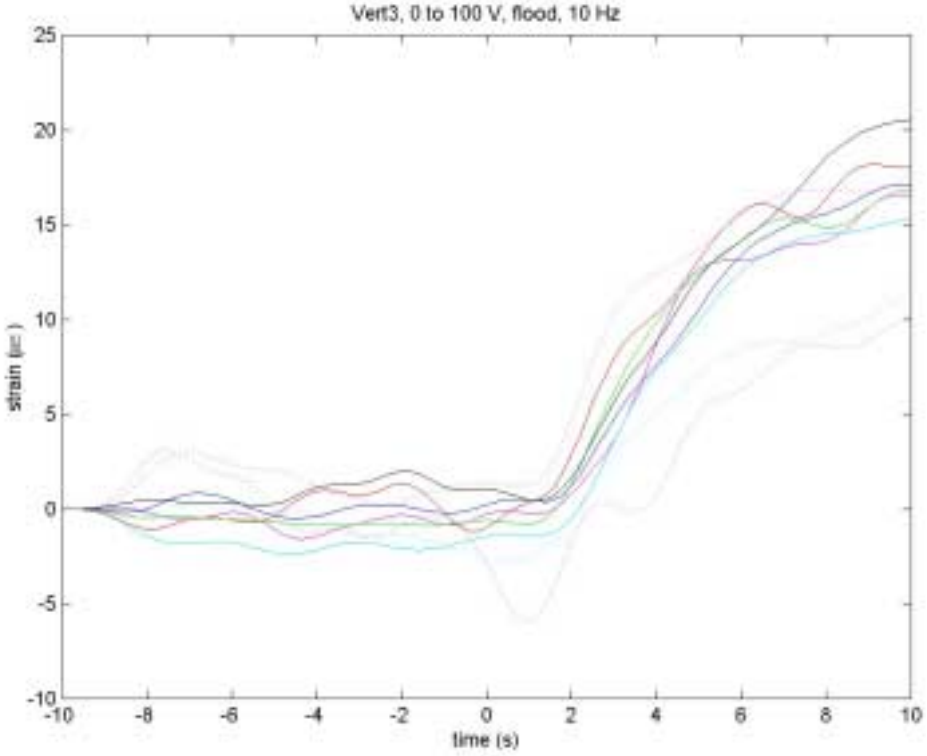
Vert3, 0 to 100 V, flood, 10 Hz
strain (με)
time (s)

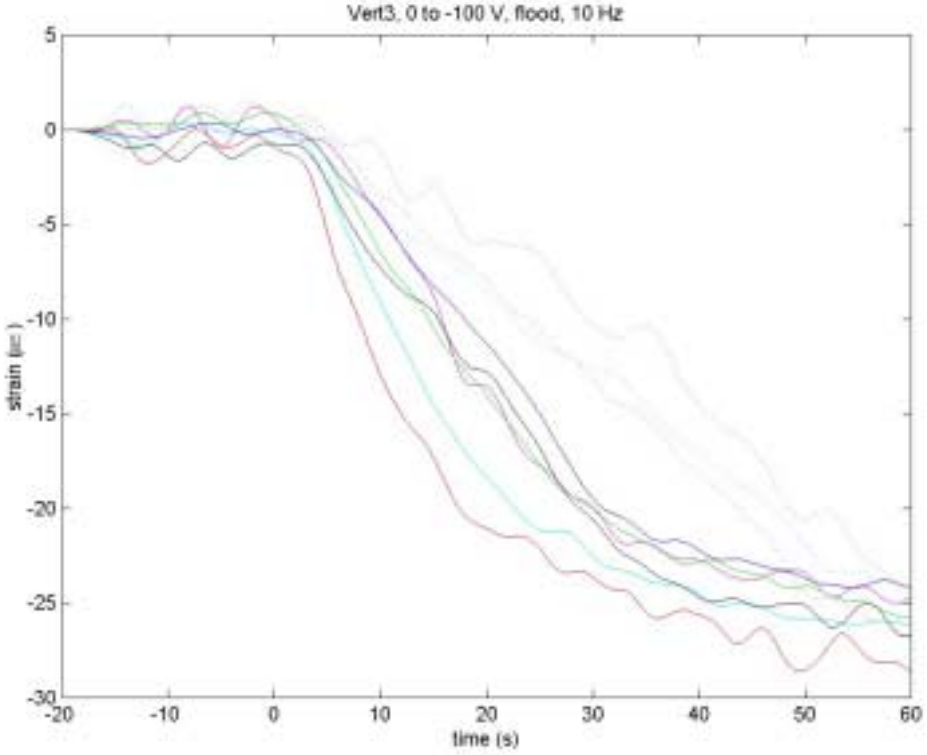
Vert3, 0 to -100 V, flood, 10 Hz
strain (με)
time (s)

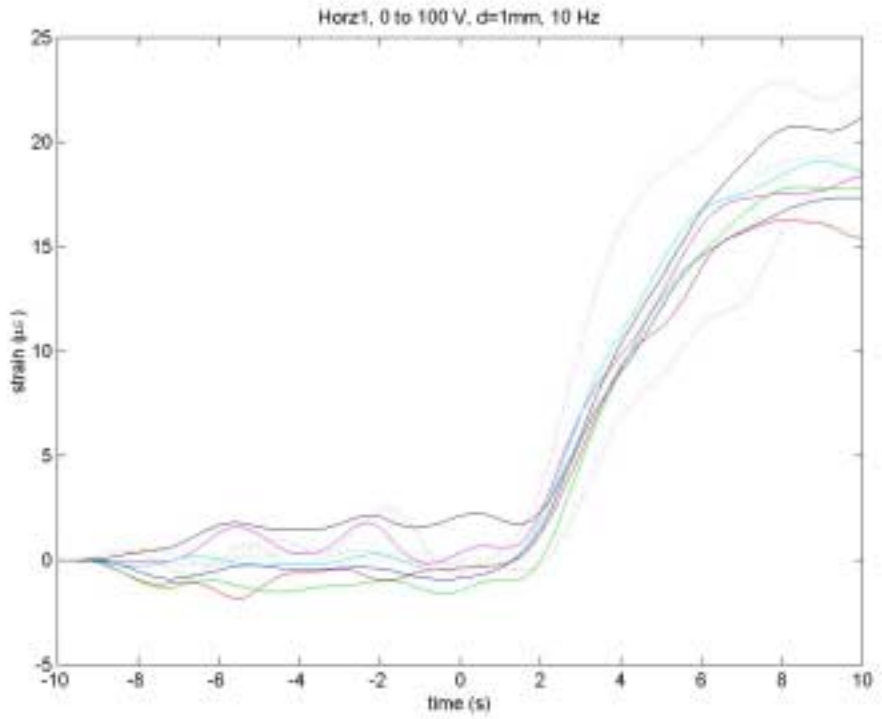
Horz1, 0 to 100 V, d=1mm, 10 Hz
strain (με)
time (s)

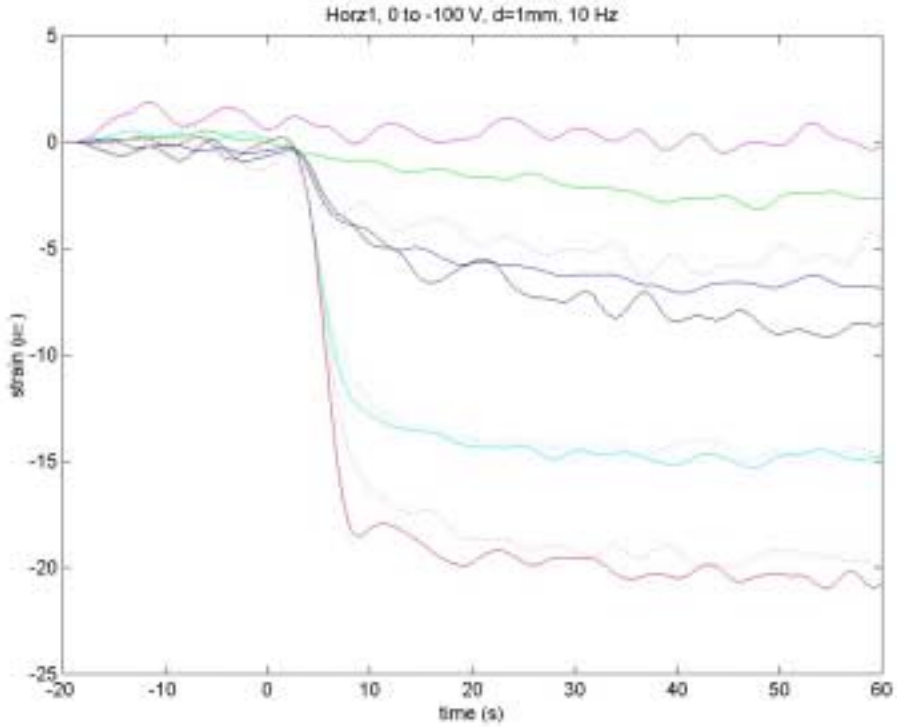
Horz1, 0 to -100 V, d=1mm, 10 Hz
strain (με)
time (s)

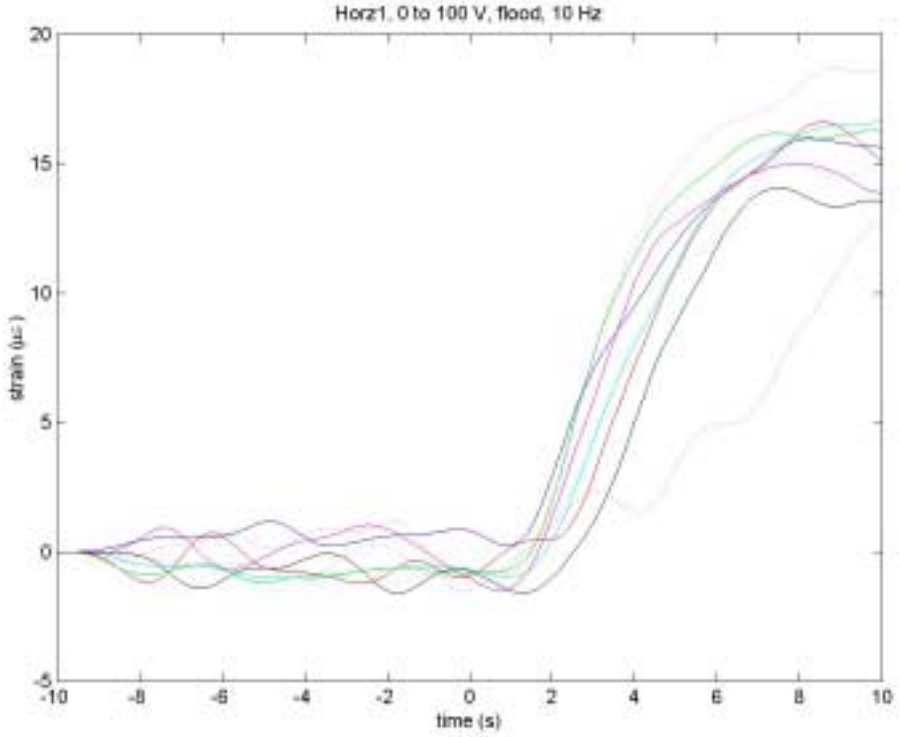
Horz1, 0 to 100 V, flood, 10 Hz
strain (με)
time (s)
20
15
10
5
0
-5
-10
-8
-6
-4
-2
0
2
4
6
8
10

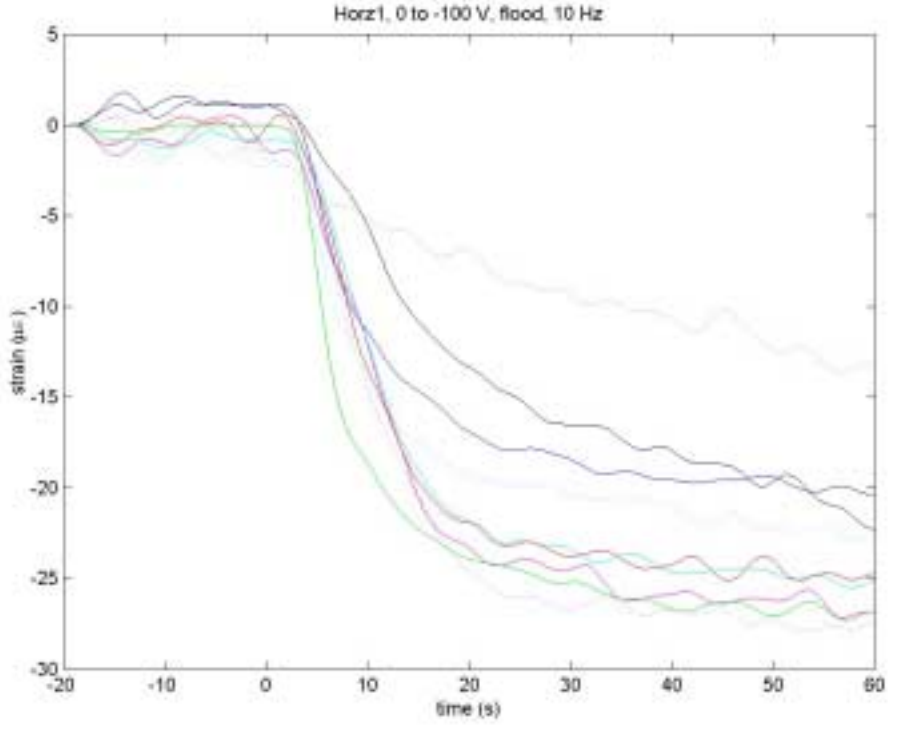
Horz1, 0 to -100 V, flood, 10 Hz
strain (με)
time (s)
5
0
-5
-10
-15
-20
-25
-30
-20
-10
0
10
20
30
40
50
60

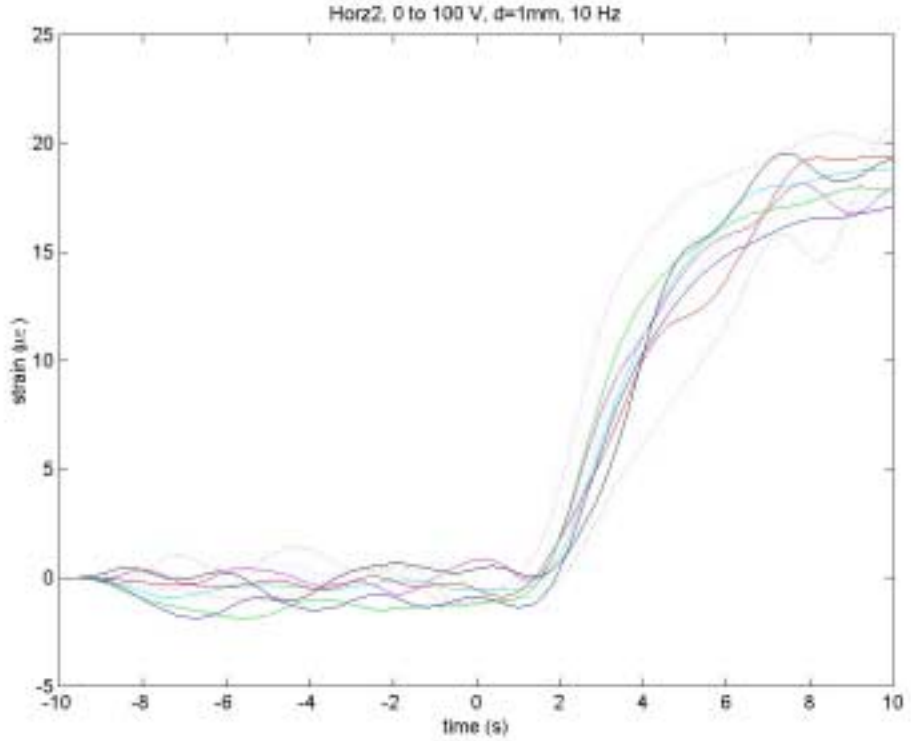
Horz2, 0 to 100 V, d=1mm, 10 Hz
strain (με)
time (s)
25
20
15
10
5
0
-5
-10
-8
-6
-4
-2
0
2
4
6
8
10

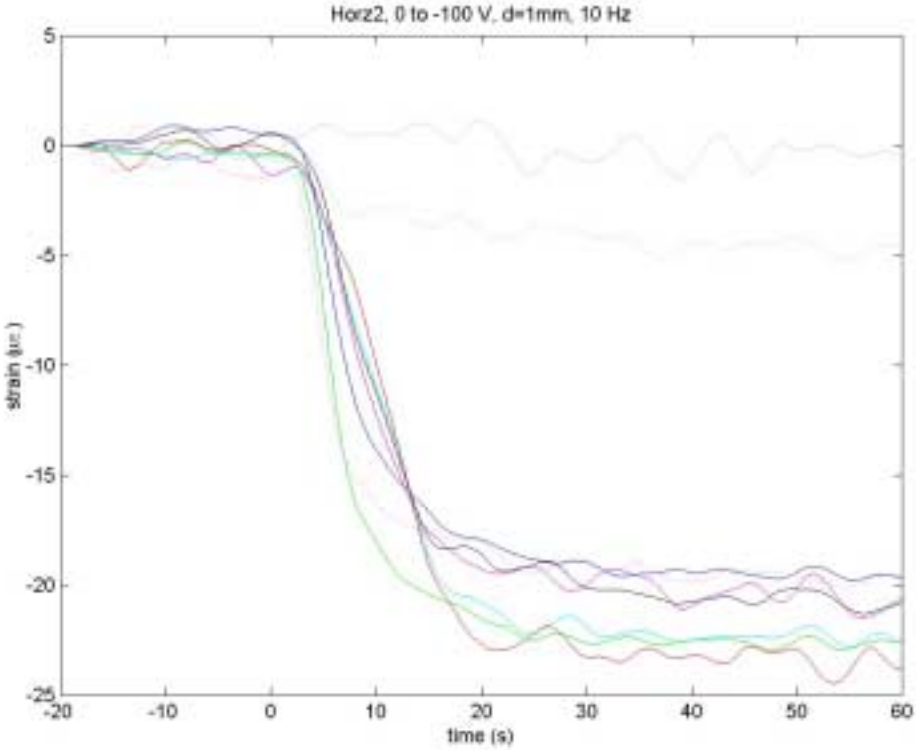
Horz2, 0 to -100 V, d=1mm, 10 Hz
strain (με)
time (s)
5
0
-5
-10
-15
-20
-25
-20
-10
0
10
20
30
40
50
60

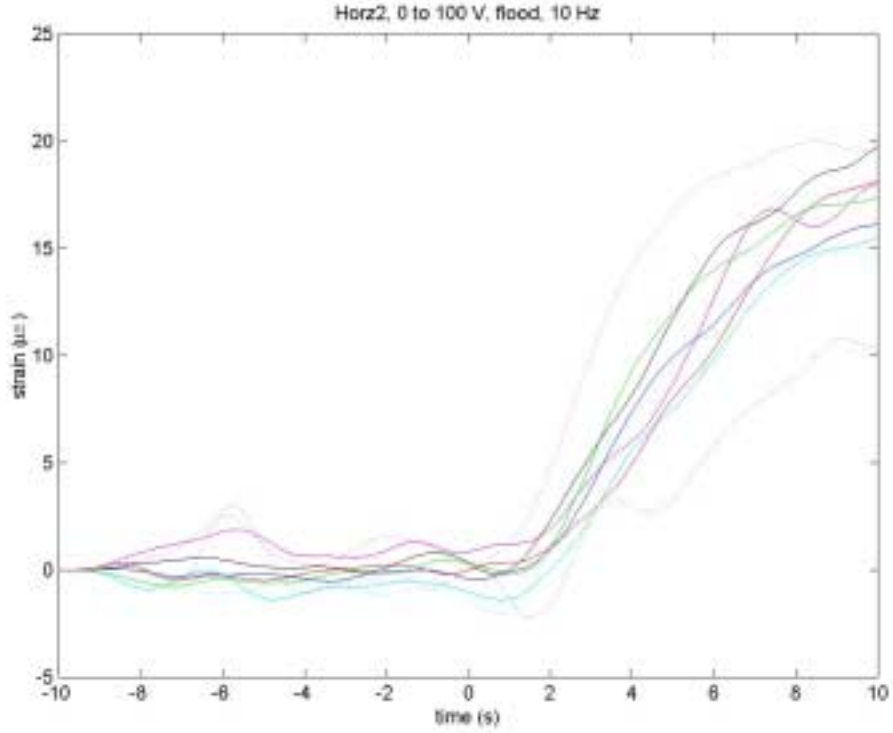
Horz2, 0 to 100 V, flood, 10 Hz
strain (με)
time (s)
25
20
15
10
5
0
-5
-10
-8
-6
-4
-2
0
2
4
6
8
10

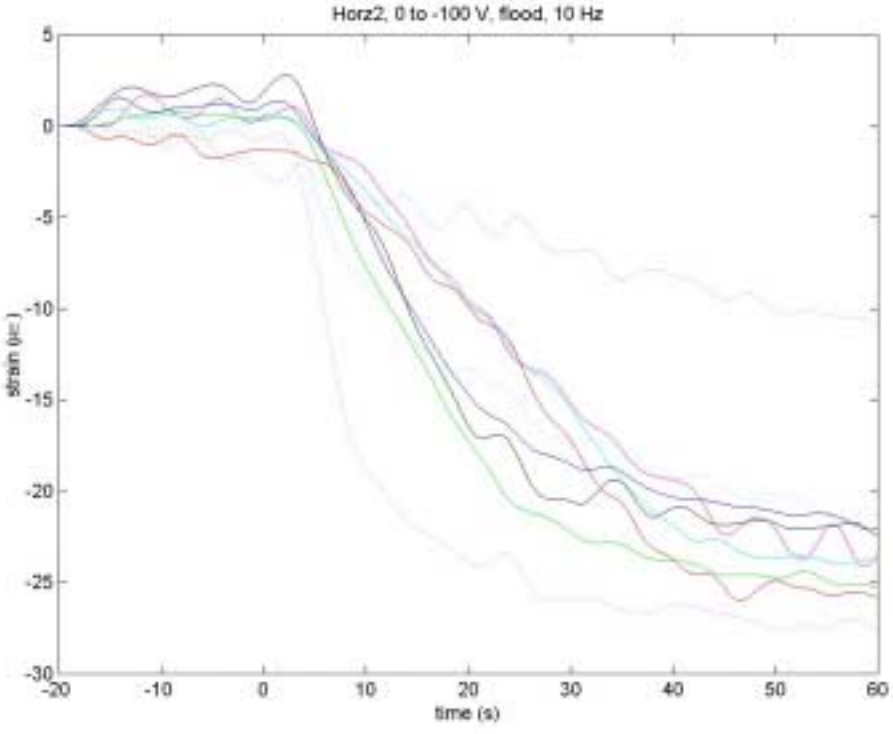
Horz2, 0 to -100 V, flood, 10 Hz
strain (με)
time (s)
5
0
-5
-10
-15
-20
-25
-30
-20
-10
0
10
20
30
40
50
60

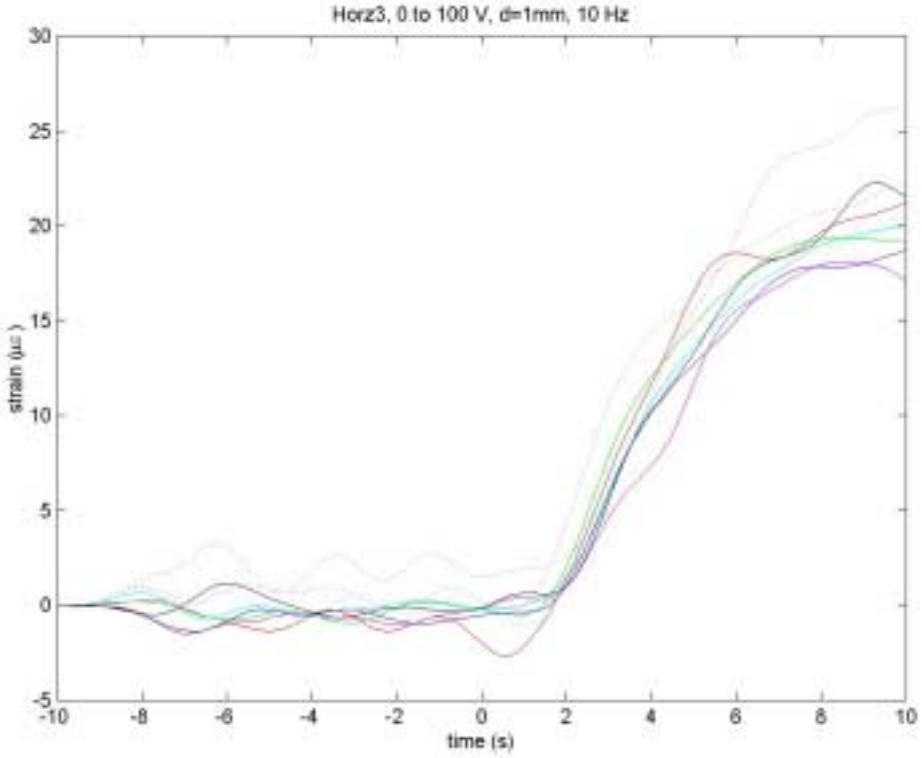
Horz3, 0 to 100 V, d=1mm, 10 Hz
strain (με)
time (s)

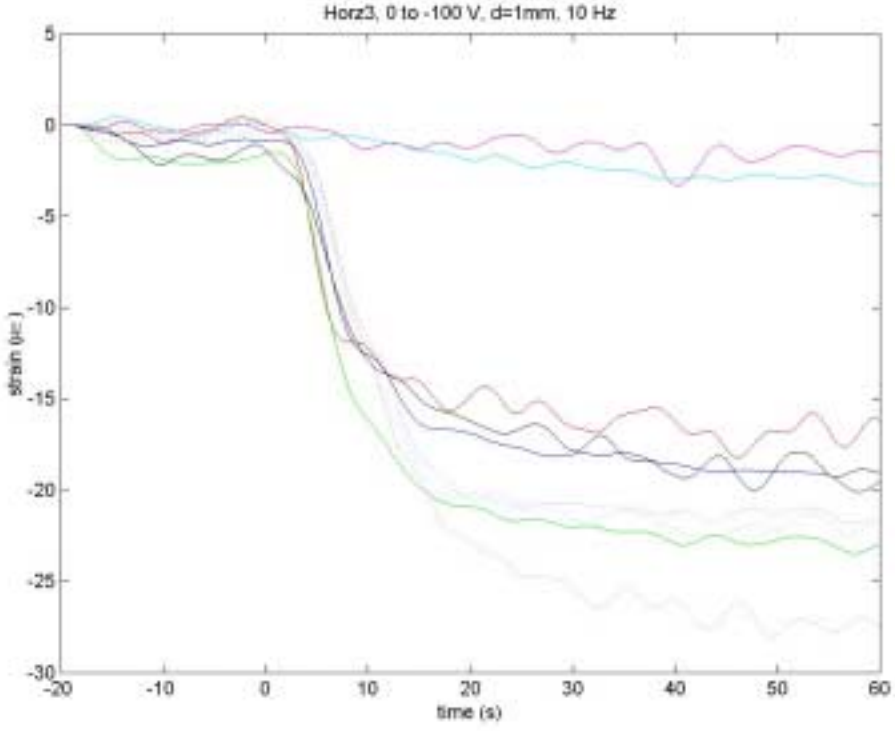
Horz3, 0 to -100 V, d=1mm, 10 Hz
strain (με)
time (s)

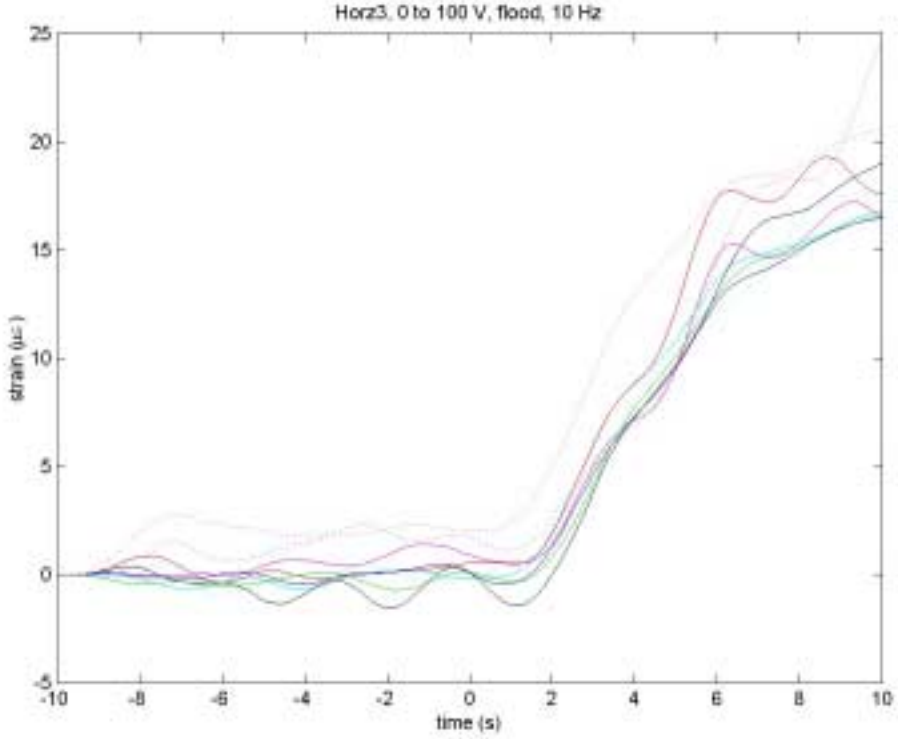
Horz3, 0 to 100 V, flood, 10 Hz
strain (με)
time (s)
25
20
15
10
5
0
-5
-10
-8
-6
-4
-2
0
2
4
6
8
10

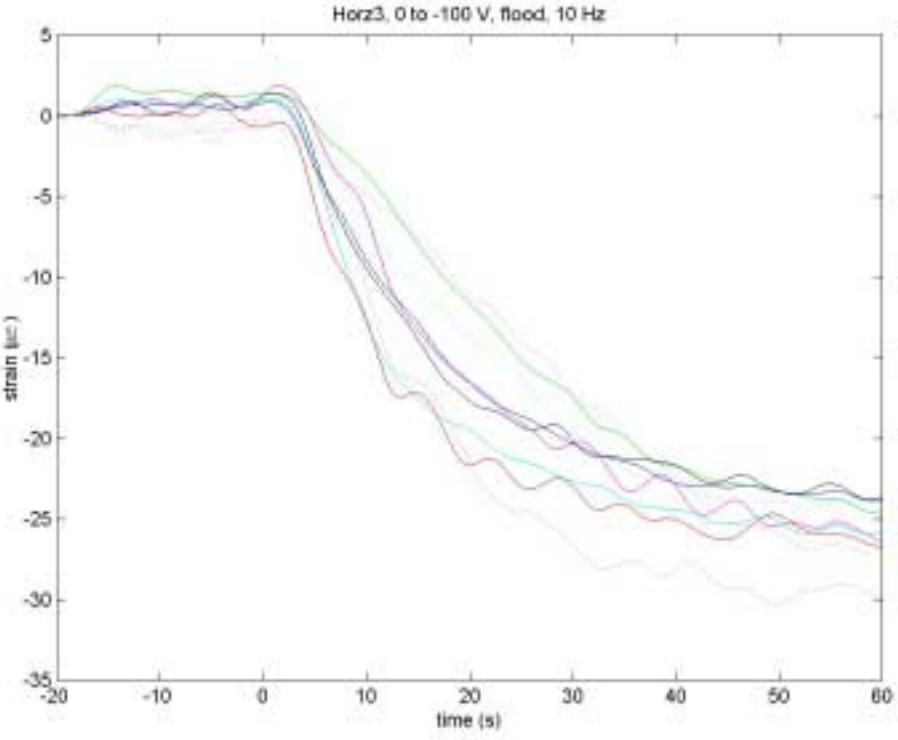
Horz3, 0 to -100 V, flood, 10 Hz
strain (με)
time (s)
5
0
-5
-10
-15
-20
-25
-30
-35
-20
-10
0
10
20
30
40
50
60

Appendix E: Nomenclature

Π = charge build-up when the electrons hit the plate, determined from the experiments.

α_1, α_2, α_3 = coordinate in 1st, 2nd, and 3rd direction

χ = mobility of the electron in the material

$\in = \in_r \in_o$

$\in_r$ = relative dielectric constant

$\in_o$ = permitivity of vacuum = 8.85×10^{-12} F/m

$\eta_k(t)$ = modal participation factor

λ = wavelength of the wave function

μ = Poisson ratio

ν = frequency of the wave function

ρ = mass density

σ = ionic mobility

ω = frequency

A = frequency factor, obtained from the probability of a jump caused by an average energy $h\omega_o$ with respect to all probable energy

A_1, A_2 = Lamé parameters

C = material capacitance

D = electric flux density

$\bar{E}$ = electric field

$\bar{E}_v$ = electric field in vacuum

$\bar{E}_i$ = electric field in i^{th} direction

E_b = energy barrier

E_p = energy of particle

E_t = the total energy received from the interaction with primary electron

M^m_{ij} = mechanical bending moments

M^e_{ij} = electric bending moments

N^m_{ij} = mechanical membrane forces

N^{e}_{ij} = electrical membrane forces

Q = the charge at time t

Q_f = the charge at initial time

Q^{m}_{ij} = mechanical transverse shear forces

Q^{e}_{ij} = electrical transverse shear forces

R = material resistance

R_1, R_2 = radii of curvature

S = strain

T = stress tensor

U = potential energy

V = potential

V_p = potential on positive surface

V_b = the potential on negative surface (backpressure voltage)

Y = Young modulus

YI = bending stiffness

a = distance between lattice

[c] = elastic constant matrix

e = electron charge (1.6×10^{-19} C)

[e] = piezoelectric constant matrix

e_{ij} = conventional mechanical stress

h = thickness of piezoelectric plate

h_P = Planck constant (6.63×10^{-34} J.s)

$\hbar = \frac{h}{2\pi}$

i = electric current

j = electric current density

k = wave number = $\frac{2\pi}{\lambda}$

m = electron mass

n = density of electron

p = particle momentum

p* = the probability that the electron flux will cause a local ion (electron) to jump across a barrier

p(x,y,t) = force acting on x-y plane

q = surface charge density

t_c = time constant

v = the speed of electron

x*,y* = the point/points where p applies

BIBLIOGRAPHY

1. Solymar, L.; Walsh, D.; Lectures on the Electrical Properties of Materials, 5th Edition, Oxford University Press, 1993

2. Bruining, Hajo, *Physics and Application of Secondary Electron Emission*, McGraw-Hill Book Co., New York, 1954.

3. Ganachaud, J.P.; Mokrani, A.; *Theoretical Study of the Secondary Electron Emission of Insulating Targets*, Surface Science v.334 no. 1-3 July 10, 1995 pp. 329-341.

4. Ganachaud, J.P.; Attard, C.; Renoud, R.; *Study of the Space Charge Induced by an Electron Beam in an Insulating Target part I: Monte Carlo Simulation*, Phys. Stat. Sol (b) 199, 1997 pp 175 – 184.

5. Attard, C.; Ganachaud, J.P.; *Study of the Space Charge Induced by an Electron Beam in an Insulating Target part II: Presentation of the Results*, Phys. Stat. Sol (b) 199, 1997 pp 455 – 465.

6. Renoud, R.; Attard, C.; Ganachaud, J.P.; Bartholome, S.; Dubus, A.; *Influence on the Secondary Electron Yield of the Space Charge Induced in an Insulating Target by an Electron Beam*, Journal of Physics: Condensed Matter, vol. 10, 1998 pp 5821 – 5832.

7. Bibi, F. Alouani; Lazurik, V.T.; Rogov, Yu V.; *Space Charge Distribution in Thin Targets Irradiated by Electrons*, IEEE Nuclear Science Symposium & Medical Imaging Conference, Proceedings of the 1996 IEEE Nuclear Science Symposium. Part 1 (of 3) Nov 2-9 1996 v 1 1996 Anaheim, CA, USA pp. 191-195

8. Bibi, F. Alouani; Lazurik, V.T.; Rogov, Yu V.; *Approximation of Charge Deposition Density in Slabs Irradiated by Electrons or Photons*, IEEE Nuclear Science Symposium & Medical Imaging Conference, Proceedings of the 1996 IEEE Nuclear Science Symposium. Part 1 (of 3) Nov 2-9 1996 v 1, 1996 pp. 196-200.

9. Bibi, F. Alouani; Lazurik, V.T.; Rogov, Yu V.; *Electric Field in Thin Dielectric Slabs Irradiated by Electrons*, IEEE Transactions on Nuclear Science Proceedings of the 1997 Nuclear Science Symposium & Medical Imaging, NSS/MIC. Part 1 (of 2) Nov 9-15 1997 v 45 n 3 pt 1 Jun 1998 pp. 617-622

10. Nazarov, V.U.; *Analytical Properties of Dielectric Response of Semi-Infinite Systems and the Surface Electron Energy Loss Function*, Surface Science Proceedings of the 14th European Conference on Surface Science Part B, September 19-23, 1994 v 331-333 pp. 1158-1162.

11. Gross, Bernhard; Giacometti, J.A.; Ferreira, G.F. Leal; *Charge Storage and Transport in Electron-Irradiated and Corona-Charged Dielectrics*, IEEE Transactions on Nuclear Science, v. NS-28, no. 6, December 1981.

12. Schou, J.; *Transport Theory for Kinetic Emission of Secondary Electron from Solids*, Physical Review B, September 1980, pp. 2141-2174.

13. Rösler, M.; Brauer, W.; Devooght, J.; Dehaes, J.C.; Dubus, A.; Cailler, M.; Ganachaud, J.P.; *Particle Induced Electron Emission part I*; Springer-Verlag, Berlin 1991

14. Halliday, David; Resnick, Robert; *Physics 3rd* Edition, John Wiley & Sons, Canada 1978

15. Pollock, Daniel D., *Physical Properties of Materials for Engineers, 2nd Edition*, CRC Press, Inc, USA 1993

16. Smith, Arthur C,; Janak, James F.; Adler, Richard B.; *Electronic Conduction in Solids*, McGraw-Hill Book Company, USA 1967

17. Batra, R.C.; Liang, X.Q.; Yang, J.S.; *Shape Control of Vibrating Simply Supported Rectangular Plates*, AIAA Journal v. 34 no. 1 January 1996 pp. 116-122.

18. Ghosh, K.; Batra, R.C.; *Shape Control of Plates using Piezoceramic Elements*, Proceedings of SPIE - The International Society for Optical Engineering Active Materials and Smart Structures Oct 10 1994 v 2427 1995 pp. 107-121.

19. Main, J.A.; Nelson, G.; Martin, J.; *Maintenance of Inflated Structure Shape Using Electron Gun Controlled Piezoelectric Materials*, Proceedings of the 39th AIAA Structures, Structural Dynamics, and Materials Conference, Adaptive Structures Forum, April 20-23, 1998, Long Beach, CA, AIAA Paper 98-1983.

20. Main, J.A.; Martin, J.W.; Nelson, G.C.; *Noncontact Shape Control of Membrane Mirrors*, Ultra Lightweight Space Optics Challenge Workshop, Napa, California, March 24-25 1999.

21. Nelson, G.C.; Main, J.A.; *Noncontact Electron Gun Strain Control of Piezoceramics*, AIAA Journal, in press.

22. Crawley, E.F.; Luis, Javier; *Use of Piezoelectric Actuators as Elements of Intelligent Structures*, AIAA Journal vol.25, no.10, October 1987.

23. Crawley, E.F.; Lazarus, K.B.; *Induced Strain Actuation of Isotropic and Anisotropic Plates*, AIAA Journal, vol.29, no.6, June 1991, pp.944-951.

24. Lee, C.K.; Moon, F.C.; *Modal Sensors/Actuators, Journal of Applied Mechanics*, vol.57, June 1990, pp.434-441.

25. Tzou, H.S.; Ye, R.; *Piezothermoelasticity and Precision Control of Piezoelectric Systems: Theory and Finite Element Analysis,* Journal of Vibration and Acoustic, vol. 116, October 1994, pp. 489-495.

26. Gopinathan, Senthil V.; Varadan, Vasundara V.; Varadan, Vijay K.; *Review and Critique of Theories of Piezoelectric Laminates*, Smart Materials and Structures, vol. 9, no.1 2000 pp. 24-48.

27. Tzou, H.S., *Piezoelectric Shells, Distributed Sensing and Control of Continua*, Kluwer Academic Publishers, Netherlands 1993.

28. Morgan Matroc, Inc., *Guide to Modern Piezoelectric Ceramics*, Electro Ceramics Division, Bedford, Ohio, 1993.

29. ANSI/IEEE, *An American National Standard, IEEE Standard on Piezoelectricity*, Standards Committee of the IEEE Ultrasonics, Ferroelectrics, and Frequency Control Society, The Institutue of Electrical and Electronics Engineers, Inc., New York 1988.

30. Horowitz, Paul; Hill, Winfield; *The Art of Electronics 2nd edition*, Cambridge University Press, 1989.

31. Eisbert, Robert; Resnick, Robert; *Quantum Physics of Atoms, Molecules, Solids, Nuclei, and Particles*, John Wiley & Sons Inc., 1974

32. Klemens, Paul; *Electrons in Test Tubes, Electrons on the Move (editor: Sharon Banigan)*, The Westinghouse Search Book, Walker and Co., New York 1964 pp. 74.

33. Kreyszig, Erwin, *Advanced Engineering Mathematics, 6th edition*, John Wiley & Sons Inc., New York 1988.

34. Ugural, Ansel C.; Fenster, Saul K.; *Advanced Strength and Applied Elasticity, 3rd edition*, Prentice Hall Inc., New Jersey, USA, 1995.

35. Hadinata, Philip C.; Main, John A.; *Time Response of Electron Gun Strain Control of Piezoelectric Materials*, Proceedings of SPIE Smart Structures and Integrated System, Smart Structures and Materials, vol. 3985, 2000, pp. 378 – 384, ISBN # 0816436038.

36. Doebelin, Ernest O.; *Measurement Systems, Application and Design, 4th edition*, McGraw Hill Book Co., Singapore 1990.

VITA

Philip Clark Hadinata was born on November 11, 1972 in Bandung, Indonesia. He earned his Bachelor of Science in Physics Engineering from Bandung Institute of Technology, April 1996. His project was Simple Cardiograph Designing Study using Ultrasonic Wave as Motion Detector. He resumed his education to master degree and received his Master of Science in Instrumentation and Control Engineering from the same institution in August 1998. His thesis was Split Spectrum Processing Application in Ultrasonic Wave Processing to Increase Signal to Noise Ratio. He continued to a doctoral degree at Mechanical Engineering Department, University of Kentucky, under advisory of Dr. John Main.

During his course of study, Philip engaged in several industrial experiences. On May-August 1995 Philip had an internship at Commander Electrindoraya Co.Ltd, as Research and Development Programmer to design an infrared remote control for fan position and speed using Motorola EPROM/OTPROM Assembler Language. On Spring 1998 he held a co-op position with Timor Indonesia, Co.Ltd, to design and analyze acoustic performance of automobile muffler using BEMAP (Boundary Element Method for Acoustic Prediction). He submitted some publications, two of them were presented on SPIE's Annual Symposium on Smart Structrures and Instrumentation, Newport Beach, CA, 2000 and 2001. He also held several certifications for seminars, workshops and tutorials.